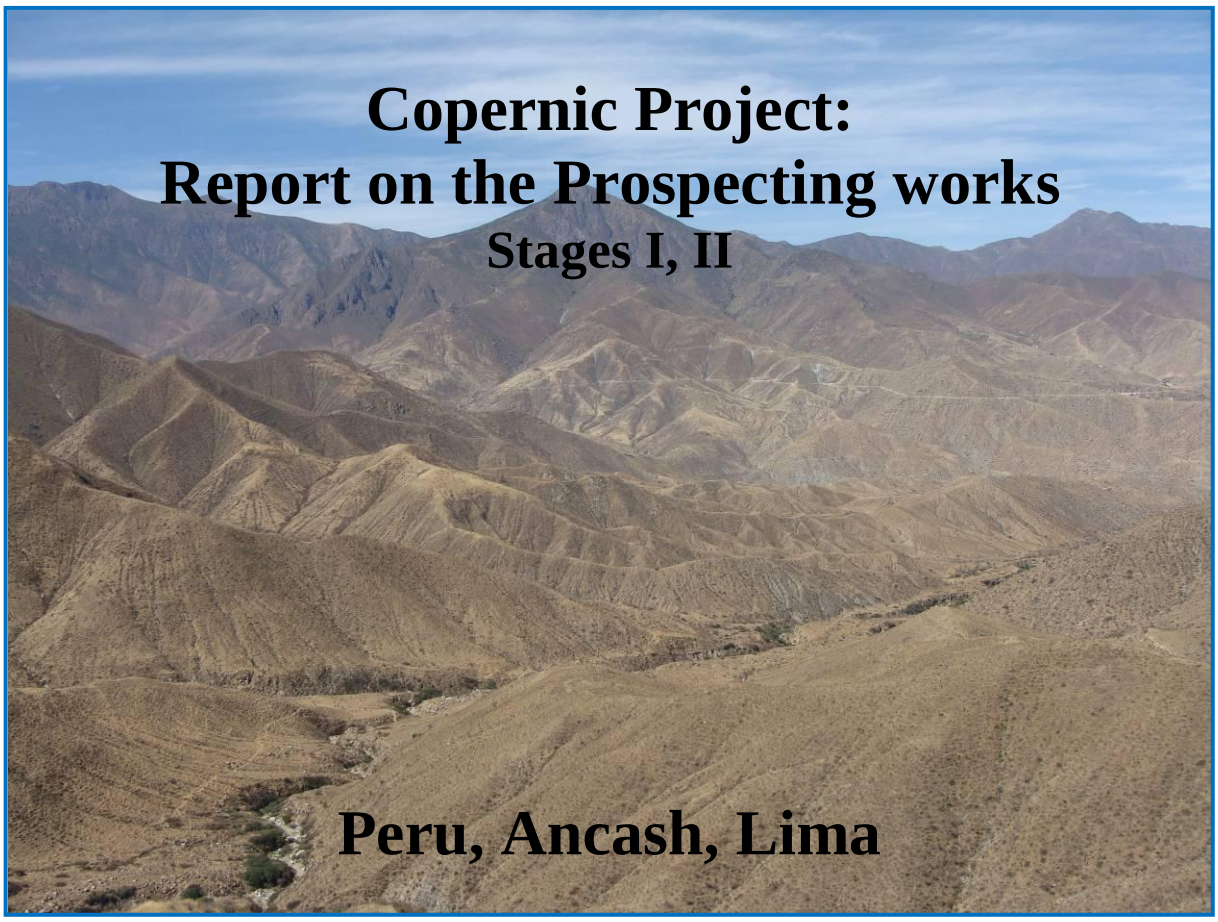

Copernic Project:
Report on the Prospecting works
Stages I, II

Peru, Ancash, Lima

Prepared by Upstream Mining S.A.C.

January 25, 2011

Contents

Tables in the text

Figures in the text

Graphic and text appendices

Appendix 1. Maps of factual data

Sheet 1. Map of factual data: observation points and routes in the studied area. Scale of 1 : 25 000

Sheet 2. Map of factual data: observation points and routes in the site of detailed prospecting. Scale of 1 : 10 000

Sheet 3. Map of factual data: samples of stream sediments in the studied area. Scale of 1 : 25 000

Sheet 4. Map of factual data: samples of bedrocks in the studied area. Scale of 1 : 25 000

Sheet 5. Map of factual data: samples of bedrocks in the site of detailed prospecting. Scale of 1 : 10 000

Sheet 6. Map of factual data: mining workings and samples of bedrocks in the site of detailed prospecting. Scale of 1 : 5000

Appendix 2. Geological maps and sections

Sheet 1. Geological map of the studied area. Scale 1 : 25 000

Sheet 2. Geological map of the site of detailed prospecting. Scale of 1 : 10 000

Sheet 3. Geological map of the site of detailed prospecting. Scale of 1 : 5000

Sheet 4. Geological section along line AB. Horizontal and vertical scales of 1 : 5000

Sheet 5. Geological section along line CD. Horizontal and vertical scales of 1 : 5000

Sheet 6. Legend to geological map

Appendix 3. Maps of monoelemental geochemical anomalies in the studied area: primary halos in bedrocks

Sheet 1. Map of **Cu** anomalies in the studied area: primary halos in bedrocks. Scale of 1 : 25 000

Sheet 2. Map of **Mo** anomalies in the studied area: primary halos in bedrocks. Scale of 1 : 25 000

Sheet 3. Map of **Ag** anomalies in the studied area: primary halos in bedrocks. Scale of 1 : 25 000

Sheet 4. Map of **Pb** anomalies in the studied area: primary halos in bedrocks. Scale of 1 : 25 000

Sheet 5. Map of **Zn** anomalies in the studied area: primary halos in bedrocks. Scale of 1 : 25 000

Sheet 6. Map of **Au** anomalies in the studied area: primary halos in bedrocks. Scale of 1 : 25 000

Sheet 7. Map of **Bi** anomalies in the studied area: primary halos in bedrocks. Scale of 1 : 25 000

Sheet 8. Map of **Fe** anomalies in the studied area: primary halos in bedrocks. Scale of 1 : 25 000

Sheet 9. Map of **Al** anomalies in the studied area: primary halos in bedrocks. Scale of 1 : 25 000

Sheet 10. Map of **S** anomalies in the studied area: primary halos in bedrocks. Scale of 1 : 25 000.

Appendix 4. Maps of monoelemental geochemical anomalies in the studied area: secondary halos in stream sediments

Sheet 1. Map of **Cu** anomalies in the studied area: secondary halos in stream sediments. Scale of 1 : 25 000

Sheet 2. Map of **Mo** anomalies in the studied area: secondary halos in stream sediments. Scale of 1 : 25 000

Sheet 3. Map of **Au** anomalies in the studied area: secondary halos in stream sediments. Scale of 1 : 25 000

Sheet 4. Map of **Ag** anomalies in the studied area: secondary halos in stream sediments. Scale of 1 : 25 000

Sheet 5. Map of **Pb** anomalies in the studied area: secondary halos in stream sediments. Scale of 1 : 25 000

Sheet 6. Map of **Zn** anomalies in the studied area: secondary halos in stream sediments Scale of 1 : 25 000

Sheet 7. Map of **Bi** anomalies in the studied area: secondary halos in stream sediments. Scale of 1 : 25 000

Sheet 8. Map of **Fe** anomalies in the studied area: secondary halos in stream sediments. Scale of 1 : 25 000

Sheet 9. Map of **Al** anomalies in the studied area: secondary halos in stream sediments. Scale of 1 : 25 000

Sheet 10. Map of **S** anomalies in the studied area: secondary halos in stream sediments. Scale of 1 : 25 000

Appendix 5. Maps of monoelemental geochemical anomalies in the sites of detailed prospecting: primary halos in bedrocks

Sheet 1. Map of **Cu** anomalies in the Western site: primary halos in bedrocks. Scale of 1 : 5000

Sheet 2. Map of **Mo** anomalies in the Western site: primary halos in bedrocks. Scale of 1 : 5000

Sheet 3. Map of **Cu** anomalies in the Eastern site: primary halos in bedrocks. Scale of 1 : 5000

Sheet 4. Map of **Mo** anomalies of the Eastern site: primary halos in bedrocks. Scale of 1 : 5000

Appendix 6. Polyelemental and muliplicative geochemical maps of the studied area: primary halos in bedrocks

Sheet 1. Polyelemental geochemical map (As, Au, Hg, Sb, W, Li) of the studied area: primary halos in bedrocks. Scale 1 : 25 000

Sheet 2. Multiplicative geochemical map of the studied area: Ki = (Cu*Mo)/(Ag*Zn). Scale 1 : 25 000

Sheet 3. Multiplicative geochemical map of the studied area: Ki = (Cu*Mo)/(Pb*Zn). Scale 1 : 25 000

Sheet 4. Multiplicative geochemical map of the studied area: Ki = (Cu*Mo)/(Ag*Zn). Scale 1 : 10 000

Sheet 5. Multiplicative geochemical map of the studied area: Ki = (Cu*Mo)/(Ag*Zn). Scale 1 : 10 000

Supplementary appendices in electronic form only

Supplementary Appendix 1. Files with analytical results
Supplementary Appendix 2. Detailed plan of prospecting (II stage), project Copernic, 2010 (rus.)
Supplementary Appendix 3. Geophysical report on magnetic, gamma spectrometry, and induced polarization surveys on behalf of Upstream Mining S.A.C., Copernic Project, Ancash, Peru, June, 2010 performed by VDG del Peru S.A.C.
Supplementary Appendix 4. Report by supervisor A.B. Nikitin on completed geophysical survey in the Copernic area, district San Pedro, department Ancash, province Ocros, Peru, 2010.(rus.)
Supplementary Appendix 5. Files with analytical results on copper leachability.(rus.)

1. INTRODUCTION

1.1. Ownership

The Copernic project was offered to Upstream Mining S.A.C. by Quippu Exploraciones S.A.C. for creating a joint venture. The JV Coppernico Exploraciones S.A.C. was created on March 31, 2010 for geological exploration of potentially economic copper occurrences in the concession territories owned by both companies and the subsequent development of the projects to prefeasibility and feasibility stages.

The area of prospecting works is spaced on territory of concessions listed in Tables 1.1, as well as approximately 1-2 km of adjacent territory.

Table 1.1. List of concessions. Titleholder is JV «Coppernico Exploraciones S.A.C.»

	Property Name	Code.	Location	Status	Hectares
1	Cayan 1	010464907	Ancash	In force	100
2	Cayan 2	010401808	Ancash	In force	400
3	Cayan 3	010401908	Ancash	In force	200
4	Cayan 4	010046809	Ancash	In force	100
5	Cayan 5	010258009	Ancash	In force	100
6	Cayan 6 *	520010509	Ancash	In force	400
7	Cayan 7	010262609	Ancash	In force	400
8	Cayan 8	010262709	Ancash	In force	500
9	La Obra de Dios	010436907	Ancash	In force	100
10	La Obra de Dios I	010437007	Ancash	In force	100
11	La Obra de Dios II	010437107	Ancash	In force	100
					2000 ga

Comment*: Titleholder of concession “Cayan 6” in present is «Upstream Mining S.A.C.».

The area of Copernic project occupies a territory of the concessions (Fig. 1):

1. Cayan 2 - 4 km^2 ,
2. Cayan 4 - 1 km^2 ,
3. La Obra de Dios - 1km^2,
4. La Obra de Dios I - 1km^2, as well as a part of adjacent territory by total area of surface 8 km^2.

The above concessions shown in Fig. 1 are localized within Map Sheet Huayllapampa–21h of the State Topographic Map on a scale of 1 : 100 000 in the southeastern part of Map Sheet 21h-II-SE. The digital topographic base on a scale 1 : 25000, Map Sheet 21h-II-SE was used during fieldwork and preparation of this report.

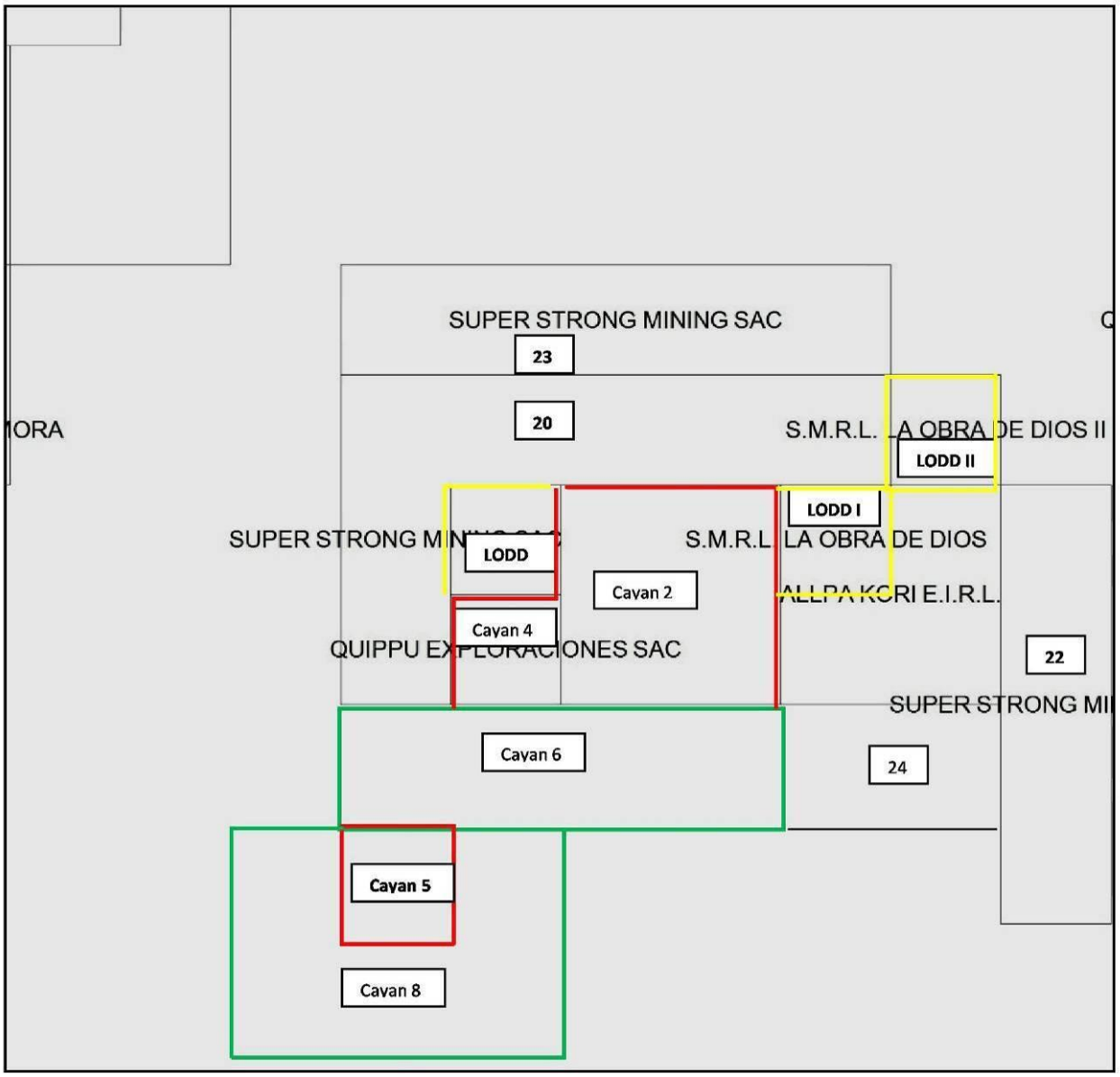

Fig. 1. Concessions covering the Copernic project area and the adjacent territory.

1.2. Property location and infrastructure

The area of the project is situated in the Ancash Region, Ocros Province, Copa District, Choque Commune close to the boundary between the Ancash and Lima regions. The settlement of Choque is closely related to the settlement of Chulin 41 km south-southwest from the former at the boundary with the Lima Region; both settlements make up a joint commune (Figs. 2, 3).

The infrastructure in the studied area and the site of forecasted deposit is favorable. Transport ways are as follows: PanAmerican Norte Highway from the Lima (Callao) port to the Pativilca Settlement (205 km; 3 h of driving) or approximately 0.6 h from the terminal of Antamina Company; then 2 h of driving by a local dirty road to the eastern boundary of concession area. To provide a direct passage to the site, it is necessary to build about 3.5–4.0 km

of road (2–3 km for drilling campaign). An electrical power line 220 kV extends 38 km south of the site; power line 14 kV reaches the Choque Settlement.

The concession area occurs near the Pacific coast of Peru at the western spurs of the Cordillera Negra in the medium-mountain semidesert zone 1300–2900 masl. Climate is arid. A short rainy season falls on January–March, when day temperature varies from +18 to +28°C; in summer, day temperature is +25 to +35°C; night temperature is +14 to +25°C. The area is beyond the zone of seasonal fogs. The Choque River is a single perennial stream. Almost all its runoff is used for agricultural needs of local habitants, so that water resource is deficient.

Population is limited because of shortage of land suitable for agriculture. Social conflicts are related to water and agricultural resources. The demand for unskilled labor force can be satisfied by local resources but strongly depends on the season of agricultural works in the Rio Choque Valley and the Barranca–Pativilca Zone.

The relationships between the Upstream Mining S.A.C. and the Choque Commune are currently favorable.

Fig. 2. Index map. The Copernic project is marked by star.

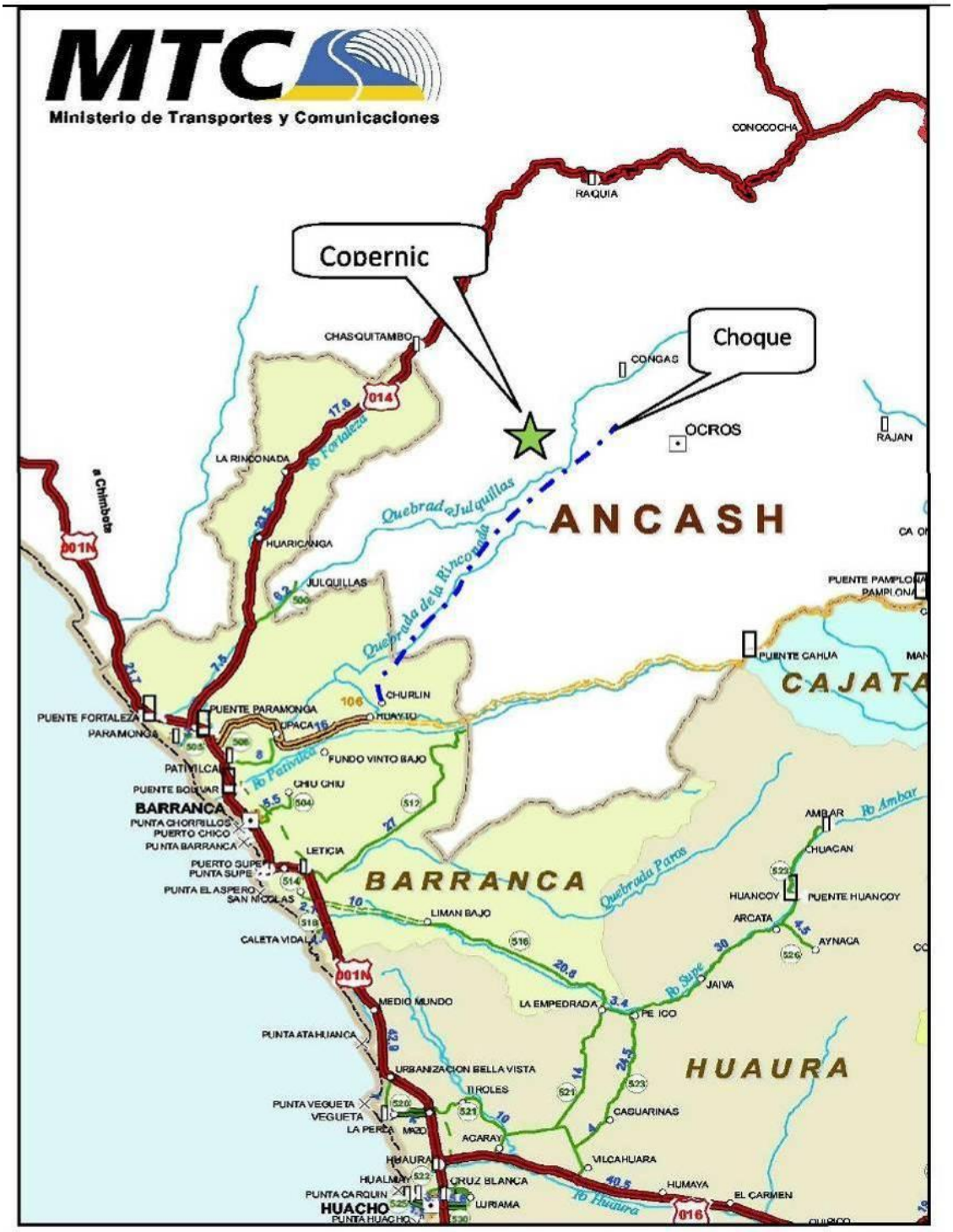

Fig. 3. Infrastructure of the Ancash region and the adjacent territory.

1.3. History and previous works

1.3.1. History

The Copernic project was offered for studying to Upstream Mining S.A.C. by Quippu Exploraciones S.A.C. in October 2008. By that date, the Quippu Company had taken ~15 samples from bedrock outcrops, debris falls, and remote fragments with visible oxidized copper mineralization. Furthermore, in February and March, 2009, the data of sampling within concessions Cayan 1 and Cayan 3 and the adjacent territories were handed over to Upstream Company.

These data comprised the analytical results for base elements and gold, coordinates of samples in PSAD-56 system, type of sampling, and brief descriptions of samples. No cartographic data were handed over. In the opinion of specialists from the Quippu Company, the sampled object was a zone of leaching of porphyry copper deposit hosted in granodiorite.

Upstream Company carried out reconnaissance prospecting in October and December, 2008. About 40 rock chip panel samples and composite channel samples were taken from bedrocks. A schematic geological plan on a scale of 1 : 5000 was drawn for the central part of mineralized zone. The occurrence of oxidized copper mineralization in stockworks and quartz veinlet zones was confirmed. No direct evidence for the mineralization characteristic of porphyry copper deposits has been furnished. As a result, speculative resources were estimated at 10–100 Mt ore depending on a possible scenario. In the course of fieldwork, it was revealed that 30–50% of promising area is located in the territory of La Obra de Dios concession belonged to other owners.

Taking into account the results obtained, a decision was made to carry out geological prospecting of the first stage focused on more detailed and thorough estimation of the Copernic prospect.

1.3.2. Previous works (the first stage, 2009)

The objective of geological prospecting of the first stage was preliminary evaluation of the Copernic occurrence as a potentially economic deposit. The following tasks were set for this purpose:

- revision and evaluation of the previously revealed mineralization,
- search for new ore occurrences,
- delineation of promising area, and
- qualitative and quantitative assessment of the revealed mineralization and, if possible, its morphogenetic, geological, and economic estimation.

To solve the above problems, geological mapping, sampling, dig holes and trenches were used.

Geological prospecting was carried out during one month by three engineers-geologists A.Yu. Mar'yan, V.M. Marchenko, and I.M. Puzankov (executive resume App. 9) with assistances of 10 called-in workers. The Cayan 2 and Cayan 4 concessions (project Copernic proper), as well as La Obra de Dios (LODD), La Obra de Dias I and La Obra de Dias II were covered. Geological mapping and prospecting over an area of 18 km^2 on a scale of 1 : 25 000 to 1 : 5000 (1 : 50 000 at flanks) were performed. The detailed prospecting was carried out in the forecasted ore zones bearing direct evidence for copper mineralization. Main attention was paid to the site with visible oxidized copper mineralization.

In the course of prospecting, 786 channel samples (up to 6 kg in weight), composite channel samples (up to 8 kg), and rock chip panel samples (up to 4 kg) were taken; 235 dig holes (12 hole lines) were sunk, and a line of 10 trenches and strippings were driven.

The following results have been achieved:

- outlook of the project was expanded due to new sites with promising mineralization;
- the project became more reliable;
- occurrences of oxidized copper mineralization were traced northward into a free at that moment territory;
- outcrops with primary sulfide Cu–Mo mineralization were found;
- speculative copper ore resources were estimated;
- depending on accepted assumptions they vary from 89 008 kt ore and 473 kt Cu to 239 783 kt ore and 857 kt Cu; this estimate is referred to oxidized ore only;
- the forecasted resources correspond to a medium-sized copper deposit.

By the onset of geological exploration in 2010, a model of the Copernic deposit was suggested as follows:

- a porphyry-type Cu–Mo deposit with stringer–disseminated mineralization hosted in the Late Cretaceous granitoids was formed first;
- then it was involved in faulting and affected by hydrothermal solutions; as a result, quartz veinlets and veins were formed;
- low-temperature hydrothermal solutions oxidized and redistributed the primary sulfide mineralization and formed oxidized ore containing 0.1–1.0% Cu.

On the basis of the results obtained, a decision was made to participate in the project and carry out geological prospecting of the second stage.

2. TECHNIQUE AND RESULTS OF GEOLOGICAL EXPLORATION (THE SECOND STAGE, 2010)

2.1. Objective

The objective of the fulfilled work was to assess the Copernic ore field revealed in 2009 as a probable economic ore object. The fieldwork was focused on the revision of previously found ore occurrences, determination of their real dimensions and character of mineralization, geological and morphogenetic estimation of the ore field as a whole, and prospecting new ore occurrences in the adjacent territories.

The works of the second stage started on April 23 and finished on June 17 and comprised both the geological prospecting and the geophysical exploration considered in section 2.3.

The geological prospecting included geological mapping on a scale of 1 : 50 000 to 1 : 5000; sampling of outcrops and talus; sampling of ore zones on a certain network; sinking dig holes and driving trenches in unexposed areas for contouring ore zones.

The detailed plan of prospecting of the second stage under the Copernic project 2010 is given in Supplementary Appendix 1. The subdivision of concessions by order of priority is presented in Fig. 4.

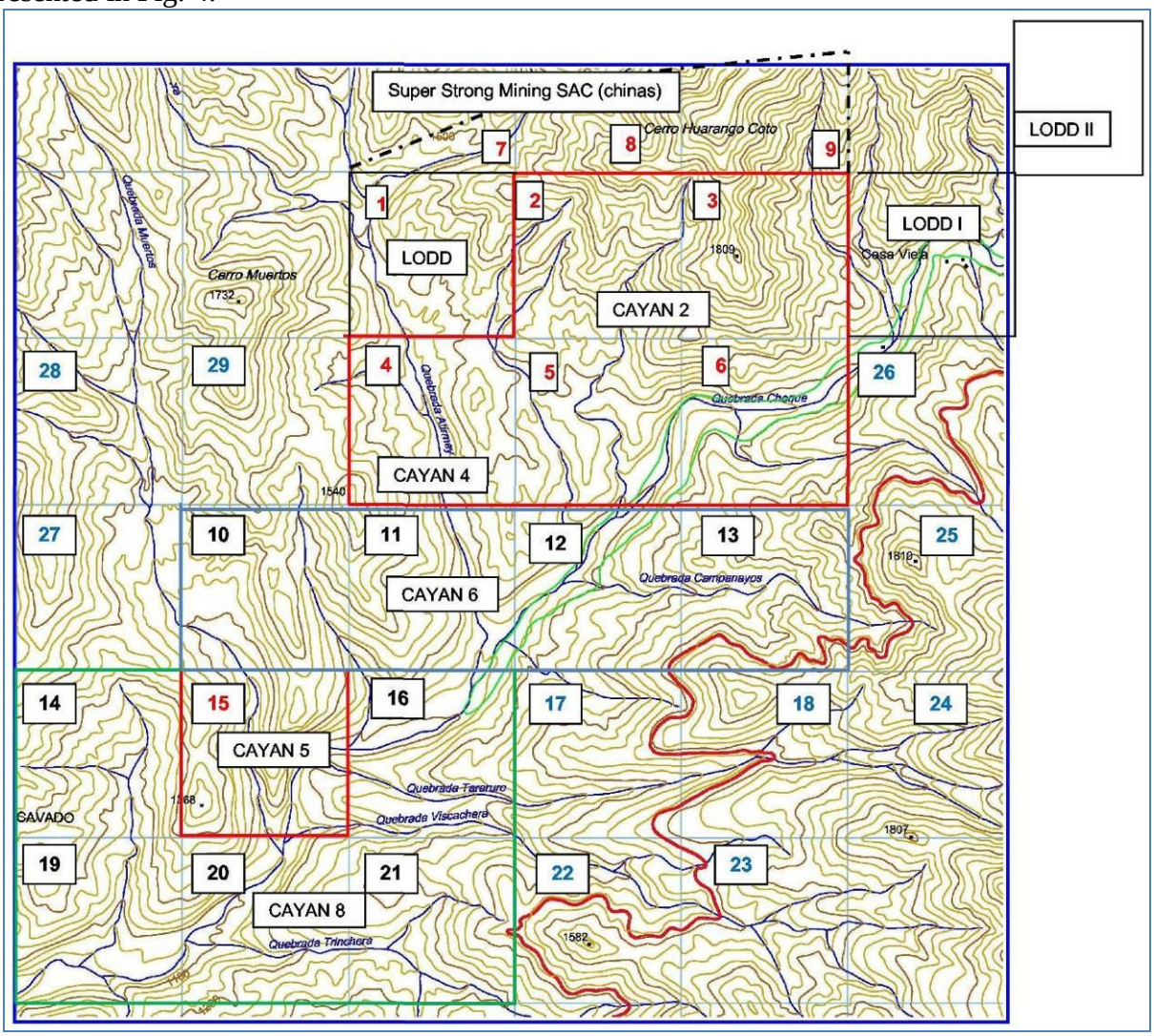

Fig. 4. Concessions covering the Copernic project area (see Fig. 3) and prospecting sites of the first (red numbers), second (black numbers), and third (blue numbers) orders of priority. (Step of grid is 1 km)

2.2. Geological prospecting (the second stage, 2010)

Geological prospecting was implemented by four engineers (A.Yu. Mar'yan, R.M. Novakov, I.M. Puzankov, V.S. Uspensky) with assistance of ten called-in workers. The field provision was carried out by Cumbrex geoservice firm (four persons). The field camp was located close to the site in the Choque River valley (Fig. 5). The fieldwork was started on July 17, 2010.

Fig. 5. Field camp in the Choque River valley.

To haul goods to the field camp from the dirty road going toward the Choque Settlement, donkeys were used. The samples were carried from site to camp by porters. During the second part of field season, a km-long passage was constructed to facilitate transportation.

Taking into account the data obtained in 2009 and disposition of concession areas (Fig. 1), the work in 2010 were conducted in the Cayan 2, Cayan 4, Cayan 5, Cayan 6, Cayan 8, La Obra de Dios, partly in La Obra de Dios I concession areas and in the adjacent tract 1–2 km wide (Fig. 4). No work was conducted in the Cayan 1, Cayan 3, Cayan 7, and La Obra de Dios II areas, because of their insignificant promise and time shortage.

The areas Cayan 2, Cayan 4, and La Obra de Dios I were combined into the Copernic project. The prospecting was also conducted in quadrangles 7–9 (Fig. 4) that adjoin the above territory in the north. The areas Cayan 5, Cayan 6, Cayan 8, the adjacent tract 1–2 km wide together with the Copernic project were conventionally combined into the Copernic project. The total working area amounts to 30 km^2. Geological mapping on a scale of 1 : 25 000 to 1 : 10 000 and 1 : 50 000 at flanks covered 26 km^2. The area of the Copernic Project was covered by geological mapping on a scale of 1 : 10 000–1 : 5000 along with prospecting.

According to the agreement between Quippu Exploraciones S.A.C. and Upstream Mining S.A.C., two thirds of geological prospecting and 100% of geophysical exploration were performed in the area covering the Copernic Project and one third of geological prospecting in the Cayan 5, Cayan 6, Cayan 8 concession areas and the adjacent territory.

The detailed prospecting was carried out in the Western (Oeste) and Eastern (Este) ore zones bearing direct prospecting guides in form of oxidized copper mineralization; in addition, copper sulfides were identified in the Eastern zone.

Five dig hole lines have been sunk (114 holes) (Table 2.2-1) and 20 trenches and strippings 680 m in total length have been driven (Table 2.2-2). Dig holes were spaced at 20 m along the line; distance between the lines was 100–200 m. Bedrock samples were taken from dig holes (Fig. 6) and trenches (331 samples), some outcrops, and along profiles (Fig. 7). In the course of the work in 2010 was taken 1810 samples. The rock chip panel samples consisted of 20–30 chips collected from an area of 1–3 m^2, up to 4 kg in total weight; composite channel samples were 2–5 m long, no less than 30 chips, up to 8 kg in total weight; channel samples were 1–2 m long, no less than 40 chips, up to 6 kg in total weight. Stream (bottom) sediments were taken from dry valleys; the weight of sieved material (2 mm) was 0.5–1.0 kg; 231 samples were taken beyond mineralized zones.

Fig. 6. Dig hole 1208 at the southern flank of a zone of oxidized mineralization, prospecting line 1.

Fig. 7. Channel sampling along prospecting line.

In summary, the following prospecting works were fulfilled in 2009 and 2010:

- 17 dig hole lines (349 holes);
- 30 trenches and strippings 708.5 m in total length;
- 2365 channel, composite channel, and rock chip panel samples, including 566 samples from dig holes and trenches;
- 231 bottom samples were taken from channels of dry valleys.

Table 2.2-1. Scope of mining workings and sampling (dig holes)

Dig holes 2010				
	Dig hole number		quantity	
Line number	from	to	dig hole	sample
1	1900	1922	26	26
	1924	1926		
2	1927	1943	17	17
3	1944	1969	26	26
4	1970	1994	25	25
5	1995	2014	20	23
total			114	117

Table 2.2-2. Scope of mining workings and sampling (trenches)

Trenches 2010							
	Executive			количество проб			
No.		Trench number	Length, m	ChS	PS	Total	In depot
1	I. Puzankov	1923	8	6		6	
2		2015	20	5		5	
3		2016	19	4		4	
4		3700	20	5		5	4
5		3701	28	6		6	3
6		3702	20	4		4	4
7		3703	24,5	6		6	
8		3704	41	10	3	13	
9		3705	24	6		6	4
10		3706	23	5	1	6	6
11		3707	20	4	1	5	3
12		3708	25	5		5	
Total			272,5	66	5	71	24
1	V. Uspensky	246	105			31	19
2		247	10,5			10	0
3		249	50			15	11
4		261	50			15	10
5		460	50			27	17
6		461	30			8	0
7		463	50			7	2
8		891	30			3	2
Total			375,5	0	0	116	61
		Total	648	66	5	187	85

Maps of factual data showing location of geological and prospecting routes, main observation points (OPs), dig hole lines, contours of the areas of detailed prospecting are combined into Appendix 1 (sheets 1–6).

All samples were analyzed at the Inspectorate Services Peru S.A.C. laboratory in June–August 2010:

(1) ICP/AES (32-44 elements), digestion in aqua regia;

(2) AAS (Cu, Pb, Zn, Mo), AA flame multielement dissolution in aqua regia; the samples with base metal contents higher than 1 wt % were analyzed;

(3) FA/AAS (Au, charge is 30 g); no more than 50% of samples were analyzed selectively and all samples from the site of detailed prospecting and all stream samples.

The following sample preparation was implemented:

(1) PREP-01 – drying, sieving, and homogenization of entire sample (up to 8 kg) and subsequent grinding of 150 g for all bedrock types.

(2) PREP-03 – drying, and screening of entire stream (bottom) sample (up to 4 kg). Sieving and drying of bottom samples was conducted at the field camp.

The detection limits for ICP/AES and FA/AA are given in Table 2.2-3.

To determine speciation of copper in ore, the following analyses were preformed in 2009 for the samples containing 1–7 wt % Cu:

(1) 4-ACID/AAS for the determination of bulk Cu content in a sample;

(2) CN/AAS for determination of soluble Cu content in secondary sulfides (chalcocite, bornite);

(3) AAS for determination of oxidized Cu ore (azurite, malachite, atacamite, chrysocolla, etc.).

The same analyses were used for control of Cu determination in samples.

The results of analyses of samples with variable leachability of Cu are given in Table 2.2-4.

The control analyses were performed at the SGS del Peru S.A.C. for 30 samples taken in 2009 and 70 samples taken in 2010. These samples were analyzed for the entire set of typical microelements in order to check quality and reproducibility of the primary analyses implemented at the Inspectorate Services Peru S.A.C.

The analyses for gold were verified with fire assay (FAA313 AAS 30 g) within a range of 5 ppb to 5000 ppb. The determination of base metals was controlled with ICP-MS for 52 elements.

Table 2.2-3. Detection limits of determination of Au, Cu, and other elements at the Inspectorate Services Peru S.A.C.

ICP Multielementos

Cantidad	Elementos	Método	Parámetro	Limite Detección
1	Detalles abajo	ICP AES	ICP Multielemento Digestión en Agua Regia	Detalles abajo

ISP-330	ISP-142									
Au	Ag	Al	As	Ba	Be	Bi	Ca	Cd	Ce	
FA/AA	ICP/AQR									
ppm	ppm	%	ppm				%	ppm		
Au	Ag	Al	As	Ba	Be	Bi	Ca	Cd	Ce	
-0,005	-0,2	-0,01	-5	-5	-1	-5	-0,01	-1	-10	

ISP-142												
Co	Cr	Cu	Fe	Ga	Ge	Hg	In	K	La	Li	Mg	Mn
						ICP/AQR						
ppm			%	ppm				%	ppm		%	ppm
Co	Cr	Cu	Fe	Ga	Ge	Hg	In	K	La	Li	Mg	Mn
-1	-1	-2	-0,01	-5	-10	-1	-10	-0,01	-2	-5	-0	-2

ISP-142										
Mo	Na	Nb	Ni	P	Pb	Re	S	Sb	Sc	Se
						ICP/AQR				
	%	ppm					%	ppm		
Mo	Na	Nb	Ni	P	Pb	Re	S	Sb	Sc	Se
-2	-0,01	-10	-1	-10	-5	-5	-0,01	-5	-1	-5

ISP-142										
Sn	Sr	Te	Ti	Tl	U	V	W	Y	Zn	Zr
			%	ppm						
Sn	Sr	Te	Ti	Tl	U	V	W	Y	Zn	Zr
-10	-1	-5	-0,01	-5	-10	-1	-10	-1	-5	-5

Cantidad	Elemento	Método	Parámetro	Rango
1	Cu Total	AAS	Análisis Cu Total AAS	10 – 10000
1	Cu Soluble	AAS	Análisis CuSol AAS	10 – 10000
1	Cu Oxidado	AAS	Análisis de CuOxd AAS	10 – 10000

Table 2.2-4. Copper speciation in ores

Analisis: Cu:ISP-112 - AA - CuOx
Cu:ISP-137 - H2SO4/AA - CuSsulfurico
Cu:ISP-140 - AA - bulk Cu

	Copper soluble in H2SO4				Oxidized copper			Bulk copper		
	ISP-137	ISP-137	ISP-137	ISP-137	ISP-112	ISP-112	ISP-112	ISP-140	ISP-140	ISP-140
Sample	CuSsulfurico				CuOx			Cu		
Description	H_2SO_4/AA	H_2SO_4/AA	H_2SO_4/AA	H_2SO_4/AA	AA	AA	AA	AA	AA	AA
	ppm	%	%	%	ppm	%	%	ppm	%	%
1524	5703	--	--	--	5296	--	--	6099	--	--
1525	1642	--	--	--	1547	--	--	1963	--	--
1526	1086	--	--	--	982	--	--	1298	--	--
1527	3199	--	--	--	2970	--	--	4298	--	--
1528	1956	--	--	--	1900	--	--	2160	--	--
1551	4921	--	--	--	4916	--	--	5519	--	--
1555	--	1,26	--	--	--	1,19	--	--	1,37	--
1557	--	--	>4.00	7,04	--	>4.00	7,09	--	>4.00	7,82
150-1	--	1,88	--	--	--	1,83	--	--	2,09	--
150-2	1567	--	--	--	1242	--	--	2510	--	--
150-3	8732	--	--	--	7271	--	--	--	1,12	--
148-1	6167	--	--	--	5519	--	--	7074	--	--
148-2	7003	--	--	--	6444	--	--	8469	--	--
148-3	8456	--	--	--	7808	--	--	9504	--	--
	ISP-137	ISP-137			ISP-112	ISP-112		ISP-140	ISP-140	
Sample	CuSsulfurico	CuSsulfurico			CuOx	CuOx		Cu	Cu	
Description	H_2SO_4/AA	H_2SO_4/AA			AA	AA		AA	AA	
	ppm	%			ppm	%		ppm	%	
091	4253	--			4111	--		4968	--	
093	6245	--			5789	--		6775	--	
094	7245	--			6549	--		7681	--	
095	6631	--			6299	--		7342	--	
1209	3278	--			2663	--		4441	--	
1208	--	1,83			--	1,69		--	1,91	
1245	6035	--			5438	--		6231	--	
1264-1	4436	--			4295	--		5610	--	
1333	1837				1559			2705		
1317	4498				4435			5815		
1318	3371				3001			3827		
1331	3066				2728			3391		
1332	2821				2419			3265		
1337-1	3558				3275			4139		
1368	2100				1696			3717		
1371	4427				3968			5272		
Detection limit	**<10**	**--**	**--**	--	**<10**	**--**	**--**	**<10**	**--**	--

2.3. Geophysical exploration

2.3.1. Scope and technique

At the request of Upstream Mining S.A.C., the VDG del Peru S.A.C. carried out a complex of ground geophysical exploration aimed at the development of geophysical basis for geological mapping and the study of the forecasted ore field to a depth of 500 m as the basis for geological exploration and drilling. The work was conducted in April–May 2010.

The results of geophysical exploration are presented in detail in the report by VDG del Peru S.A .C. placed in Supplementary Appendix 3 and in the report by geophysicist-supervisor A.B. Nikitin (Supplementary Appendix 4). The summary of these documents is given below.

The complex of geophysical exploration comprised:

- magnetic survey (32.5 km^2, network 100 × 5 m),
- gamma spectrometry (40.0 km^2, network 100 × 50 m) in static (stop-and-go) regime and kinematic regime with continuous recording, and
- electrical pole-dipole survey with recording of apparent resistance and induced polarization (30.0 km^2, network 200 × 100 m) with corresponding DGPS topographic support.

Ground magnetic exploration consisted in measurement of the natural magnetic field at the surface along profiles. The method is sensitive to the occurrence of ferromagnetic minerals in rocks and makes it possible to detect geological contacts, faults, and anomalous concentrations of ferromagnetic minerals.

Gamma spectrometry determines Th, U, and K concentrations and can be used for geological mapping, in particular, for mapping of potassic alteration, e.g., in porphyry copper systems.

Electrical exploration method of induced polarization consists in measurement of chargeability and electrical resistance of rocks. The dispersed sulfides in porphyry-type mineralization are characterized by elevated polarization and are detected by measurements of chargeability. The measurement of apparent resistance facilitates the detection of argillic alteration zones and zones of elevated permeability favorable from circulation of ore-bearing hydrothermal solutions. Such zones are commonly characterized by a low resistance.

2.3.2. Results

(1) As follows from electrical exploration, an extensive low-resistance zone of elevated conductivity about 200 m thick extends downward from the surface.

(2) A highly contrasting anomaly of chargeability (elevated polarization) was established in the western part of the studied area (Fig. 43 in section 4.2).

(3) The studied area is divided into the western part with relatively quiet, slightly differentiated magnetic field and the eastern part with differentiated, sharply variable field (Fig. 44 in section 4.2).

(4) The U, Th, and K contents are clearly correlated with the fields of intrusive rocks differing in composition.

Conclusions and recommendations:

(1) A hypothesis is supported that the Copernic ore field can be a porphyry copper–molybdenum deposit up to 1700–1900 m in diameter.

(2) In compliance with revealing of sulfides at the surface, a probability is strengthened that shallow-seated disseminated sulfide mineralization is combined with widespread oxidized copper mineralization.

(3) It should be emphasized that the results of electrical exploration in the western and the eastern parts of the area are controversial and allow us to interpret the structure of the studied area and evaluate the prospect in different ways.

(4) To date, no reasonable explanation can be proposed for absence of anomalous conduction and chargeability beneath the Eastern ore zone.

In the opinion of geophysicist-supervisor A.B. Nikitin, the performed geophysical exploration merits a positive rating. The fieldwork has been performed with due quality and timely without a substantial objection. The preparation of final report was delayed for two weeks. The conclusions and recommendations stated in the report presented by the the VDG del Peru S.A.C. are extremely conservative and restrained, though when the report was preparing, they estimated the studied territory in obviously positive terms.

3. GEOLOGY OF EXPLORATION AREA

3.1. Overview

On a metallogenetic map of Peru Copernic project falls at juncture of two metalogenic belts: VII - Cu-Fe-Au minefields of Middle Jurassic - Lower Cretaceous и X - Volcanogenic massive sulfide deposits Pb-Zn-Cu of Upper Cretaceous (Fig. 8).

According to the available data, the ore district is mainly composed of several granitoid complexes and units combined into the Cretaceous Coastal Batholith. On the sheet 21h (Fig. 9) to determine the absolute ages are not available. Our age of intrusive rocks is taken as the Cretaceous. Several intrusive units, which are recognized in the geological map on a scale 1 : 100 000 published by IGEMMET (Fig. 9), are composed of Cretaceous gabbro, gabbrodiorite, diorite, and various granitoid rocks. Configuration, morphology of intrusive bodies, and their mutual relationships are not simple. The oldest Patap and Paccho complexes consist of gabbro–gabbrodiorite and diorite, respectively, which occur as roof pendants in younger granitoid plutons pertaining to the Santa Rosa Complex comprising the Cortaillo granodiorite and granite; the Puscao monzogranite, adamellite, and granite; and the San Jeronimo syenogranite. The Coastal Batholith is cut through by dikes of granitic aplites and pegmatoid leucogranitic dikes.

Table 3.1-1. Correlation of rock complexes recognized in the studied area in 2010 with mappable units and complexes shown in the State Geological Map compiled by INGEMMET

Complexes recognized in the studied area in 2010 (from younger to older)	**Complexes shown in the State Geological Map compiled by INGEMMET**	**Comment**
Trinchera Complex: andesite dikes	Microdiorite dikes	Andesite dikes are widespread in the studied area but not shown in the State Geological Map. Microdiorite dikes are known in the adjacent territory
Copernic Complex: plagiogranite, granite; granite porphyry, rhyolite, dacite, pegmatite (dikes)	San Jeronimo Unit: syenogranite; Puscao Unit: granite, monzogranite, adamellite	Syenogranite and monzogranite were not identified as a result of the performed work
Atirmey Complex: amphibole–biotite tonalite, metagranodiorite, leucogranite, aplite dikes	Tonalita Corralillo Unit: granite and granodiorite	Confirmed by the performed study
Choque Complex: gabbro, gabbrodolerite, gabbronorite, diorite	Patap Complex: gabbro and gabbrodiorite; Paccho Complex: diorite	Confirmed by the performed study
Pararin Formation	Pararin Formation	Confirmed by the performed study

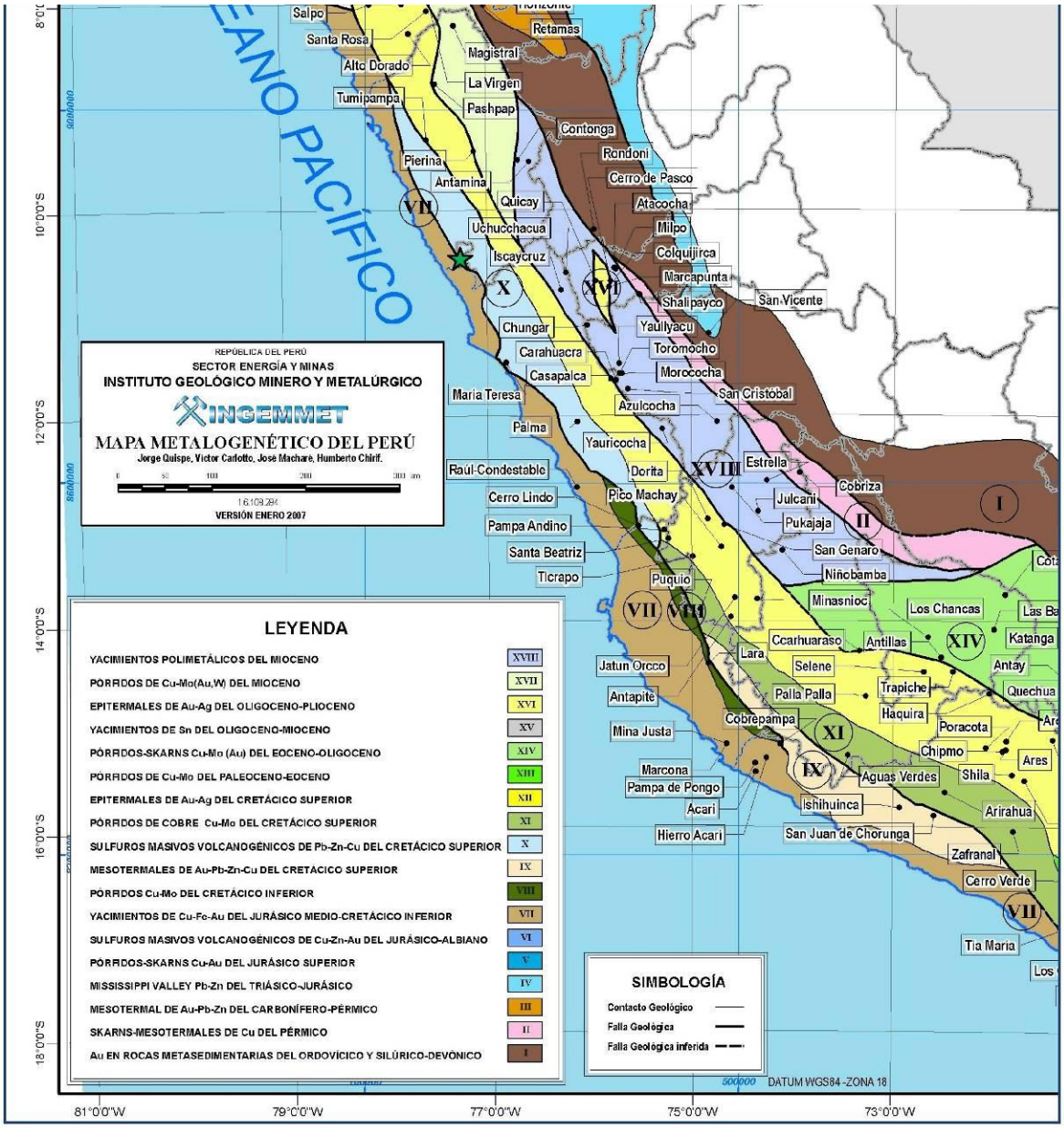

Fig. 8. Regional metallogenetic map. Copernic project is marked by star.

When mapping the area of the ore district on a detailed scale, we had to introduce our own taxons, which partly coincide with intrusive complexes and units shown in the published geological map. Their correlation with the previously established intrusive sequence is presented in Table 3.1-1. We also mapped numerous faults, which are not shown in the regional geological map. The faults make up a polygonal system with predominance of the fractures oriented in the northeastern, nearly meridional, and northwestern directions. The blocks bounded by these faults underwent vertical displacements, so that the intrusive rocks differing in age are exposed now on the same hypsometric level. It was previously noted that the intrusive rocks are affected by hydrothermal metasomatic alteration in form of chloritization, propylitization, silicification, and argillic alteration. In general, our data obtained in 2010 confirm this statement.

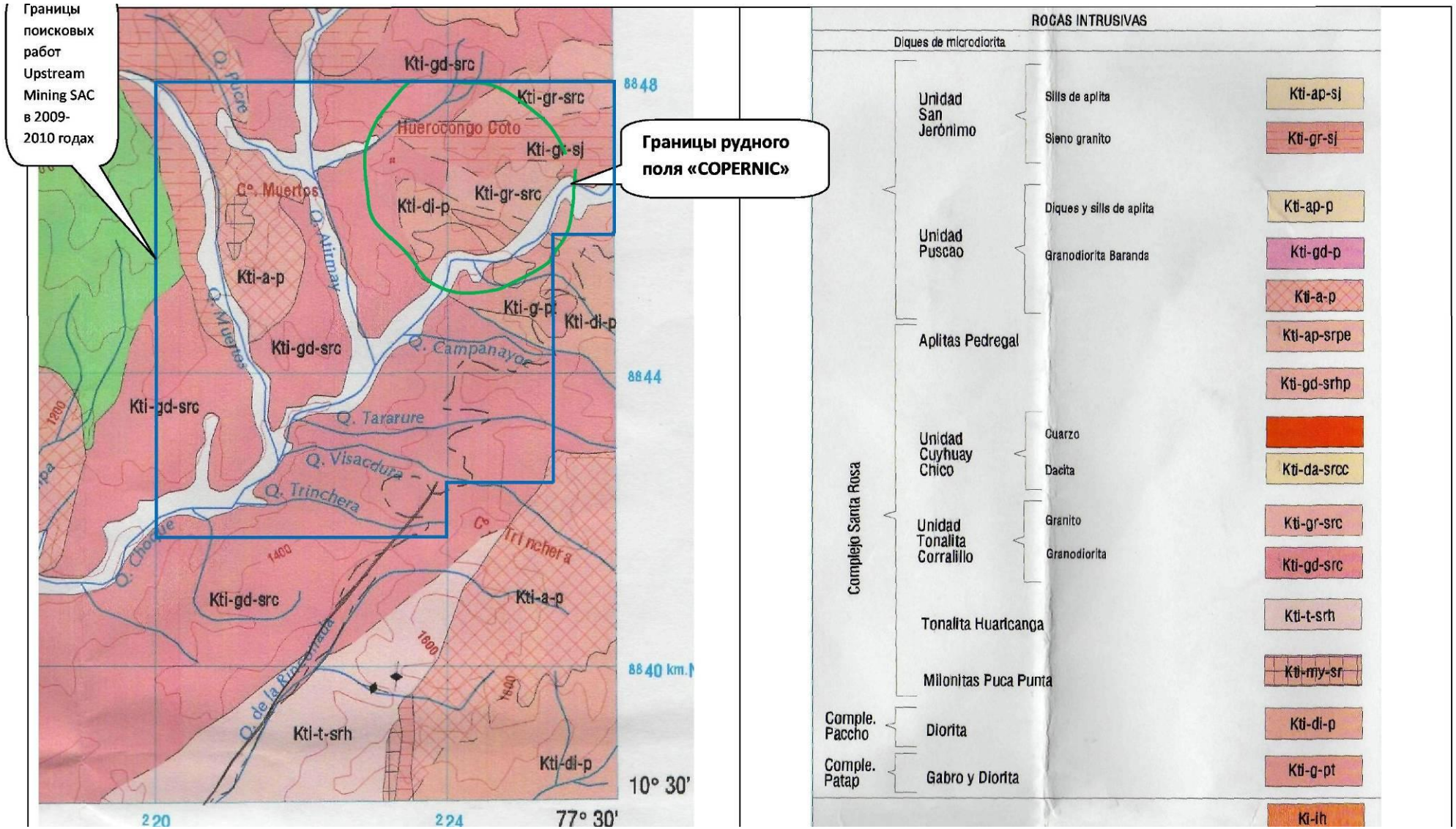

Fig. 9. A fragment of map sheet 21h of the State Geological Map and its legend.

3.2. Stratigraphy

The stratified rocks are of subordinate abundance in the studied area and are limited by the Lower Cretaceous Pararin Formation and loose Quaternary sediments.

The Pararin Formation consists of andesitic lavas, agglomerates and related sills and dikes of the same composition. The altered sandstone and tuff are noted as well. The intrusive contact of the Atirmey and Copernic intrusive complexes (see below) with rocks of the Pararin Formation was documented on the right bank of the Muertos Valley. The host rocks are transformed into hornfels at the contact. In general, volcanic rocks are intensely propylitized. Quartz and quartz–epidote veinlets as thick as 1–3 cm are abundant; chlorite and epidote replace the rock as a whole. Altered volcanic rocks occasionally contain sulfide mineralization, including chalcopyrite and products of its oxidation.

Fig. 10. Alluvial and proluvial sediments at the terrace of an intermittent stream.

The Quaternary colluvial and hillside sediments on slopes, proluvial and alluvial sediments in valleys and on their terraces (Fig. 10), as well as mudflows in their channels occur throughout the district. They are commonly omitted in geological map, where only covers 5–10 m thick are shown on gentle slopes. The loose sediments are not sorted and composed of blocks

and rubble with sand and grus. The large fragments vary in size from tens of centimeters to a few meters. The valleys are commonly filled with sand, silt, and coarse clastic material. Silt and sand on terraces are commonly clearly bedded. The thickness of loose sediments varies from a few to 10–20 m.

The mudflows are known in the Tararure Valley, where they form high terraces with steep scarps up to 30–40 m high at its walls and are composed of unsorted, slightly rounded and angular large fragments combined with rubble, sand, and silt. These sediments are cut down by a stream to its base; the apparent thickness is about 50 m.

3.3. Intrusive rocks

The studied territory is composed largely of intrusive rocks. Four Cretaceous intrusive complexes are recognized here (from older to younger):

(1) The Choque Complex: gabbro, gabbrodolerite, gabbronorite, and diorite.

(2) The Atirmey Complex: biotite–amphibole tonalite, metagranodiorite, leucogranite, and aplite dikes.

(3) The Copernic Complex: granite and granite porphyry; plagiogranite, granite, granite porphyry; granite, granite porphyry, fine-grained granite, aplite, rhyolite, dacite, and pegmatite dikes.

(4) The Trinchera Complex: andesite dikes.

All these taxons are described below; the summary of petrographic descriptions is given in Appendix 10.

The Choque Complex is composed of gabbro, gabbrodolerite, gabbronorite, and diorite, which are exposed in the northeastern part of ore district. These intrusive rocks are the oldest and cut through by granitoids of the Atirmey and Copernic complexes.

Gabbro and gabbrodolerite are dark gray to black fine-grained rocks consisting of calcic plagioclase, olivine, clino- and orthopyroxene, and ore mineral. Plagioclase phenocrysts are incorporated into the groundmass with doleritic microstructure (Fig. 11).

Fig. 11. Photomicrograph of porphyritic gabbrodolerite with plagioclase phenocrysts and doleritic groundmass. Crossed polars.

Biotite–hornblende gabbro (thin sections 723-1, 664-2, 589-1, 692, 3524-8A, 550, 3524-8) is a dark gray massive, medium- to fine-grained rock. Its modal composition (vol. %): calcic plagioclase (50–70), hornblende (25–45), biotite (up to 10), clinopyroxene (up to 5), ore mineral (up to 5); orthopyroxene (thin sections 3524-8A, 692) and quartz (thin sections 723-1, 554-2, 589-1) are noted. Structure is hypidiomorphic-granular, ophitic, poikiloophitic, and cryptic (Fig. 12). Secondary alteration is expressed in propylitization.

Leucogabbro is distinguished by enrichment in plagioclase up to 70 vol % and panidiomorphic-granular aggregates of this mineral.

Fig. 12. Photomicrograph of hypidiomorphic-granular hornblende gabbro. Crossed polars.

Biotite–hornblende gabbronorite (thin sections 485-1, 494-1, 559, 560, 495-1, 556, 561-25) is a dark gray and greenish massive, medium- to fine-grained rock. Its modal composition (vol. %): calcic plagioclase (up to 50–55), orthopyroxene (15–25), hornblende (up to 25), clinopyroxene (up to 10), biotite (up to 5), ore mineral (up to 3); olivine (thin sections 569, 560) and quartz are noted. Structure is ophitic, poikiloophitic, and cryptic; some varieties are porphyritic; sideronite structure is rare. Secondary alteration is expressed in propylitization.

Diorite and quartz diorite (2741-2, 787-1, 313-1, 554-3, 577) are gray massive, medium- to fine-grained rocks. Their modal composition (vol. %): calcic and intermediate plagioclase (55–75), hornblende (up to 25–30), biotite (up to 5–10), quartz (up to 5 and 10 in quartz diorite). Albite, K-feldspar, and ore mineral are noted in insignificant amounts. Structure is hypidiomorphic-granular (Fig. 13). Large, newly formed biotite crystals and rocks with acicular hornblende appear at the contact with granitoids. Secondary alteration is expressed in propylitization and chloritization.

Hornblende andesite (thin sections 352, 1875) has seriate porphyritic structure. Phenocrysts occupy no less than 35% of the rock volume. Andesine crystals up to 7 mm in size are predominant among phenocrysts in association with hornblende rimmed by opacite and magnetite; a small quartz phenocryst is noted in thin section 1875. The microgranular quartz–feldspar aggregate with magnetite dust is a product of devitrification of glass. The groundmass is often replaced with sericite–illite–smectite aggregate.

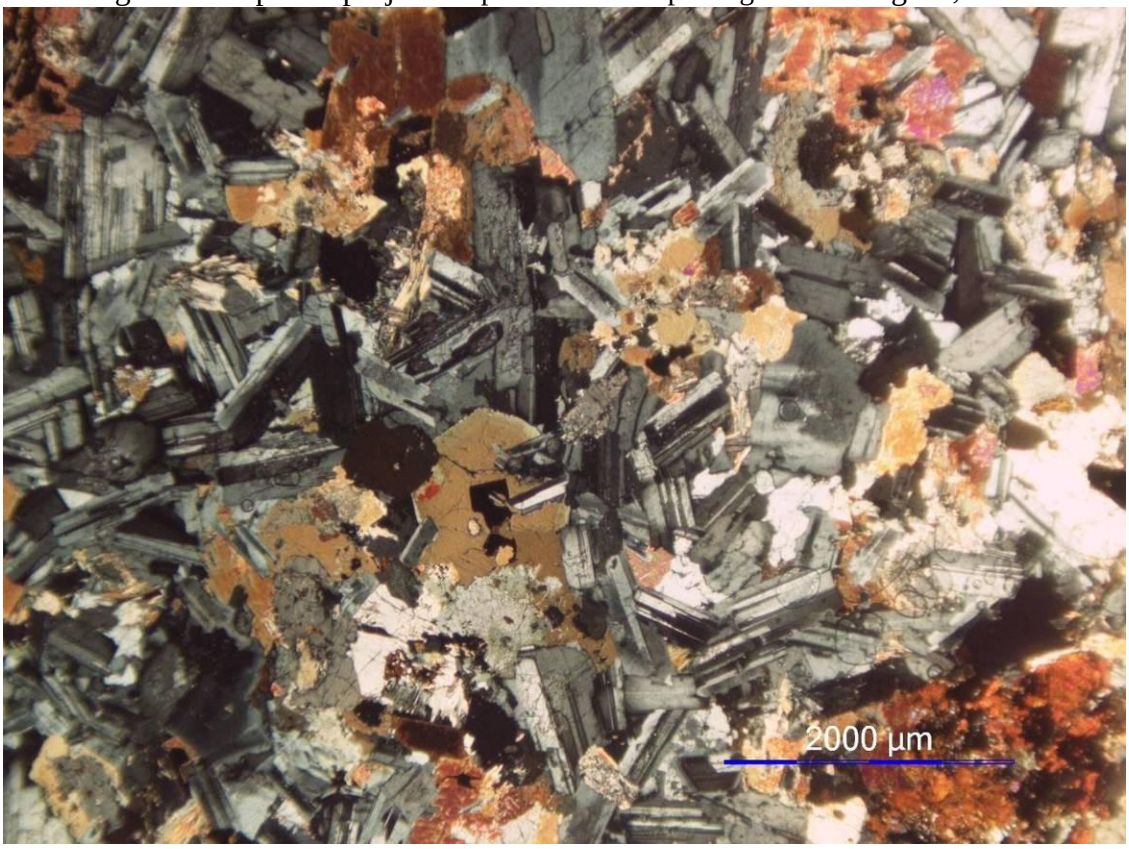

Fig. 13. Photomicrograph of hypidiomorphic-granular diorite. Crossed polars.

At the drainage divide to the east of the Choque River, blocks of black hornblendite were observed in Quaternary loose sediments.

Sporadic inclusions of leucocratic diorite up to 20 cm across are incorporated into gabbro (Fig. 14). The aggregates of large amphibole crystals characteristic of these inclusions contain sulfides. Dark-gray dolerite with sulfide disseminations is noted as well.

The Choque Complex is correlated with gabbro and gabbrodiorite of the Patap Complex and diorite of the Paccho Complex.

Fig. 14. An inclusion of leucocratic diorite in gabbro.

The Atirmey Complex: amphibole–biotite tonalite, metagranodiorite, leucogranite, and aplite dikes. These rocks occupy most studied area along both walls of the Choque River valley and in basins of its left and right tributaries: the Muertos, Capcabao, Atirmey, Copa Vilca, Piedra Pintada, Trinchera, Viscachera, Tararure, Campanayos rivers and the lower reaches of the Tacpa River. Light gray tonalite with numerous xenoliths of diorite, porphyritic diorite, and rocks of the Pararin Formation (Figs. 15, 16) occupies large areas. Commonly rounded xenoliths are 10–20 cm in size. Leucogranite occurs in the Cerra Muertos district and in the southwestern part of the studied territory. Widespread aplite dikes a few centimeters to one meter thick cut through older granitoids.

Intrusive rocks of the Atirmey Complex cut through gabbro and diorite of the Choque Complex and volcanic and sedimentary rocks of the Paparin Formation. Contacts of large intrusive bodies are commonly accompanied by rather thick (tens to 200–200 m) zones of intrusive breccia consisting of fragments of country rocks cemented by granitoids (Fig. 17). Rounded and angular fragments are tens to a few meters in size. The stratified rocks of the Pararin Formation are transformed into hornfels. Intrusive contacts are often tectonized.

Fig. 15. Xenoliths of country rocks in tonalite of the Atirmey Complex.

Fig. 16. Xenoliths of country rocks in tonalite of the Atirmey Complex.

Fig. 17. Intrusive breccia: fragments of diorite pertaining to the Choque Complex and rocks of the Pararin Formation cemented by tonalite of the Atirmey Complex

Tonalite (thin sections 2246-7, 857-3a, 301-2, 471-D, 471-A, 246-17, 890, 868-1, 468-1, 857-2, 837-1, 246-17, 571-1, 553, 672-1, 643-1, 246-48, 297-2, 246-49, 246-7, 299-1, 246-17, 247-5, 246-5, 579-1, 298-2, 2889-1, 2883-1, 552-1, 610-1, 892, 893, 579-2, 246-21, 247-7, 247-5, 246-2, 246-23-1, 216-16, 247-5) are light gray, gray, and occasionally light brown massive, medium- to coarse grained rocks with prominent biotite and amphibole crystals up to 3–10 mm in size. Their modal composition (vol %): andesine (55–70), quartz (15–25), amphibole (5–20), biotite (5–15), K- and Na-feldspar (up to 5%). Accessory minerals are apatite, titanite, zircon, and an ore mineral. The hypidiomorphic-granular structure is combined with the micropoikilitic structure with plagioclase laths incorporated into quartz (Figs. 18–20). Secondary alteration is expressed in silicification, biotitization, propylitization, beresitization, and argillic alteration.

Fig.18. Photomicrograph of coarse- to medium-grained tonalite.

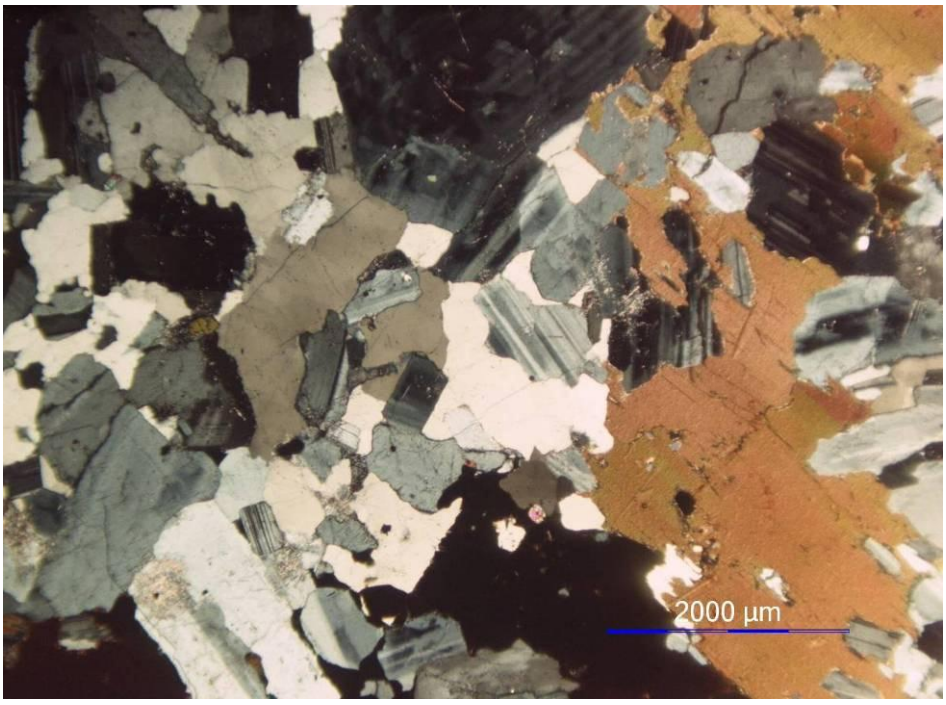

Fig.19. Photomicrograph of coarse- to medium-grained tonalite.

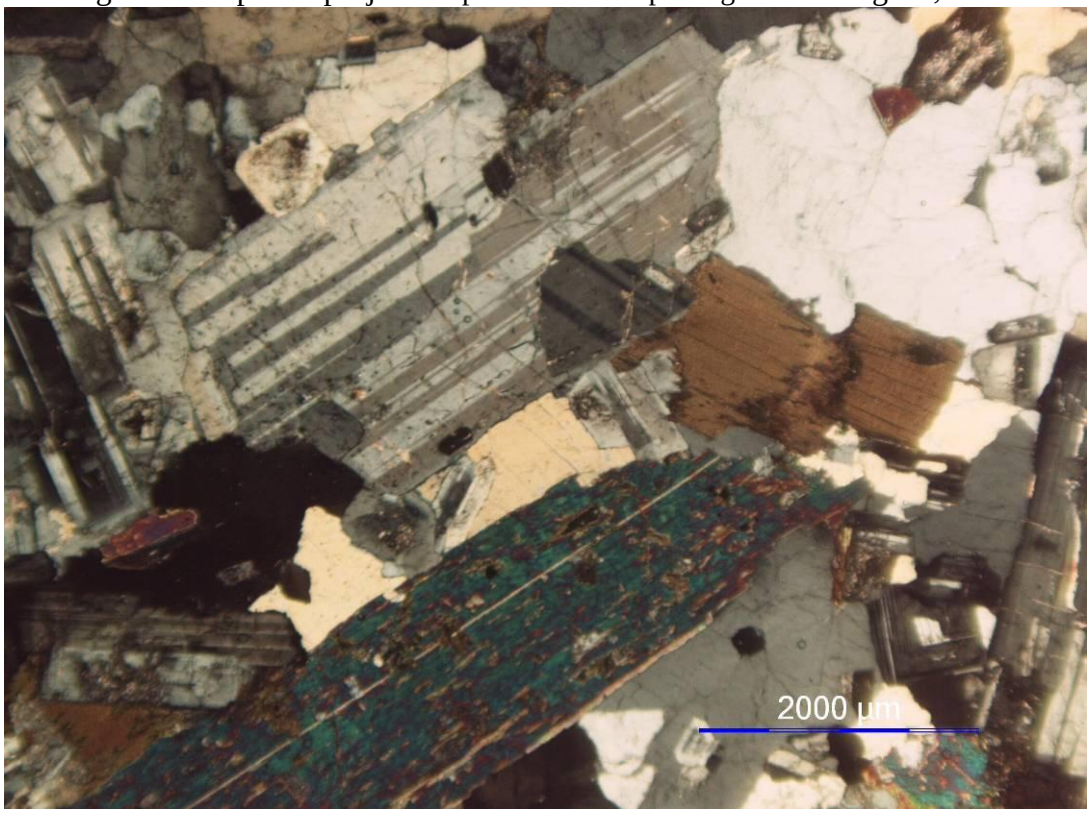

Fig.20. Photomicrograph of coarse- to medium-grained tonalite.

Metagranodiorite (thin sections 302-5, 1833-8, 691-2, 890-1, 1846, 461-4, 461-7, 551) is an intensely fractured rock that differs from tonalite by a higher K-feldspar content. This is medium- to coarse-grained rock consisting (vol. %) of oligoclase–andesine (45-60), quartz (15–24), green hornblende (5–15), biotite (5–15), and K- and Na-feldspars (up to 20%). Accessory minerals are apatite, titanite, zircon, and an ore mineral. The hypidiomorphic-granular structure is combined with micropoikilitic and pegmatoid structures (thin sections 551, 691-2, 1846). Hornblende is often replaced with finely flaky biotite, which also crystallized along fractures; the primary biotite is recrystallized. The intensely of secondary alteration is widely variable. In addition, silicification, biotitization, propylitization, beresitization, and argillic alteration are noted.

Leucogranites (thin sections 2585-1, 2745-1, 2923-2, 2829-2) are light gray massive coarse- medium-, and fine-grained rocks with sporadic dark-colored minerals. These rocks are composed (vol %) of sodic plagioclase (25–35), quartz (30–35), biotite and hornblende (up to 3–5), and microcline-perthite (25–40%). Apatite, titanite, and ore minerals are accessories. Epidote, chlorite, albite, and sericite are secondary minerals. Structure of the rocks is granitic and locally pegmatoid. Intensity of secondary alteration is low.

Aplite is a light gray, almost white fine- to medium-grained equigranular leucocratic quartz–feldspar rock.

The granitoids pertaining to the Atirmey Complex host stockwork mineralization. Oxidized copper mineralization is hosted in propylitized metagranodiorite.

The Atirmey Complex is compared with the Tonalita Coralillo Unit shown in the previously published map.

The Copernic Complex comprises plagiogranite, granite, and granite porphyry intrusive bodies irregular in shape more than 1 km^2 in area and dikes of the same composition, as well as aplite, pegmatite, and dacite dikes. These rocks occur largely in the northeastern part of the study territory—in the upper reaches of the Tacpa River, a left tributary of the Atirmey River, at the slopes and drainage divide of the Cerrro Huarango Goto, attaining a height of 1610 masl.

Granitic intrusions cut through granitoids of the Atirmey Complex, gabbro and diorite of the Choque Complex, and volcanic and sedimentary rocks of the Pararin Formation. The contact of large granitic bodies are accompanied by wide (up to 200–300 m) zones of intrusive breccia (Fig. 21) with numerous xenoliths of country rocks incorporated into granitic cement (Figs. 22–24). Angular or irregular in shape fragments (Fig. 22) vary from tens of centimeters to a few meters in size. When xenoliths and cement are close in composition, it is difficult to identify them with confidence (Figs. 23, 24). Dikes are commonly 2–3 m thick and are commonly not accompanied by wall-rock alteration. They are often complexly bent and variable in thickness. Pegmatite veins are 0.2–0.3 m thick.

Fig. 21. Intrusive breccia, the Copernic Complex.

Biotite plagiogranites are light gray or almost white fine-, medium-, and coarse-grained rocks with variable amounts of small biotite flakes. Rocks often become brown due to the development of iron hydroxides. The model composition (vol %): albite–oligoclase and rarely oligoclase–andesine (45–60), quartz (25–30), green hornblende (up to 15), biotite (5–15), potassium (up to 10) and sodic (up to 15) feldspars. Biotite occurs in all varieties, whereas hornblende does not. When both minerals coexist, biotite prevails over hornblende. Apatite, zircon, and opaque minerals are present in accessory amounts. The microstructure is hypidiomorphic-granular. Biotitization, propylitization, and beresitization are characteristic types of hydrothermal alteration.

Biotite (thin sections 2512-1, 2523-2, 2013, 474-1) and biotite–hornblende (thin sections 2568-1, 2680-2) plagiogranite porphyries are light gray massive rocks consisting of the relatively fine-grained groundmass and rounded quartz and plagioclase phenocrysts (thin sections 2523-2, 2013, 2680-2) readily visible to the naked eye; biotite phenocrysts are noted as well (thin section 2013). The groundmass is allotrimorphic-granular, granitic, or granophyric (for example, in thin section 2568-1) and consists (vol %) of plagioclase (50–65), quartz (25–35), biotite (5–10), potassium (up to 10) and sodium (up to 5) feldspars, and ore mineral (up to 2). Green hornblende

occurs locally (up to 10%). Epigenetic biotitization, propylitization, and beresitization are characteristic.

Fig. 22. Shadow granodiorite xenoliths in andesitic dacite of the Copernic Complex.

Fig. 23. Granodiorite xenoliths in andesitic dacite of the Copernic Complex.

Fig. 24. A granodiorite xenolith in granite porphyry of the Copernic Complex.

Aplite (thin section 572-1) is a leucocratic fine-grained rock consisting (vol %) of quartz (40), K-feldspar (30), sodic plagioclase (25), and micas (5), including of biotite, muscovite, brownish and colorless hydromica; accessory apatite is noted. The structure of rock is aplitic.

Rhyolite and dacite are light-colored, partly argillized porphyry rocks with small (up to 2–3 mm) phenocrysts of feldspars, biotite, and quartz; the latter are rounded in outlines.

Rhyolite (thin sections 569, 570) is a yellowish light gray rock with seriate structure. Phenocrysts 4–5 mm in size occupy 30–40% of rock volume and consist of plagioclase, quartz, biotite, and magnetite. Plagioclase phenocrysts are commonly oscillatory zoned; quartz phenocrysts are commonly rounded and embayed. Some biotite phenocrysts are completely replaced with hydrobiotite, epidote, and chlorite. Epidote–chlorite pseudomorphs after hornblende phenocrysts are suggested. The felsitic quartz–feldspar groundmass is a product of devitrification of glass. The quartz content in groundmass is as high as 25 vol %. All dark-colored microlites except for magnetite are replaced with epidote and/or brown hydromica. Epigenetic propylitization and beresitization are characteristic.

Dacite (thin sections 306-3, 471D-a, 463-2-1)—a yellowish light gray and occasionally banded rock—is distinguished from rhyolite by a lesser number of quartz phenocrysts and a lesser amount of quartz in groundmass. The structure of rock is porphyritic or seriate. Phenocrysts 3–6 mm in size occupy 20–40% of rock volume and consist of oscillatory zoned andesine with saussuritized cores, quartz, biotite, and magnetite. Quartz phenocrysts are commonly rounded and embayed; they are smaller (0.5–1.5 mm) in comparison with other phenocrysts. Plagioclase phenocrysts are albitized, sericitized, and saussuritized. Some biotite phenocrysts are completely replaced with hydrobiotite, epidote, and chlorite (thin section 471D). Small columnar phenocrysts of green hornblende are noted in thin section 306-3. The felsitic quartz–feldspar groundmass is a product of devitrification of glass. This is a microcrystallime quartz–feldspar aggregate with ore dust and flakes of hydrobiotite. The quartz percentage in moderately altered groundmass is estimated at 10–15 vol %. The groundmass can be partly

silicified (thin section 306), albitized, and replaced with chlorite, epidote, and hydromica. Silicification, propylitic, and argillic alterations are characteristic of dacite.

Pegmatites were observed in the basin of the Muertos River, along the right bank of the Atirmey River to the north of Cerro Muertos (Fig. 25). Pegmatites are composed of coarse-crystalline quartz and feldspar, biotite, and in some cases, of columnar actinolite and sheetlike chlorite. K-feldspar and K-feldspar-perthite are the most abundant; sodic plagioclase occurs as well. The structure of rocks is micropegmatitic and granophyric (locally). Myrmekite quartz segregations are detected in perthite ingrowths. Biotite forms the flakes up to 2 mm in size and is replaced with chlorite (mainly clinochlore) and epidote. Feldspars are pelitized (up to 25%).

Fig. 25. Pegmatoid vein in granite porphyry of the Copernic Complex (observation point 139).

The vein is more than 70 m long and 20 m thick.

The intrusive rocks pertaining to the Copernic Complex underwent argillic and propylitic alterations and silicification. Thin (~1 mm) sulfide and sericite veinlets are observed. Microscopic examination showed partial chloritization of biotite, slight sericitization of plagioclase, and limonitization along small fractures.

Sporadic sulfide pockets with chalcopyrite and molybdenite, a few millimeters across, are noted in rocks of the Copernic Complex (Fig. 26).

Fig. 26. Sulfide mineralization in granite porphyry of the Copernic Complex.

In the published geological map, the rocks of the Copernic Complex fall into the field of the San Jeronimo Unit composed of syenogranite, but the latter rock is actually absent here.

The Trinchera Complex consists of andesitic dikes mainly extending in the northwestern direction. The dikes are widespread throughout the studied territory, mostly at the Atirmey–Choque interfluve close to the Western stockwork. Dikes are commonly about 1 m thick; thinner (<0.5 m) and thicker (up to 3–5 m) dikes are less abundant. The dikes extend as far as 900 m and are clearly interpreted in aerial photographs. They are poorly expressed in topography as small mounds against the background of less hard country granitoid rocks (Figs. 27, 28)

Fig. 27. Andesite dike cutting through granite of the Copernic Complex.

Fig. 28. Andesite dike near the stockwork Oeste.

Andesite is a gray to black massive hard rock commonly with clearly visible phenocrysts; aphyric andesite is less abundant. Phenocrysts are composed of zonal plagioclase (up to 5 mm in size) and less frequent hornblende; biotite phenocrysts occur sporadically. The fine-grained groundmass (thin section 552) consists of plagioclase and subordinate quartz; pilotaxitic groundmass is distinguished by oriented plagioclase laths.

A thin (few centimeters) chilled zone is traced along the contact (Fig. 29).

Epigenetic alteration of andesitic dikes is poorly developed. Sporadic propylitized dikes are replaced with chlorite and epidote. The wall-rock propylitization often develops along dike contacts. Malachite and azurite are identified along the fractures of the andesite dikes that cross the zones of copper mineralization.

Fig. 29. Contact of andesite dike with country rock.

Petrochemical characterization of intrusive rocks is based on major oxide contents in 24 bulk analyses. The samples were taken from the least altered rocks. Nevertheless, the microscopic petrographic examination has shown that six analyses should be omitted. Samples 551, 889, 890-1, and 470-1 are propylitized or contain newly formed biotite. The K_2O content in sample 2829-2 is probably overestimated in comparison with K-feldspar content established under a microscope. The low SiO_2 content in sample 298-2 of amphibole–biotite granite is inconsistent with the high quartz content (up to 30 vol %) in the corresponding thin section. Eventually, the representative selection of chemical analyses characterizing intrusive rocks has been reduced to 18 samples, which served as the basis of the conclusions drawn below (Table 3.3-1).

Table 3.3-1. Correlation of chemical and petrographic nomenclature of igneous rocks

Sample and thin section	Chemical nomenclatur	Petrographic nomenclature	Major rock-forming minerals
Choque Complex: 554-3, 561	Diorite	Hornblende diorite	Plagioclase, amphibole, orthopyroxene, ore mineral
Choque Complex: 550	Gabbro	Biotite–hornblende gabbro	Plagioclase, amphibole
Choque Complex: 495-1	Gabbronorite	Biotite–hornblende gabbronorite	Plagioclase, olivine, amphibole
Complex Atirmey 552-1, 577, 579-1, 890, 2883-1, 2889-1	Tonalite	Biotite–hornblende tonalite	Plagioclase, quartz, amphibole, biotite
Complex Atirmey 579-2, 892, 893	Granodiorite	Fractured amphibole–biotite granodiorite	Plagioclase, quartz, amphibole biotite
Complex Copernic 474-1, 479-1	Granite, plagiogranite	Biotite granite, plagiogranite	Plagioclase, quartz, biotite
Complex Copernic 1849-1	Plagiogranite	Biotite granite porphyry	Plagioclase, quartz, biotite
Complex Copernic 2652-2, 2680-2	Granite porphyry	Biotite granite porphyry	Plagioclase, quartz, biotite, amphibole

All rocks belong to the normal petrochemical series of moderately potassic rocks that make up a natural evolutionary trend from gabbro to granite (Fig. 30). In the SiO_2 vs. FeO* classification diagram (Fig. 31), the data points of almost all granitoids fall in the field of calc-alkaline series; gabbro, gabbronorite, and diorite of the Choque complex belong to the tholeiitic series. The diagrams confirm the correctness of the allocation of intrusive complexes, since the figurative points of each of them occupied a separate position.

The petrographic and petrochemical data show that in the course of evolution of magma source, the melts become saturated in silica but increase in potassium content was moderate, likely due relatively shallow magma generation in the frontal zone of the Andean volcanic–plutonic belt. As a result, a intrusions formed rock series of diorite-granodiorite plagiogranite, and in granitoids mainly crystallized of plagioclase and to a lesser extent potassium feldspar.

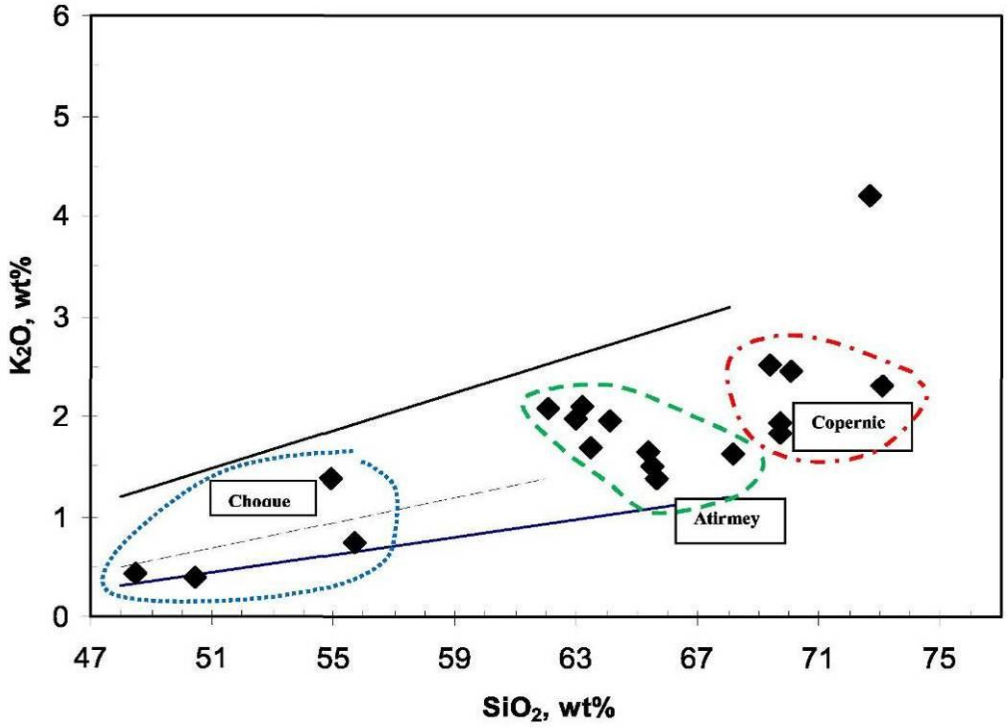

Fig. 30. Compositions of igneous rocks plotted on the K_2O vs. SiO_2 classification diagram.

The lines bound the field of moderately potassic rocks.

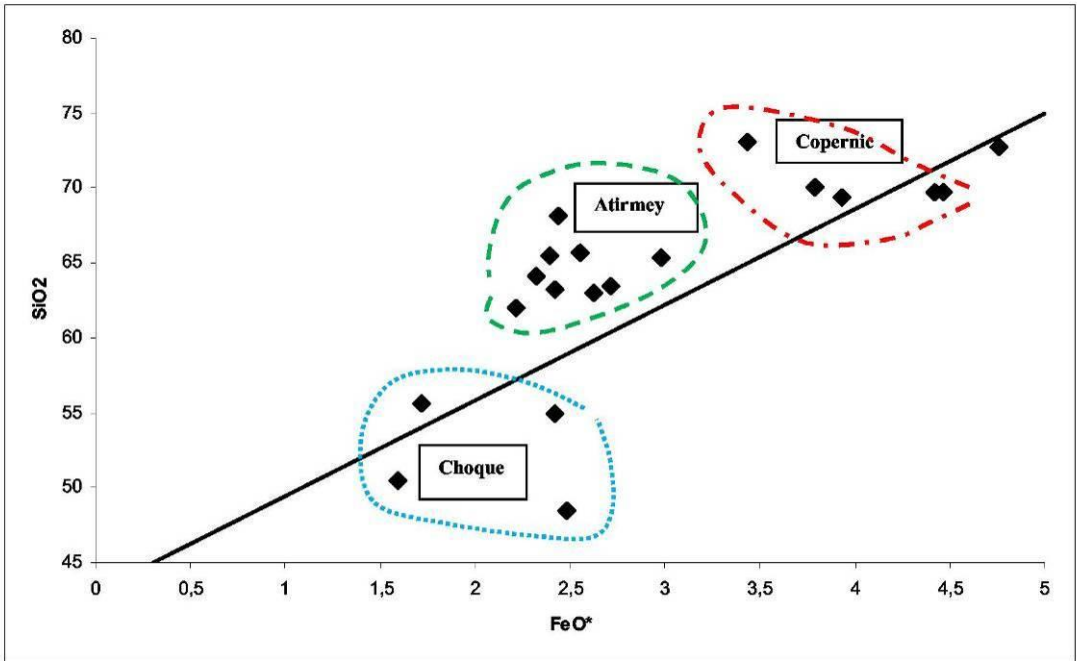

Fig. 31. Miyashiro diagram. Compositions of igneous rocks plotted on the SiO_2 vs. FeO* classification diagram.

The line bounds the fields of calc-alkaline and tholeiitic series.

3.4. Metasomatically and hydrothermally altered rocks

3.4.1. Types

Propylitic alteration is widespread throughout the Copernic ore field. In the Western, Central, and Eastern ore zones, propylites are ore-bearing metasomatic rocks. Propylitic alteration also develops in the adjacent areas and along the left tributary of the Atirmey Valley in the north of the studied territory.

Propylitic alteration mainly affects metagranodiorite (biotitized granodiorite) of the Atirmey Complex. In stockworks, the host rocks are dissected by numerous quartz and quartz–epidote–chlorite veins and veinlets often with hematite and limonite and undergo pervasive silicification. Biotite and hornblende are replaced with chlorite and epidote partly or completely. Pyrite disseminations develop along fractures and, to a lesser extent, in rocks as a whole. The metasomatic zoning: granodiorite – propylitized granodiorite – chlorite–epidote propylite corresponds to the transition of hypidiomorphic-granular to shadow structure. Oxidized copper mineralization as crusts, sinters, and spots along fractures and microfractures is hosted in propylites of the Eastern and Western zones. The intensity of oxidized copper mineralization in the Central zone is much lower. In addtition, sporadic chalcopyrite and molybdenite disseminations were identified in silicified and propylitized rocks of the Eastern zone.

Quartz–kaolinite metasomatic rocks occur as small fields to the south and the west of the Eastern Zone. The quartz–kaolinite aggregate with a small amount of sericite replaces amphibole–biotite granodiorite of the Atirmey Complex. The primary structure of plutonic rocks has been oblitered. Metasomatic rocks are rich in limonite and hematite and because of this acquire yellowish brown color with red spots. These rocks are locally cut by thin (1–2 mm) quartz veinlets and contain fine-grained pyrite disseminations. Small linear zones as thick as 1 m and up to a few meters long were observed in some routes.

Fig. 32. Quartz–sericite–limonite veinlets in shattered metagranodiorite.

Quartz–sericite metasomatic rocks occur locally in selvages of quartz veins and veinlets (Fig. 32). Such wall-rock alteration develops in the Eastern and Western zones. In the Eastern zone sericitization and silicification were observed in trenches 246, 249, 460, 461 and in a number of routes. In the Eastern zone, such alteration is the most intense north of the stockwork at the eastern slope of drainage divide of the spot height of 1809 m. In addition, similar alteration was documented in the site of detailed prospecting near dig hole lines 1 and 5 and to the north and the east of the Eastern zone.

Monomineralic quartz aggregates metasomatically replace host plutonic rocks in selvages of quartz veins in zones of silicification. Such selvages consist of quartz for 70–100%; relics of silicified wall rocks are retained locally.

Biotite metasomatic alteration. The newly formed biotite is observed in limonitized granodiorites around stockworks; these rocks are called metagranodiorite in this report. They are intensely fractured and limonitized along fractures. Locally, limonite pervades a rock as a whole, and it becomes brown in color. Amphibole crystals are often replaced with fine-grained biotite aggregate. Biotite fringes occur in selvages of quartz veins; biotite veinlets along fractures are noted as well.

Silicification is widepread throughout the Copernic ore field and is only sporadically occurs beyond their limits. The fields of silicified rocks coincide almost completely with stockworks of the Eastern, Central, and Western zones.

Argillic alteration occurs throughout the Copernic ore field as linear, lenticular zones confined to fractures and faults of different orders. The thickness of such zones varies from a few meters to a few tens of meters; their length ranges from a few tens to a few hundreds of meters.

The argillized granite porphyry were observed to the north of the Eastern Zone in the site of detailed prospecting near dig hole line 1, in the upslope part of line 5, and at the drainage divide along trench line T-3703–T-3707. The primary minerals of granite porphyry are partly or completely replaced by white, brownish white, or gray quartz–kaolinite aggregate. Rounded quartz grains mark a relict porphyry structure. Slight limonitization is characteristic.

A field of argillized metagranodiorite has been mapped to the southeast of the Eastern Zone along the left wall of the Copa Vilka Valley. The primary minerals are replaced here partly or completely with clay aggregates and, to a lesser extent, with quartz. Quartz veinlets occur locally. The rocks are limonitized and hematitized.

3.4.2. Petrographic description of metasomatically and hydrothermally altered rocks

The description presented below is based on microscopic examination of thin sections collected and prepared in June and July 2010.

Propylites (thin sections 246-5-1, 247-5-1, 247-5-2, 247-7-1, 469, 468-2, 247-5-3,1846, 571-1, 472, 1840, 890-1). In the propylitized biotite–hornblende granodiorite with primary hypidiomorphic-granular medium-grained structure partly obliterated by metasomatic alteration, plagioclase is replaced with albite, saussurite aggregate, and to a certain extent, with sericite. Biotite and hornblende are replaced partly or completely with chlorite and epidote. The content of altered plagioclase varies from 40 to 70 vol % and the amount of biotite and hornblende replaced with chlorite attains 10–25 vol %. The chlorite pseudomorphs after hornblende often retain characteristic shape of amphibole crystals. As a rule, propylitized rocks are dissected by a network of quartz veinlets (5–25% of the total area of thin section). Chlorite, epidote, prehnite, and sericite aggregates occupy 5–30% of selvages of these veinlets and occur as disseminations throughout the rock. Irregular clusters of epidote and prehnite grains are occasionally observed in cores of zonal plagioclase crystals. Sericite occurs as fanlike and radiated spots.

The formation of chlorite and epidote pseudomorphs after biotite and hornblende is accompanied by crystallization of magnetite as small isometric grains. Apatite and titanite are identified as accessory minerals (Figs. 33, 34).

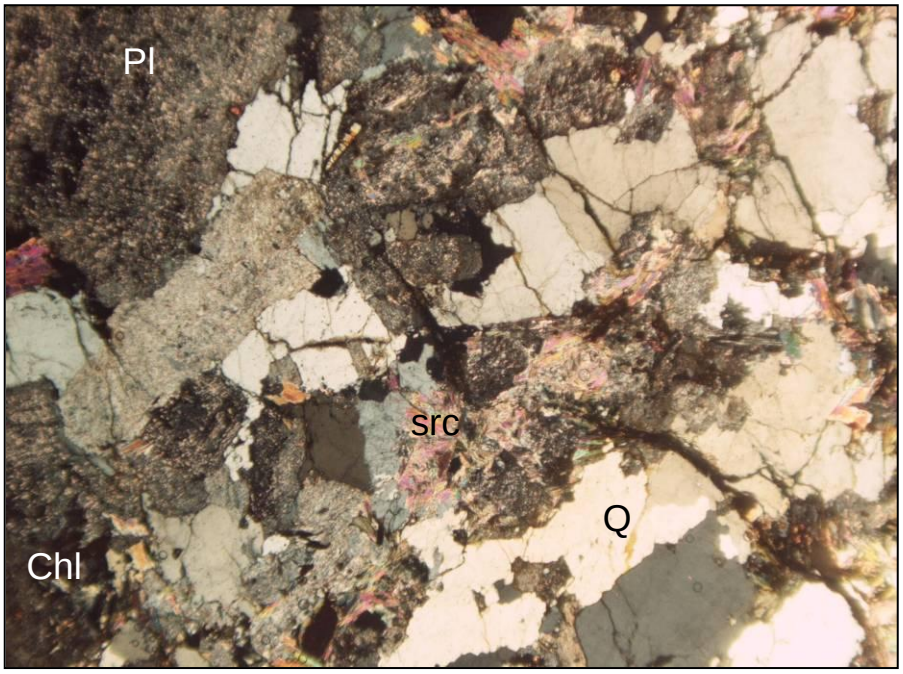

Fig. 33. Photomicrograph of quartz–sericite–chlorite–epidote veinlet in propylitized granodiorite (thin section 246-5-1); src - sericite; Chl - chlorite; Pl - plagioclase; Q - quartz. A field of vision is 7.73 mm across; crossed polars.

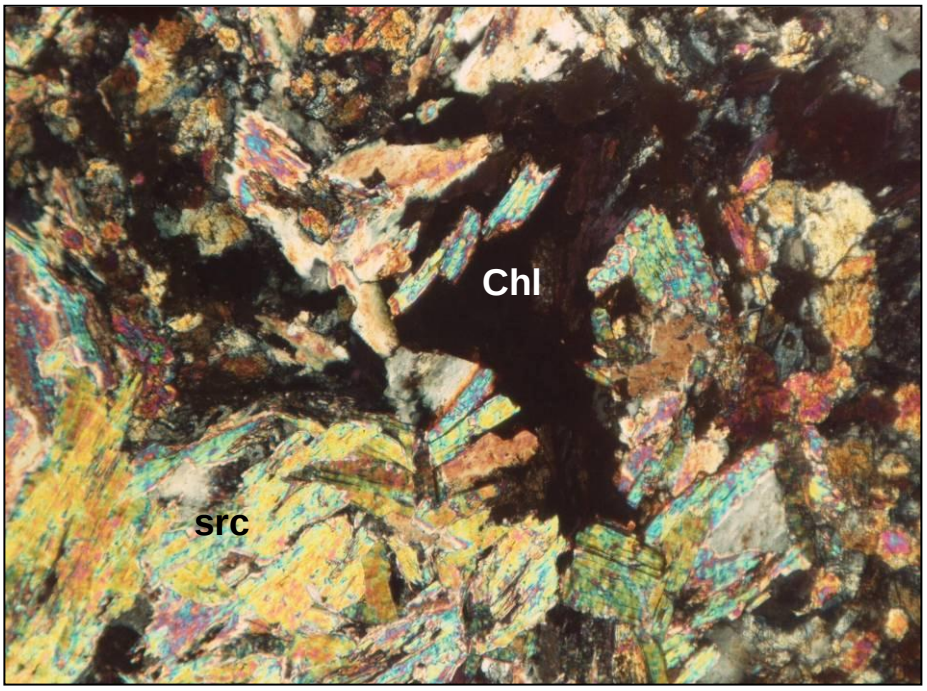

Fig. 34. Photomicrograph of sericite–chlorite aggregate in propylitized granodiorite (thin section 247-5-1); src - sericite; Chl - chlorite. A field of vision is 1.67 mm across; crossed polars.

Quartz–kaolinite metasomatic rocks are colorless aggregates of isometric micrograins of quartz, clay minerals, and a small amount of sericite. The rocks are dissected by thin brownish microveinlets filled with still finer mineralic mass (Fig. 35).

Quartz–sericite metasomatic rocks (thin sections 472-2, 573-1, 754-1) have microgranular, microveinlet, and allotriomorphic-granular structures (Figs. 36, 37). The rocks are composed of radiated, tabular, and allotriomorphic-granular sericite (60–70 vol %) and quartz grains (30–40 vol %) and crossed by quartz and quartz–limonite microveinlets.

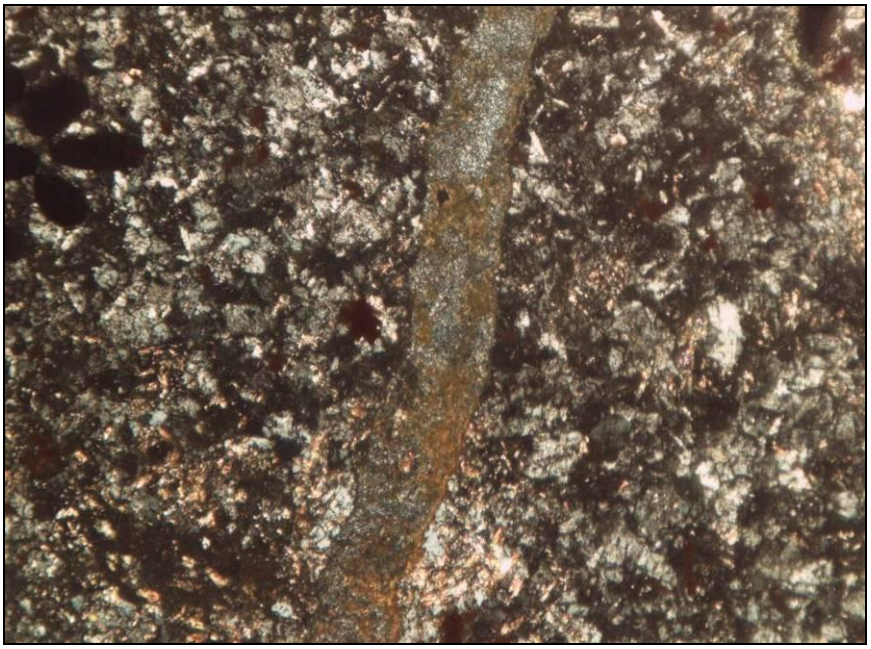

Fig. 35. Photomicrograph of quartz–kaolinite metasomatic rock (thin section 474). A field of vision is 1.67 mm across; crossed polars.

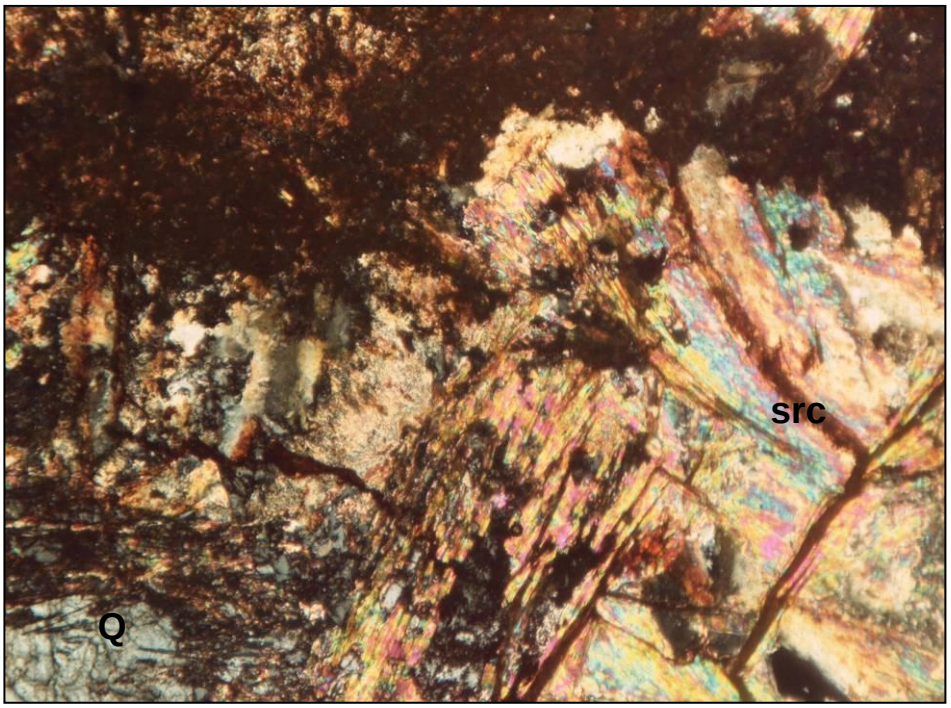

Fig. 36. Photomicrograph of quartz–sericite metasomatic rock (thin section 472-2): a fan-like quartz–sericite aggregate and quartz–limonite veinlet in the upper part of photomicrograph; src - sericite. A field of vision is 1.67 mm across; crossed polars.

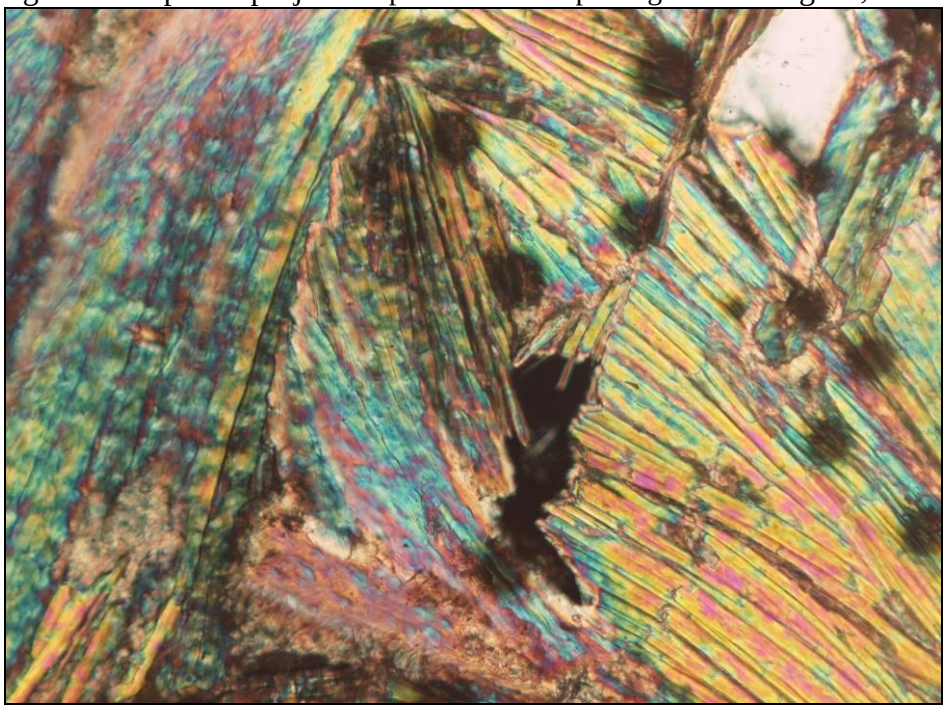

Fig. 37. Photomicrograph of radiated sericite aggregate in quartz–sericite metasomatic rock

(thin section 754-1); A field of vision is 0.67 mm across; crossed polars.

Monomineralic quartz aggregates have migrogranular or allotriomorphic-granular structures consisting of quartz by 70–100 vol %. The relics of quartz–albite–sericite metasomatic rock (Fig. 38) replaced with isometric quartz grains at margins are retained locally (thin sections 567-1, 734-2).

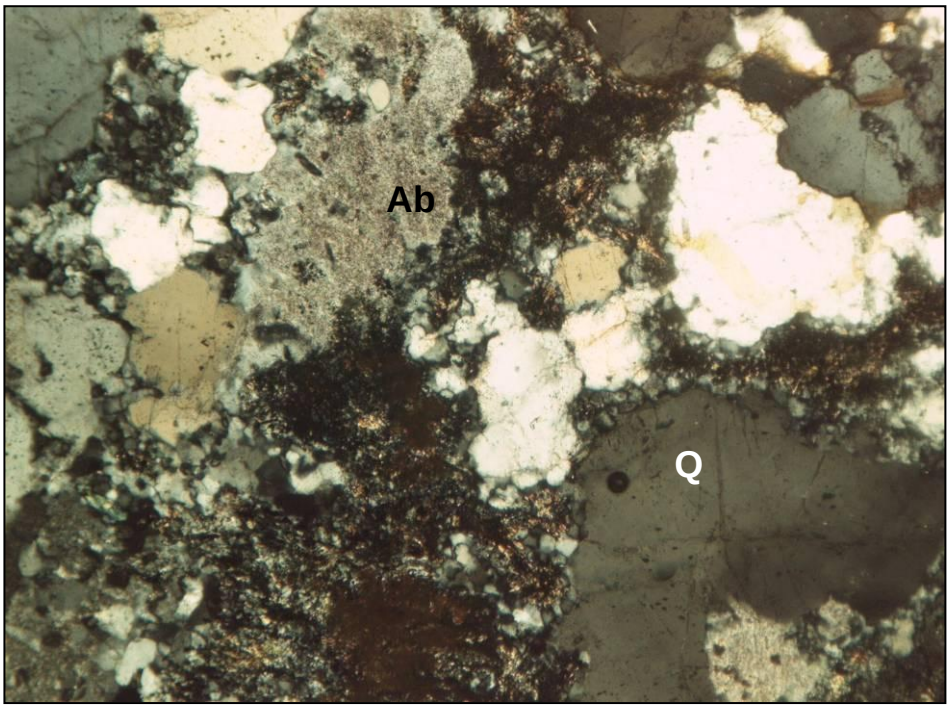

Fig. 38. Photomicrograph of quartz metasomatic rock: aggregate of allotriomorphic–granular quartz with relict albite (thin section 567-1); Q, quartz; Ab, albite. A field of vision is 1.67 mm across; crossed polars.

Silicified rocks have relict, microgranular, and allotriomorphic-granular structures. Quartz (10–40 vol %) incompletely replaces a protolith, mainly near quartz veinlets. The advanced replacement is noted in thin sections 567-1, 688-1, 734-2, 572-1, and in some propylitized rocks.

Biotitized rocks (thin sections 551, 551A, 472-1) are characterized by replacement of hornblende with bioite and development of biotite veinlets. Microgranular aggregates of biotite, albite, quartz, epidote, and magnetite replace hornblende as characteristic pseudomorphs. The biotite content varies from 60 to 100 vol % (Figs. 39, 40).

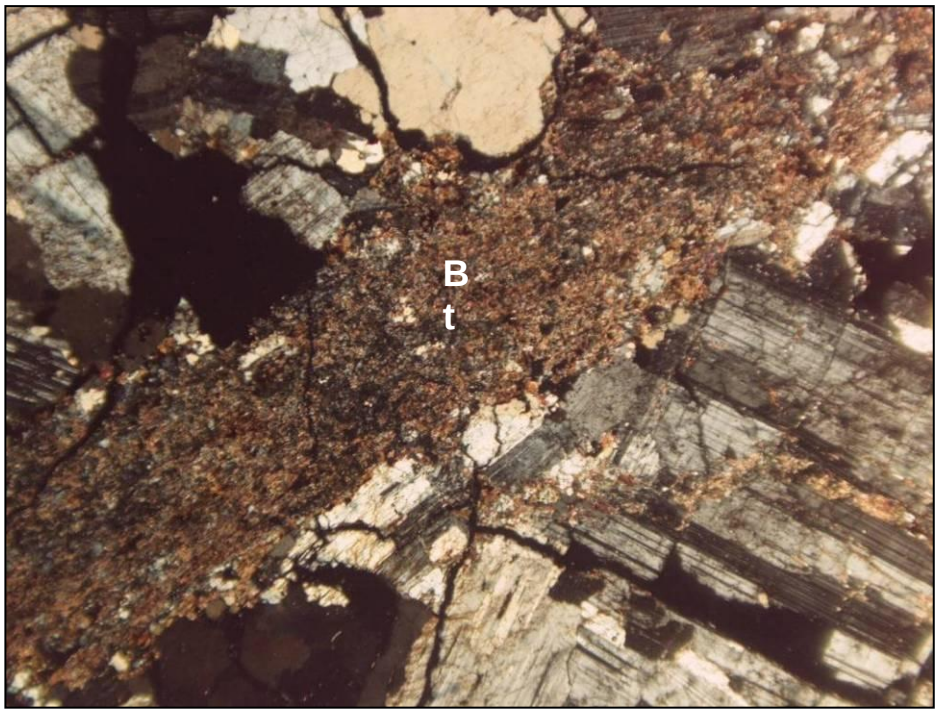

Fig. 39. Photomicrograph of microgranular (<0.01 mm) biotite replacing hornblende (thin section 551A); Bt, biotite. A field of vision is 7.73 mm across; crossed polars.

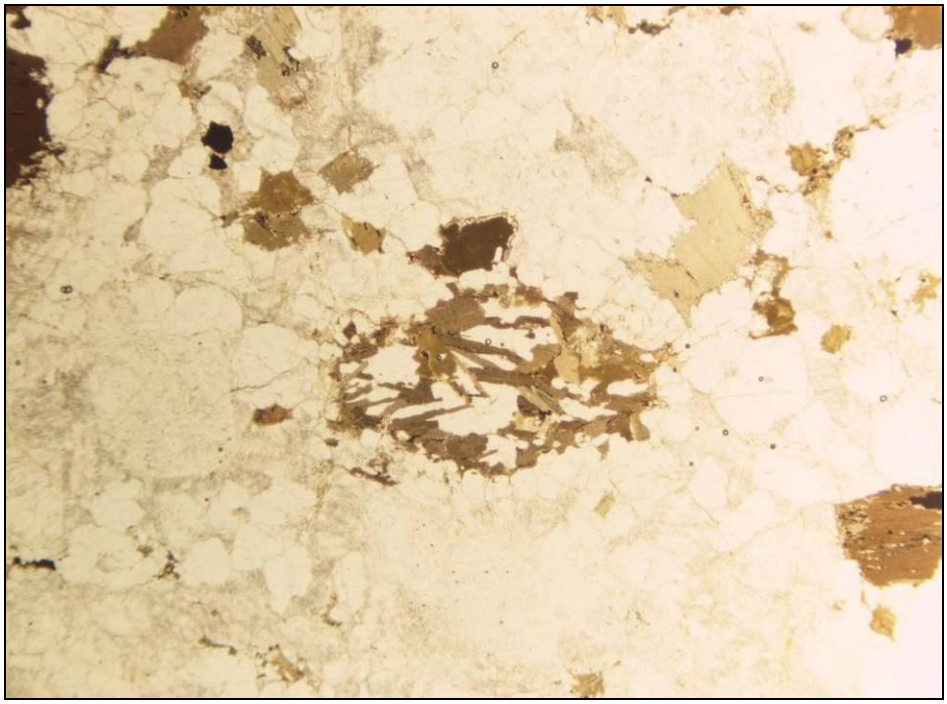

Fig. 40. Photomicrograph of biotite pseudomorph replacing hornblende (thin section 472-1). A field of vision is 7.73 mm across; plane light.

3.5. Tectonics

Faults make up a polygonal network with predominance of the tectonic lines oriented in the northeastern, nearly meridional, and northwestern directions. Blocks of intrusive rocks underwent vertical displacements along the faults. As a result, the rocks differing in age turned out to be exposed at the same hypsometric level.

Faulting at a relatively low temperature led to mechanical crushing and grinding of intrusive rocks with formation of cataclasites and kaolinite–quartz mylonites accompanied by slight argillic and propylitic metasomatic alteration. The metasomatic zones vary from a few meters to tens and hundreds of meters. The gently dipping cataclastic and mylonitized zones are observed.

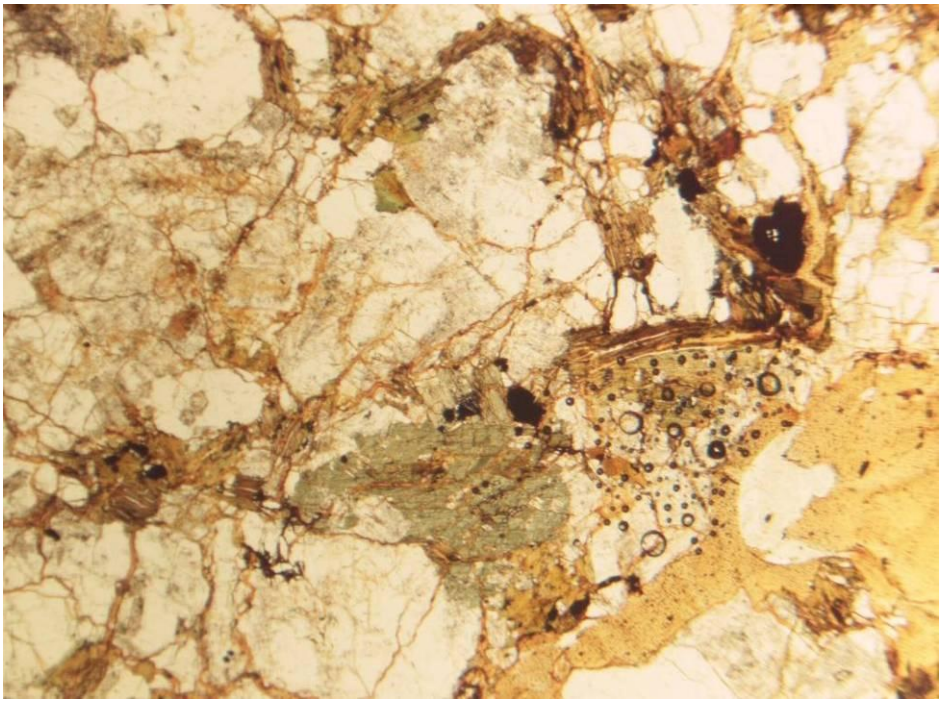

Fig. 41. Photomicrograph of shatter breccia (kakirite), thin section 892. A field of vision is 7.73 mm across; plane light.

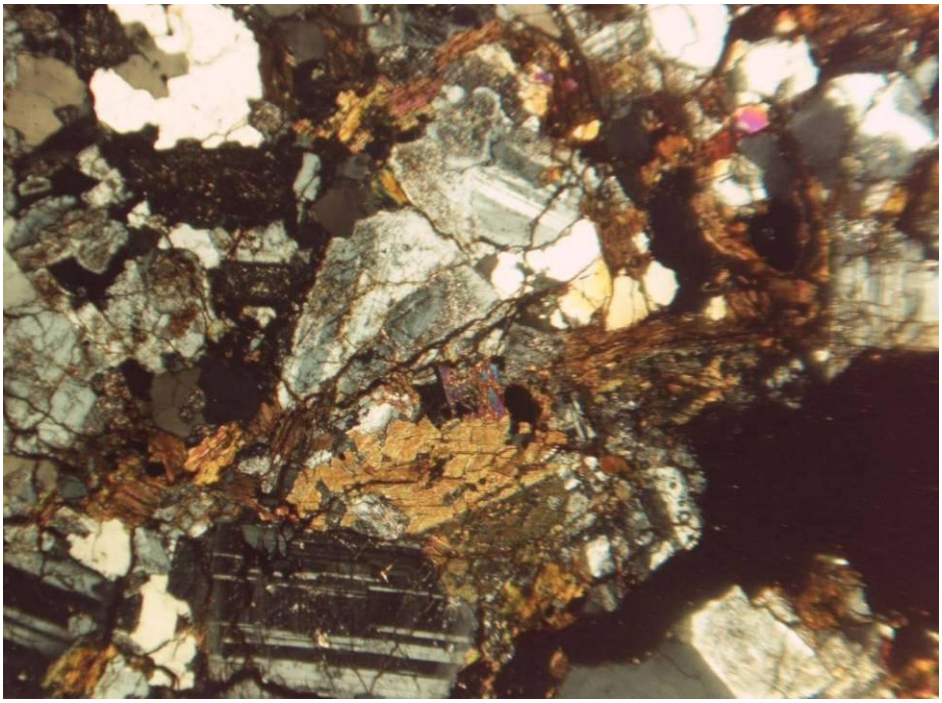

Fig. 42. Photomicrograph of shatter breccia (kakirite), thin section 892. A field of vision is 7.73 mm across; crossed polars.

Shatter breccias (kakirites) formed aside from fault planes are widespread in the studied area. These are severely shattered rocks disintegrated in hands. Particular fragments are not displaced relative to one another and retain their primary mineral composition and structure (Figs. 41, 42). In the ore field, the biotitized granodiorite transformed into shatter breccia is characterized by tiny fractures with iron hydroxides, which impart brown color to the rock.

In the fault zone that controls the trend of the Atirmey River, diorite and related intrusive breccia are locally foliated and transformed into a gneissose quartz–biotite–feldspar rock.

4. GEOLOGY OF THE COPERNIC ORE FIELD

4.1. Geology

The geological mapping accompanied by prospecting covered about 30 km^2, including 5 km^2 on a scale of 1 : 10 000 and 3 km^2, on a scale of 1 : 5000; the rest of territory was mapped on a scale of 1 : 25 000. The Copernic ore field comprises stockwork ore zones and numerous occurrences of sulfide and oxidized copper mineralization over an area of ~7.5 km^2 (App. 2. sheet 1). The southern and eastern boundaries extends along the left wall of the Choque River valley, the western boundary, along the Atirmey Valley and limiting ore occurrences in the LODD-I concession.. The northern boundary is unknown and situated to the north of the concessions belonging to the Upstream Mining S.A.C.

The ore field is composed largely of metasomatically altered biotitized granodiorite pertaining to the Atirmey Complex. Granite and granite porphyry of the Copernic Complex occur in the northern and western parts of the ore field. Gabbro, gabbrodiorite, and diorite of the Choque Complex occupy the southern and northern parts of the ore field.

The fields of plutonic rocks belonging to the aforementioned complexes are characterized by irregular configuration and are bounded by tectonic and intrusive contacts. The latter are commonly accompanied by intrusive breccia.

Large granitoid plutons are cut through by extended andesite dikes of the Trinchera Complex 0.5 to 2–3 m thick. The dikes commonly strike in the northwestern direction. Like other intrusive rocks, the dikes are diplaced along faults for a few meters and in some cases contain oxidized copper mineralization. Small aplitic dikes that complete emplacement of the plutons pertaining to the Atirmey Complex are widespread. The aplite dikes are 1–10 cm to 0.5 m thick, oriented in the northwestern direction, and dip to the northeast at angles 60–90^o (OPs 012, 018, 1092, 1523). Beyond the ore field, the strike and dip of aplitic dikes is chaotic. Granite porphyry, rhyolite, dacite, and andesite dikes of the Copernic Complex are less abundant. Their thickness is measured by few meters; they are often complexly curved and inconsistent in thickness.

The metasomatic alteration in the ore field largely affects granodiorite of the Atirmey Complex and is expressed in development of biotite, which replaces hornblende and fill microfractures in this rock. Zones of propylitization are characterized by replacement of dark-colored minerals and plagioclase with epidote and chlorite. Veinlike zones of quartz–epidote rock occur in granitoids. Argillic and quartz–sericite alterations are less abundant and commonly localized as linear zones and lenses. Zones, crusts, and disseminations of limonite occur almost overall.

The hydrothermal stockworks are composed of quartz veins, veinlets, and breccia bodies. The thickness of veins and veinlets ranges from a few centimeters to a few meters. The gangue material occupies up to 30–50% of stockwork volume. The milky white quartz is coarse-crystalline, occasionally comb and of rock-crystal type, contains muscovite and sericite, often is limonitized along fractures, and brecciated. The host rocks in selvages of quartz veins and veinlets and between them are metasomatically altered (silicification, argillic and propylitic alterations are the most characteristic).

The largest site of veins, veinlets, and breccia bodies making up a stockwork is the NNW-trending lenticular zone 200–400 m thick that extends for 600–700 m and probably declined to the northeast at angles of 60–80^o (Western stockwork zone).

Copper mineralization of the oxidation zone is composed of malachite, azurite, chrysocolla, and some other minerals and localized in three extensive sites and several local occurrences, where it is hosted in propylitized metagranodiorite and quartz veins and veinlets as mineralized aureoles, stockworks, brecciation and linear zones. Copper minerals of oxidation zones occur as crusts, sinters, spots in veins, veinlets, and their host rocks, as well as in microveinlets and pockets. In one case (OP 1527), chalcopyrite and molybdenite disseminations were identified in silicified and propylitized granodiorite.

In the course of prospecting, three sites with potentially economic oxidized mineralization were contoured in concessions Cayan 2, LODD, and LODD I (Appendix 2, sheet 2) and called Western, Central, and Eastern sites.

The granitoid rocks of the Copernic Complex and host rocks of the Atirmey Complex bearing low-grade Cu and Mo sulfide mineralization are regarded as ore-bearing, as well as numerous ocurrences of oxide mineralization.

The available data allow us to outline the following sequence of ore formation:

- During the emplacement of Copernic Plagiogranite in the Atirmey Granodiorite, magmatic breccia was formed at the roof of the younger intrusion and the Atirmey Granodiorite underwent biotitization close to the intrusive contact.
- The stockwork porphyry copper deposit was formed as a result of the subsequent hydrothermal processes.
- The largest stockwork "Oeste" was formed in the zone of elevated permeability, probably, at the intersection of long-living NE- and NW-trending faults.
- The Trinchera dike complex is postmineral; the dikes were emplaced along the faults striking in the northwestern direction.
- Geochemical zoning characteristic of porphyry copper deposit is obliterated by asymmetry of permeable zones. Mineralogical zoning inherent to porphyry copper mineralization is not expressed with certainty.

4.2. Geophysics

4.2.1. Geophysical fields and their interpretation

The scope and technique of geophysical exploration are described in section 2.3.1. According to geophysical data, the explored area is divided into two parts with geophysical fields differing in their complexity. The southeastern block, where the Eastern anomalous zone is hosted, substantially differs from the northwestern block with the Western anomalous zone in low induced polarization (Fig. 43) [Fig. 4][1].

A hypothetical NE-trending fault at an azimuth of 40–50^{o} NE cuts off the southeastern part of the IP anomaly ring in plan view and toroidal in 3D space. This fault controls the NE-trending Central anomalous zone closely related to this fault and the northwestern flank of the Eastern zone. The fault is expressed in topography by linear arrangement of contour lines along it and by linear segments of valleys 400–600m in extent striking at the same azimuth in the central part of territory.

The fault is also expressed in the magnetic field [Fig. 5-7], gamma spectroscopic data (total count) [Fig. 10], distribution of U [Fig. 12] and K [Fig. 13]. The localization of anomalies of the observed magnetic field relative to the sites with copper mineralization revealed in 2009 is shown in Fig. 44.

[1] Here and below, the references to figures from the report presented by supervisor A.B. Nikitin (see Additional Appendix 4) are bracketed.

The cut-off part of the ring IP anomaly is of special interest for its search in the northeastern or southwestern directions.

The boundary of the forecasted porphyry copper system is clearly seen in the map of electrical resistance contour lines at a relative depth of 100 m [Fig. 3], where it can be drawn conventionally at a contour line of 1000 Ω·m.

Zones of lower resistance are commonly caused by elevated permeability of rocks favorable for the migration of hydrothermal ore-bearing solutions or by enrichment in the minerals conducting electrical current.

According to the geophysical data, the forecasted porphyry copper system is a nearly vertical cylinder 1700–1900 m in diameter and heterogeneous in the internal structure (Fig. 45).

The western boundary of the inferred porphyry copper system is clearly marked by IP anomaly conventionally drawn at contour line of 20 mV/V [Fig. 4], gamma spectroscopic data (total count, 90 pulses/min [Fig. 10], Th (11 ppm) [Fig. 11], U (3.6–4.0 ppm) [Fig. 12], and K (2.2%) distribution). In space, this segment of boundary coincides with the eastern wall of the Atirmey Valley in its southwestern and western one third. This obvious boundary most likely is caused by a contact, probably, tectonic, of rocks differing in composition.

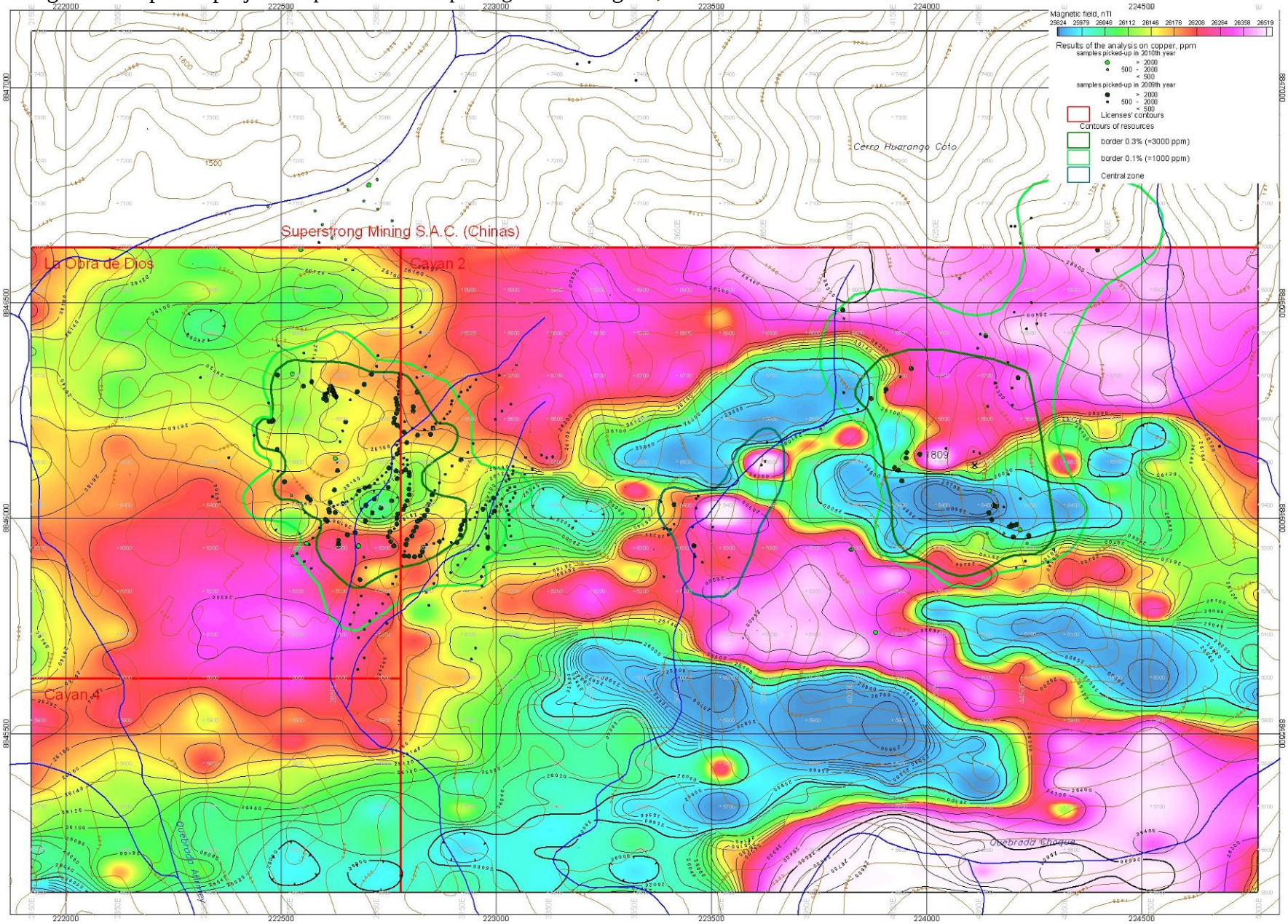

Fig. 43. Relationships between IP anomalies (pink) and the sites with visible copper mineralization revealed in 2009

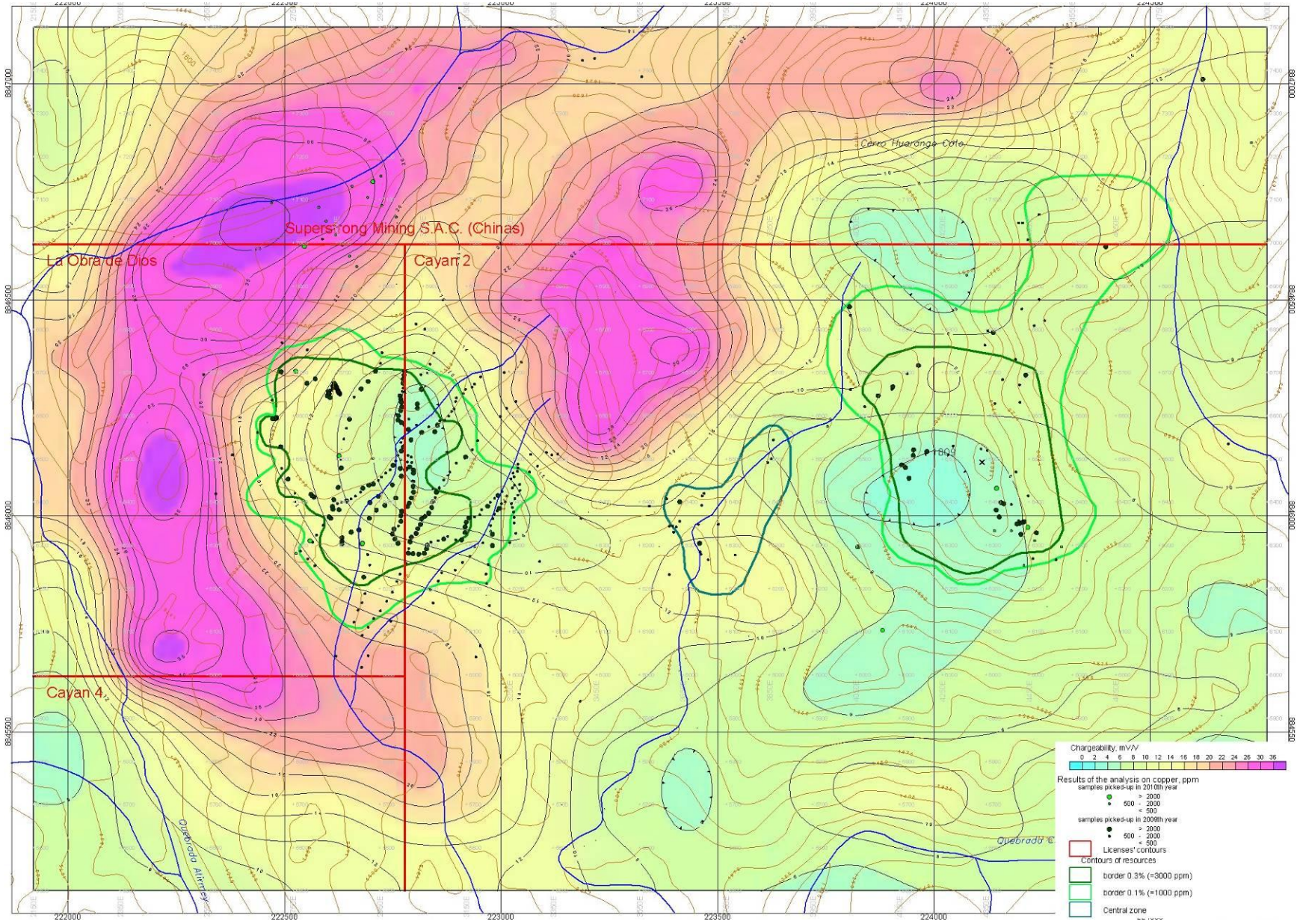

Fig. 44. Relationships between anomalies of observed magnetic field and the sites with visible copper mineralization revealed in 2009.

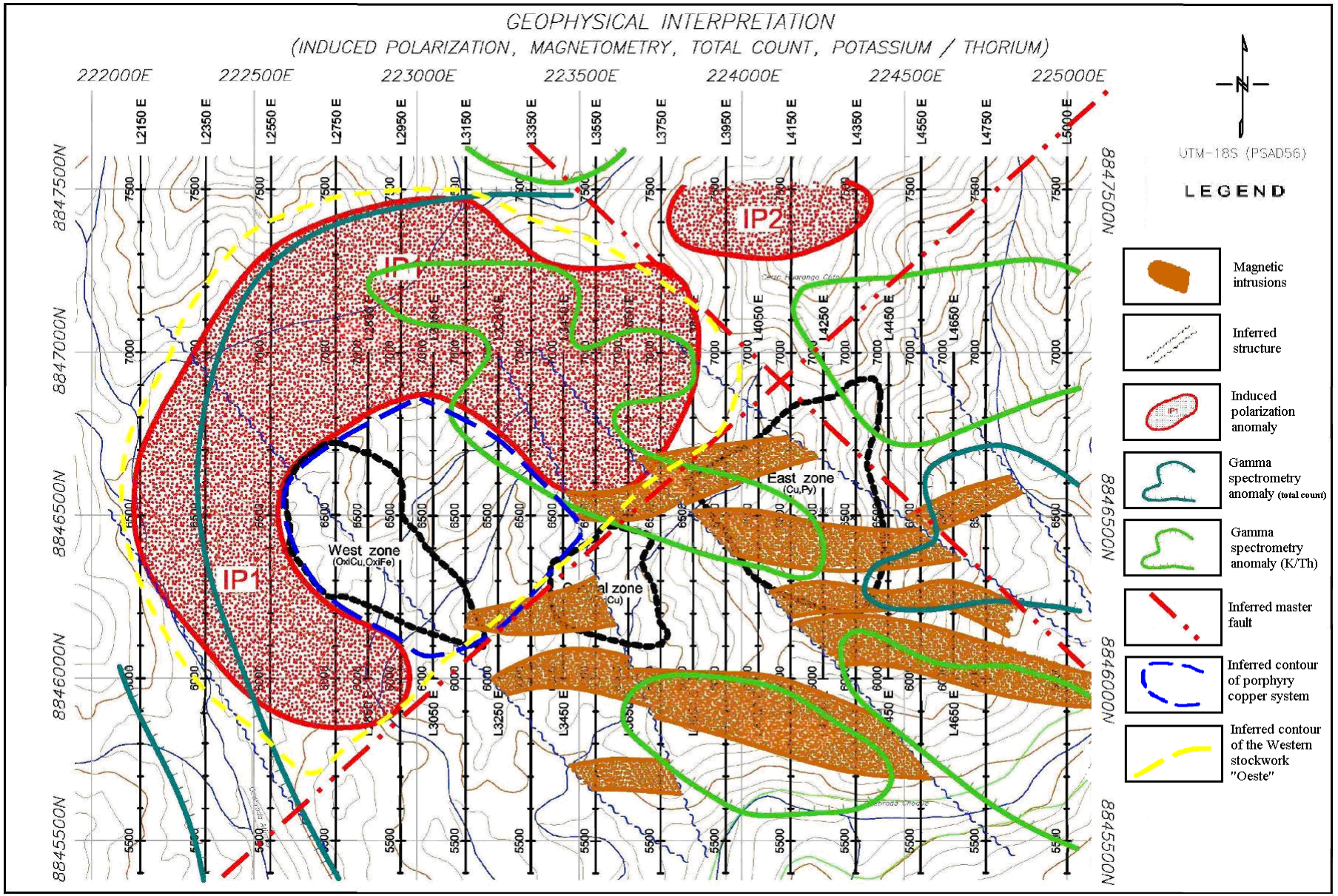

Fig. 45. Interpretation of induced polarization, magnetic, and gamma spectrometry anomalies, after the data of VDG del Peru S.A.C.and A.B. Nikitin.

4.2.2. Conclusions

Highly contrasting physical properties of rocks confirm the validity of the previously made decision to conduct geophysical exploration in the studied area and the proper choice of geophysical methods.

The degree of geophysical development of the territory and the depth of exploration down to ~500 m are sufficient for conduction of prospect drilling. The number of detected anomalies turned out to be much greater than previously expected.

The high chargeability (20–20 mV/V and higher) can be caused by sulfide, including pyrite; magnetite, graphite, clay, or extensive argillic alteration. Because neither magnetite and graphite nor extensive argillic alteration are known in the studied area, and at the same time economic copper contents are established mainly in form of oxidized mineralization, the relationship of the revealed IP anomalies with copper sulfides at a depth is highly probable (Fig. 45).

4.2.3. Recommendations

As our experience shows, the high Cu and Au concentrations are related to the marginal parts of geophysical anomalies (including IP) rather than to their central parts. Geophysical gradients can be treated in geochemical terms as barriers, where the medium changes its properties, giving rise to the precipitation of ore minerals. Therefore, it is not sensible to drill in epicentrum of IP anomalies, at least, at the first stage of drilling program.

Further processing and comparison of new geochemical and already available geophysical data should be helpful for optimal location of drill holes and their orientation.

As is clearly seen from [Fig. 6], 380 of 707 (53.7%) geological observation and sampling points and 354 of 646 (54.8%) significant Cu contents fall into the interval of observed magnetic field of 26 000– 26100 nT.

No direct cause–effect links between the copper content determined with ICP/AQR and AAS for predominant oxidized mineralization and the values of the observed magnetic field has not been established as yet. At the same time, the joint statistical processing revealed an interval of magnetic fields (26 000– 26100 nT), which spatially corresponds to most number (most percentage) of samples taken in 2009 with significant copper mineralization.

Digital geophysical data are useful not only to the qualitative interpretation but also for quantitative solutions of problems. Therefore, it would be reasonable to correlate a 3D model of Cu contents and 3D IP anomalies.

It should be noted that the results of electrical exploration in the western and eastern parts of the studied area remain controversial and allow different variants of their interpretation and estimation. To date, we cannot explain, why the Eastern ore zone does not reveal anomalous conductivity and chargeability.

4.3. Ore zones and sites

4.3.1. Western site

The Western site is located in the western part of the Copernic ore field. The study of this ore field under the Copernic project began precisely from this site. Owing to good exposure and passability in combination with its high ore resource potential, this site is the best studied to date. The site is almost completely localized in the Cayan 2 and LODD concessions. Its northern flank extends for 300–500 m to the north beyond the boundary of the concession belonging to the Upstream Mining S.A.C.

The site is largely composed of intrusive rocks pertaining to the Atirmey and Copernic complexes, including minor intrusions and dikes. The biotite–hornblende granodiorite and metagranodiorite (biotitized granodiorite) of the Atirmey Complex are severely fractured, propylitized, and limonitized. The zone of intense propylitization coincides with the Western stockwork. The Copernic Complex comprises plagiogranite, biotite granite porphyry, and fine-grained granite and aplite dikes. Andesite dikes of the Trinchera Complex 10–20 cm to a few meters in thickness occur as well.

The Western site consists of several ore and potentially ore zones (Fig. 46):

- Western ore zone (stockwotk);
- the inferred northern extension of this zone;
- zone of quartz veins and veinlets at the northern termination of the Western site at the left bank of the left tributary of the Atirmey Valley; and
- zone of porphyry copper mineralization forecasted from geophysical data (Fig. 45).

Geological prospecting routes were conducted in the site of hydrothermally altered rocks; eight trenches 375.5 m in total length, seven dig hole lines (2009), several lines of rock chip panel and channel sampling are located in this site. These lines spaced at 50–100 m crossed the potential ore zone mainly in near-meridional direction. The points of sampling were spaced at 10–20 m along the profiles and 50–100 m in geological routes. In the trenches, channel samples were taken by discrete sections 2–5 m long in the areas with visible mineralization and 10–20 m, where such mineralizationis absent. Hydrothermal metasomatic rocks comprise propylites and products of argillic and quartz–sericite–muscovite alteration. Together with zones of quartz veinlets, veins, and breccia bodies, they make up a large stockwork zone (Figs. 47–50).

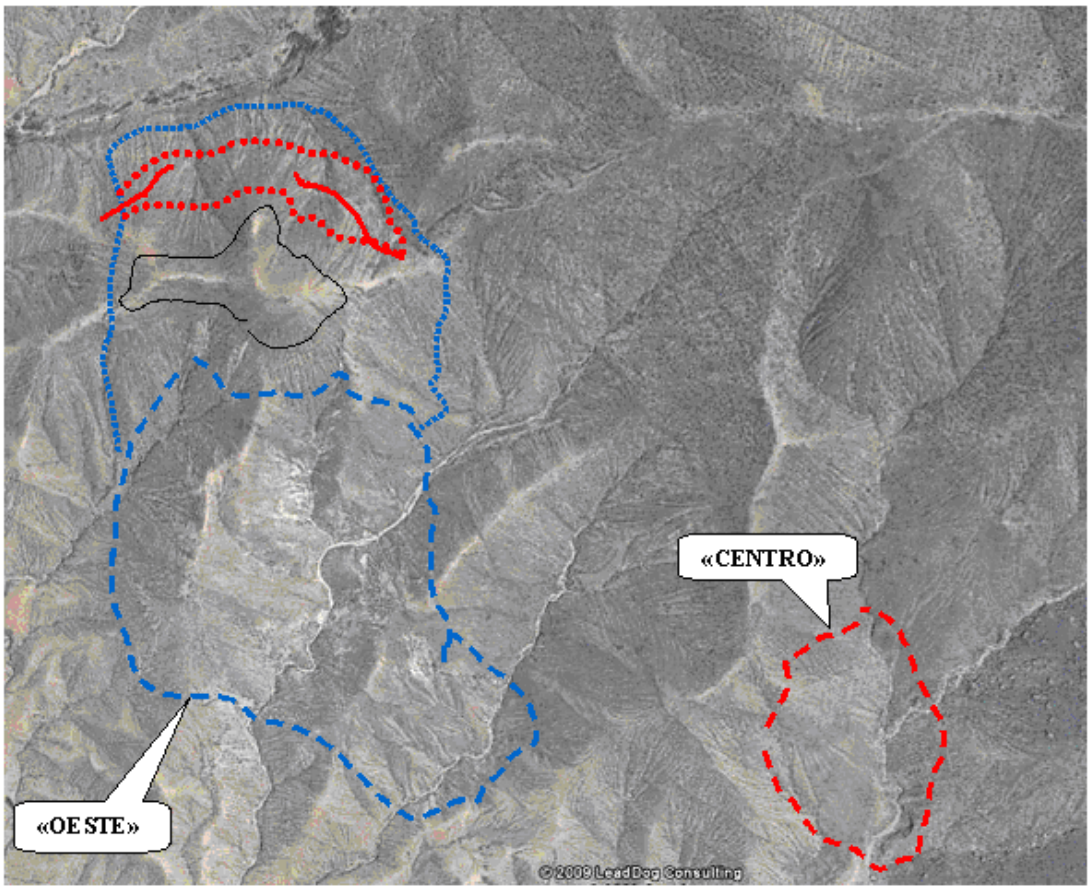

Stockwork «OESTE»:

(a) mapped contours

(b) inferred contours

Zone of quartz veinlets

Zone «CENTRO» of quartz veinlets and stockwork

Granite porphyry

Quartz reefs

Fig. 46. Contours of the Western (Oeste) and Central (Centro) sites of copper mineralization plotted on Google satellite image.

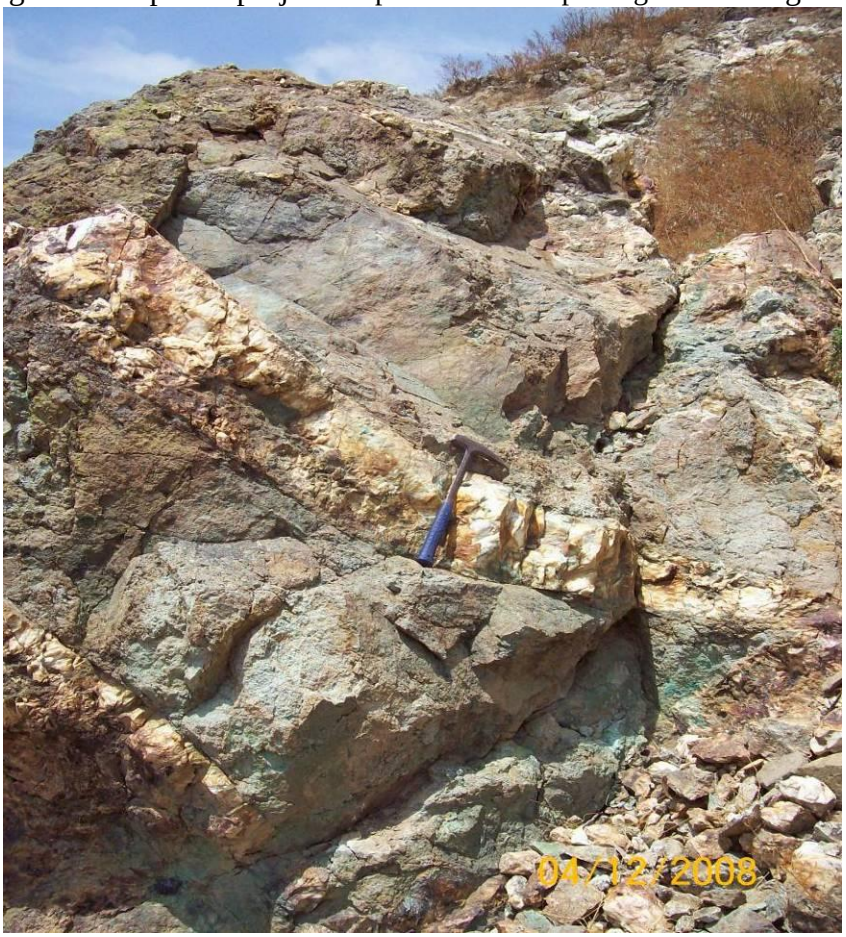

Fig. 47. Quartz veins in silicified and propylitized metagranodiorites and oxidized copper minerlaization localized along microfractures and dispersed in quartz veins and host rocks.

Fig. 48. Quartz breccia.

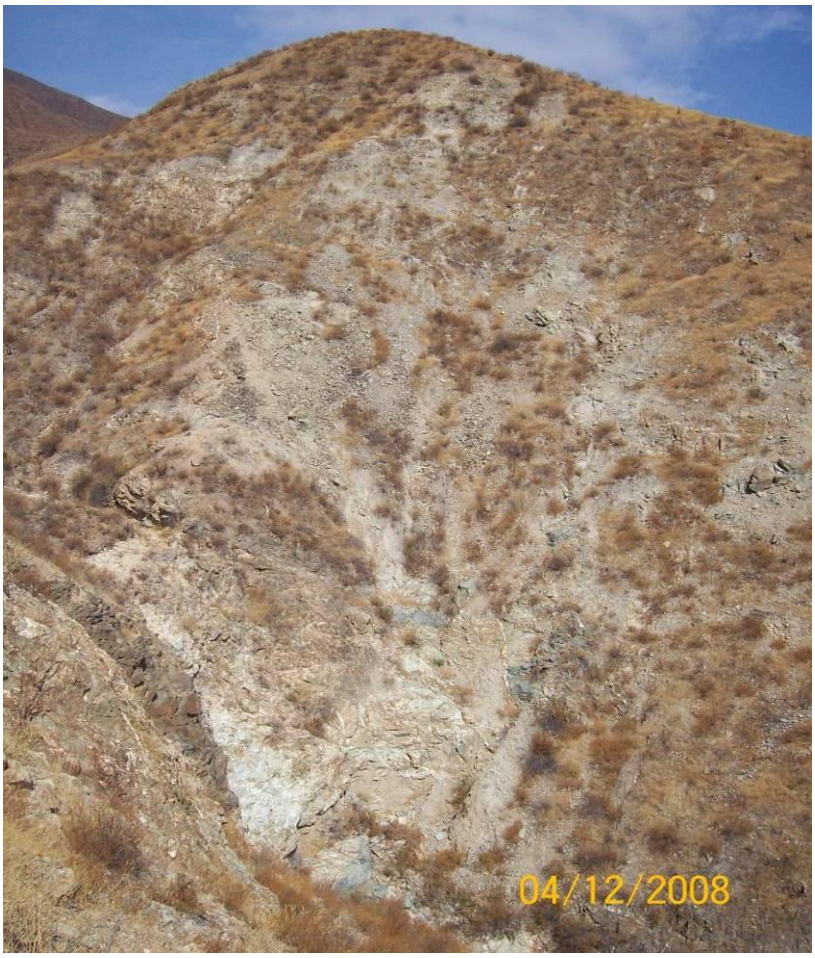

Fig. 49. Stockwork of quartz veinlets with oxidized copper mineralization hosted in metagranodiorite, site “Oeste”.

Fig. 50. Abundant oxidized copper mineralization localized along joints of parting in metagranodiorite of the site “Oeste” (location of channel sample 102).

It has been established that the stockwork with visible ore mineralization consists of a series of lenticular, probably, steeply dipping bodies of severely propylitized and silicified metagranodiorite with abundant quartz veinlets and quartz breccia. They are characterized by variable thickness, steeply dip to the northeast, and have not distinct boundaries. The intensely silicified rocks are separated by slightly propylitized granodiorite without quartz veinlets and visible copper mineralization. The contacts and mutual transitions of such zones are irregular, with bays, lenses, and interveining. A suite of extended andesite dikes occurring in the center of stockwork zone is accompanied by thin zones of cataclasis and argillic alteration. The western and southern boundaries of the stockwork are diffuse, with gradual transition to slightly propylitized metagranodiorite. These boundaries are crossed by trenches 248, 249, 261, 460, and 461. The northern boundary plunges beneath the drainage divide along a low-angle (20–30^{o}) fault zone. The footwall of this zone (OPs 316, 317) is filled with mylonite and catacalsite with intense copper mineralization. The silicified and propylitized granodiorite devoid of copper mineralization occurs in the hanging wall. In the northwest, the stockwork is disrupted near OPs 018–019, 317 and then strikes to OPs 1593 and 1343. At the eastern flank, the stockwork crops out (OPs 090–106, 016, 797).

The stockwork extends for ~600 m and reaches 400 m in width. It is suggested that it extends further northward for 200–250 m (OPs 463, 2524–2527, 575). According to geophysical data (Figs. 45, 46), the stockwork is traced in the northeastern direction for 300–400 m further and becomes oval, with the long axis attaining 700–800 m.

The anomalous Cu concentrations vary from 100–200 ppm to 1% and higher. The Mo contents are 50–300 ppm, occasionally higher; a maximum content is 0.21%. Average Cu content within the limits of an inferred orebody is above the cutoff of 0.2–0.3 % Cu and 0,01@% Mo accepted for typical porphyry copper deposit.

The mouth of a sanded-in old adit is located at the southern flank of the site (OP 148, coordinates WGS 84 – E 222.612; N 8 846.015). We fail in opening it by trench 247. The transition zone from ore-bearing to barren granodiorite was crossed by trenches 246, 249, 261.

Bulk samples were taken from the dump of this adit. The total area of the dump is about 1500 m^2; the thickness varies from 0.3 to 0.7 m; a probable length of adit is 50–100 m. The rock fragments in dump largely consist of propylitized and silicified metagranodiorite enriched in quartz veinlets to a certain extent, as well as of disintegrated quartz veins. All rock varieties in dump contain oxidized copper mineralization in form of stains, spots, sinters along joints and as disseminations in rocks. At first glance, copper mineralization was not identified at the surface of large fragments, but was revealed by their further comminution. The bulk samples were collected along a line of 10 m; the entire material was put in a sample and then crushed and reduced by hand to 7.5–8.0 kg.

The results of sampling are given in Table 4.3-1. The results of analyses of bedrock close to the adit's mouth are presented for comparative purposes.

The average Cu content in the selection of bedrocks from trench 247 and dig hole 120 is 0,622%; in ore dump is 0.827%; the average of tailings after washing is 1.083%, and the average of outcrops close to the adit's mouth is 0.963%. These contents are appreciably higher than those in calculated anomalous blocks of the Western site used for calculation of speculative resources (Section 7.2). These data increase a promise of the WEstern site to a depth, where the Cu and Mo contents are expected to be higher.

Table 4.3-1. Results of sampling of adit ore dump and tailings of washed ore samples

Results of sampling of adit ore dump and tailings of washed ore samples						FA/AA	ICP/AQR								
						Au	Ag	**Cu**	Fe	K	**Mo**	Na	**Pb**	S	**Zn**
						ISP-330	ISP-142								
	Sample			Roca	Mineral	ppm	ppm	ppm	%	%	ppm	%	ppm	%	ppm
1	148-1	Handful	Ore dump	gr-drBiHgt +Q	oxiCu	-0,005	1,4	**6453**	2,19	0,15	73	0,05	8	0,01	75
2	148-2	Handful	Ore dump	gr-drBiHgt	oxiCu	-0,005	0,7	**8062**	2,71	0,27	65	0,05	12	0,01	89
3	148-3	Handful	Ore dump	gr-drBiHgt +Q	oxiCu	0,005	1,5	**9005**	2,13	0,16	170	0,05	20	0,02	75
4	148-4	Handful	Ore dump	gr-drBiHgt +Q	oxiCu	0,008	2,3	**9613**	2,16	0,14	83	0,05	29	0,01	88
5	150-1	Handful	Tailing	massQ+gr-drBiHgt	oxiCu	**0,021**	1,3	**19700**	2,72	0,26	119	0,04	35	0,04	101
6	150-2	Handful	Tailing	massQ+gr-drBiHgt	oxiFe	**0,011**	0,7	**2368**	3,51	0,47	106	0,05	7	0,01	79
7	150-3	Handful	Tailing	massQ+gr-drBiHgt	oxiCu	**0,020**	0,5	**10400**	3,29	0,38	57	0,05	9	0,01	99
	среднее				**average**	**0,008**	1,200	**9371,6**	2,673	0,261	**96,1**	0,049	17	0,016	**86,6**
Bedrock samples taken near the adit mouth															
	Sample					**Au**	Ag	**Cu**	Fe	K	**Mo**	Na	**Pb**	S	**Zn**
1	149	ChS	bedrock	gr-drBiHgt	oxiCu	0,008	1,3	**4948**	2,54	0,15	32	0,08	2,5	0,03	70
2	dh1208	ChS	bedrock	gr-drBiHgt	oxiCu	0,008	2,3	**19200**	2,36	0,16	63	0,03	24	0,01	123
3	dh1208-1	ChS	bedrock	gr-drBiHgt	oxiCu	0,008	1,6	**4808**	2,55	0,13	**153**	0,04	9	0,01	82
	K-247								0,00	0,00	0	0,00	0	0,00	0
4	247-1	ChS	bedrock	gr-drBiHgt +Q	сл. oxiCu	0,016	1,8	**2099**	2,55	0,12	67	0,07	6	0,01	68
5	247-2	ChS	bedrock	gr-drBiHgt	сл. oxiCu	0,014	1,8	**2428**	2,78	0,19	51	0,07	7	0,01	81
6	247-3	ChS	bedrock	gr-drBiHgt	oxiCu	0,016	1,9	**9575**	2,56	0,17	40	0,06	18	0,005	101
7	247-4	ChS	bedrock	gr-drBiHgt +Q	oxiCu	**0,021**	1,4	**4740**	2,81	0,24	54	0,08	7	0,005	86
8	247-5	ChS	bedrock	gr-drBiHgt +Q	oxiCu	0,011	1,4	**6462**	1,96	0,14	60	0,06	14	0,005	65
9	247-6	ChS	bedrock	gr-drBiHgt		0,015	1,4	1929	2,55	0,21	86	0,09	8	0,02	69
10	247-7	ChS	bedrock	gr-drBiHgt	oxiCu	0,010	1,4	**8975**	2,13	0,14	35	0,07	13	0,005	77
11	247-8	ChS	bedrock	gr-drBiHgt	сл.oxiCu	0,015	1,2	**4564**	2,87	0,18	46	0,08	8	0,005	72
12	247-9	ChS	bedrock	gr-drBiHgt +Q	oxiCu	0,011	0,7	**7347**	2,75	0,20	40	0,07	6	0,005	109
13	247-10	ChS	bedrock	gr-drBiHgt	сл.oxiCu	0,011	1,0	**3810**	2,83	0,19	57	0,09	5	0,005	90
	average				**average**	**0,013**	1,5	**6221,9**	2,56	0,17	**60,3**	0,07	10	0,010	**62,9**

4.3.2. Central site

The Central site irregular in outlines is the smallest in area and completely situated in the Cayan 2 concession in the center of the Copernic ore field (Fig. 46). It cannot be ruled out that this site is connected with the Western site (Oeste).

The inferred ore zone is hosted in metasomatized biotite–hornblende granodiorite (metagranodiorite) of the Atirmey Complex and abuts in the north against melanocratic fine-grained biotite diorite of the Choque Complex.

Quartz veinlets and breccia (OPs 008-012) and sporadic quartz veins, which are hosted in propylitized metagranodiorite, do not reveal regular orientation. The thickest (up to 1.5 m) veins and brecciated zones (OPs 012-3, 012-6) strike at an azimuth of 300° NW and dip to the southwest at angles of 45–50°. Most veinlets, veins, and brecciated zones are 0.05–0.30 m in thickness.

No anomalies in resistance and induced polarization, as well as in Th, U, and K contents have been established. Magnetic anomaly at the southern flank is likely related to diorite. The oxidized copper mineralization is confined to zones of quartz veinlets and breccias and occasionally occurs in host rocks at the lowermost hypsometric levels, disappearing at the upper levels (dig holes 1401, 1420–1427). The detected vertical range of mineralization is not wider than 50 m. Anomalous Cu and Mo contents are 0.1–0.2% and 50–100 ppm, respectively.

4.3.3. Eastern site “Este”

The Eastern site is situated in the Cayan 2 concession and extends northward beyond its boundary. This is a ridge that separates the Tacpa and Copa Vilca valleys and extends further to the north up to the left tributary of the Atirmey Valley.

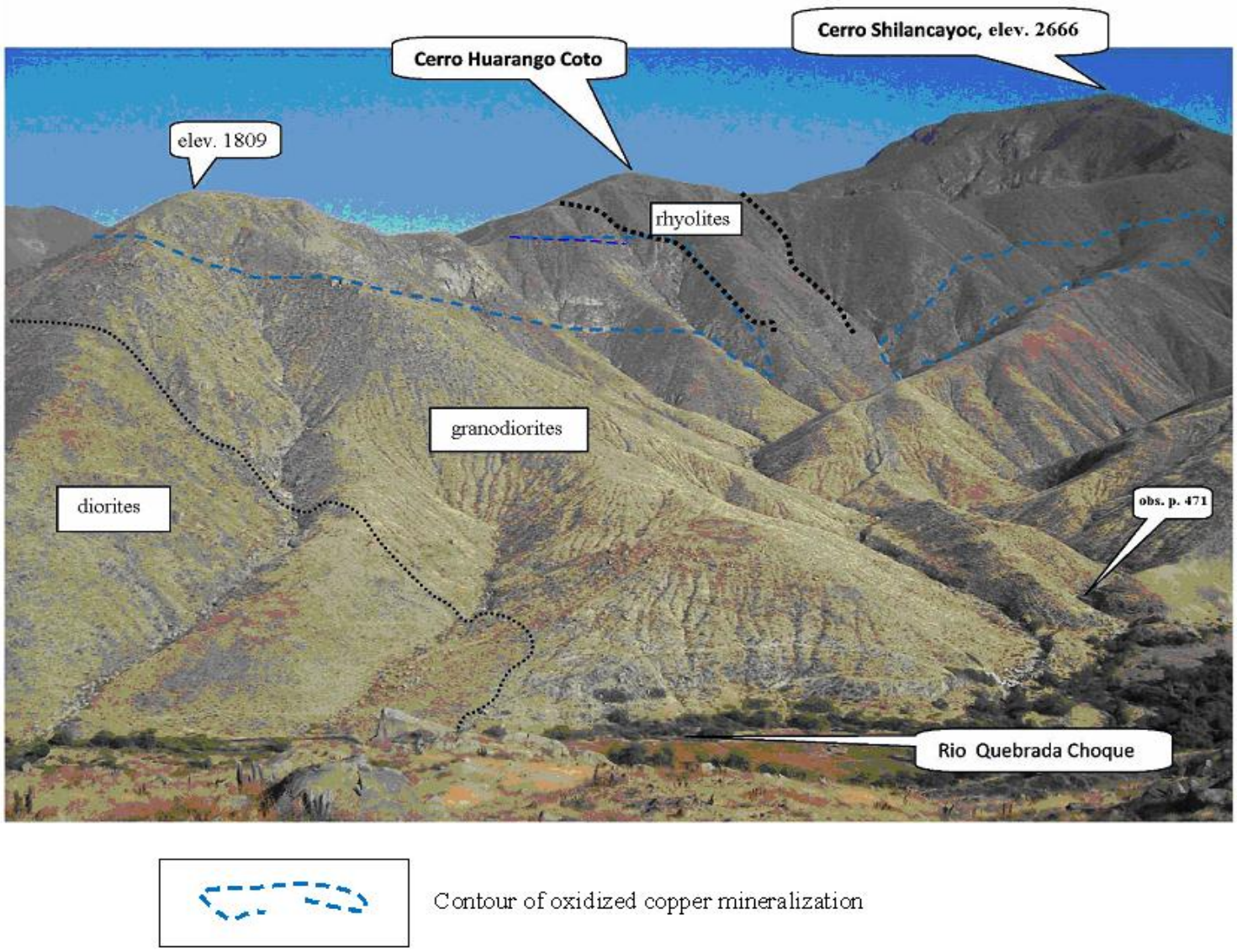

Fig. 51. The Eastern site, a view from the road to the settlement of Choque.

The site is characterized by dissected topography, the highest elevations, steep slopes, and rocky outcrops along the right wall of the Tacpa Valley (Fig. 51).

Geological and prospecting routes performed in this site were accompanied by sampling. Eleven trenches and strippings crossed a zone of argillic alteration at the southern flank and one trench (3708) was driven at the crest of ridge near spot height of 1809 m. About 400 samples were taken in total; 56 samples were used for estimation of speculative resources.

Diorite of the Choque Complex exposed in the southern part of this site is cut through by metasomatically altered granodiorite (metagranodiorite) of the Atirmey Complex. In the northern part of the site, metagranodiorite blocks are incorporated into granite porphyry pertaining to the Copernic Complex (OPs 2661, 2663, 2664, 2905, 2906, 2908, 2909).

The oxidized copper mineralization is prevalent in the Eastern site (OPs 489, 490, 491, 492, 567, 568, 1833, 1838, 2641, 2642, 2653, 2654, 2655, 2656, 2662, 2675, 2676, 2682). Sulfide mineralization (chalcopyrite and molybdenite were identified with confidence) was detected in propylitized and silicified granodiorites (OPs 1527,1551, 2644) and in granite porphyry as uniformly dispersed disseminations. Chalcopyrite and molybdenite grains are 1–3 mm and occasionally up to 5 mm in size. In some cases, sulfide mineralization is localized in quartz veinlets (molybdenite at OP 302). Sulfide mineralization was detected at the lowermost hypsometric levels.

To date, the Eastern site is distinguished by the largest area of occurrence of oxidized copper mineralization in comparison with other sites of the Copernic project. This mineralization is localized in altered granodiorite and granite porphyry as disseminations in host rocks, sinters and crusts along fractures.

The zone of sporadically developed oxidized copper mineralization identified during geological routes extends along the eastern slope of the Cerro Huarango Coto–spot height of 1809 m drainage divide from the southern boundary of the site (OP 1183) northward for approximately 800 m up to OP 2683 + 80 m. The vertical range of visible mineralization and the width of mineralized zone are about 100 m. An isolated field of oxidized copper mineralization (OPs 298-300, 302, 305) and points with sulfide mineralization (OP 302) were established in the north of the site in the basin of the Atirmey River (northwestern slope of the Cerro Huarango Coto Mountains). The total area of sporadic development of oxidized copper mineralization is about 0.25 km^2.

The inferred ore zone is localized within the Eastern stockwork at the southern and southwestern slopes of the spot height of 1809 m. The Cu and Mo contents vary from 0.1 to 1.5% (a maximum is 7.7%) and 0.05 to 0.07%, respectively. The general visible vertical range of mineralization is 175 m (locally 50–100 m).

Anomalous zones with economic Cu and Mo contents typical of porphyry copper–molybdenum deposits were contoured in the sampled area (Table 4.3-2).

Table 4.3-2. Ranking of Cu and Mo anomalies in the site of detailed prospecting, 2010

		Global mean	Zone of removal	Background		Slightly anomalous		Highly anomalous	Cut-off	Cut-off	Minimum economic	Economic	
Cu	ppm	**20-55**	<25	25-50,00	50-100	100-300	300-500	500-999	1000-2000	2000-3000	3000-5000	5000-10000	> 10000
			Zone of removal	Background	Slightly anomalous	Highly anomalous		Cut-off	Minimum economic	Minimum economic	Economic		
Mo	ppm	**1-1,1**	<2	2-9	10-19	20-49		50-99	100-299	300-499	500-999	> 1000	
			1	2	3	4		5	6	7	8	9	

4.3.4. Showings beyond the sites

Showings of copper mineralization beyond the sites were established in OPs 257, 2946, 2969, 2972, 3554, and 3563. As a rule, these are clusters of quartz veinlets hosted in propilitized rocks. The thickness of veinlets varies from 1–3 to 10–25 cm; the veinlets extend for a few meters to tens of meters. Mineralization comprises hematite, pyrite, and chalcopyrite stringers often accompanied by products of oxidation. Some showings are localized in the Cayan 5 concession; as follows from the available data, they are not of economic importance.

In some observation points the spots of oxidized copper mineralization occur in unaltered rocks without obvious relations to hydrothermal alteration or fractures.

All showings found beyond the ore field are unpromising except for an area on the eastern slope of the Cerro Negro in the northwestern part of the site, where large fragments and blocks of altered volcanic rocks of the Pararin Formation incorporated in loose sediments contain sulfides and oxidized copper mineralization. There are grounds to suggest that the altered rocks in the roof of pluton beyond the eastern boundary of the studied area are promising for prospecting.

5. GEOCHEMICAL EXPLORATION

5.1. Technique

The rock chip panel, channel, composite channel, and grab samples were taken in the studied area (2365 samples in total, including 566 samples from dig holes and trenches); 231 samples were taken from bottom sediments in channels of intermittent streams.

As a result of processing of the available data of sampling, the statistical parameters of particular selections have been estimated. The chemical elements with less than 25–30% significant determinations have been omitted.

The geochemical maps characterizing spatial distributions of Cu, Mo, Ag, Pb, Zn, Au, Bi, Fe, Al, and S have been compiled (Appendix 3, sheets 1–10). The maps of spatial Cu and Mo distribution have been prepared for the Western and Eastern sites (Appendix 5, sheets 1–5). The anomalous area of the Central Site was added to the Western site. Graphic appendices demonstrate Cu and Mo anomalies differing in ranks up to the concentrations corresponding to economic grades characteristic of porphyry copper–molybdenum deposits (Tables 7.2-1, 7.2-2).

The maps of monoelemental geochemical anomalies in the studied area: primary halos in bedrocks (Appendix 3) and in stream sediments (Appendix 4) on a scale of 1 : 25 000; maps of monoelemental geochemical anomalies in the sites of detailed prospecting: secondary halos in loose sediments (Appendix 5) on a scale of 1 : 5000; polyelemental and muliplicative geochemical maps of the studied area: primary halos in bedrocks on a scale of 1 : 25 000 and 1 : 10 000 (Appendix 6) are presented in the report.

Statistical processing of analytical data for particular selections was carried out using Golden Software Surfer 8.0 and Golden Software Grapher 3.0. The background concentrations (C_b), and anomalous concentrations of elements of the first (C_{a1}), second (C_{a2}), and third (C_{a3}) levels were calculated further. Various levels of anomalies were chosen on the basis of the obtained values and taking into account detection limits of elements and frequency of their occurrence.

The maps of geochemical anomalies were plotted in program Surfer using kriging method on a network, which was calculated automatically depending on the total area of sampling and a number of vertical and horizontal lines that divide the surface into columns and rows (squares). For the maps on a scale of 1 : 25 000, a number of lines was 100, while for the maps on scales of 1 : 10 000 and 1 : 5000, a number of lines was 300. The final graphic design was carried out in Autocad 2009 and ArcGIS 9.1.

5.2. Results of geochemical exploration in the Copernic project area

5.2.1. Sampling of stream sediments

The sampling of channel sediments of dry streams was performed beyond the area studied in 2009 and out of the area of detailed prospecting. The objective of stream sediment sampling was prospecting the areas adjoining the Copernic ore field.

As follows from Table 5.2-1, the distribution of elements in bottom sediments of intermittent streams is close to normal. All analyzed elements are characterized by background concentrations close to global means of intermediate igneous rocks or lower than these values.

The background Mo concentration elevated by 2–3 times and still much higher (approximately 10 times) Au concentrations are only exceptions.

The anomalous Cu and Mo concentrations shift to the flanks of the ore field.

Local areas with anomalous Cu points of the 1st–3rd levels (30–60 and 60–80 ppm, respectively) are related to the fields of metasomatic rocks and zones of quartz veinlets. No promising, highly contrasting anomalies were revealed. Only exception is the eastern slope of the Cerro Negro, where prerequisites for discovery of copper mineralization are related to the contact zone of Atirmey and Copernic granitoids with sedimentary and volcanic rocks of the Pararin Formation.

A single area of anomalous Mo points of the 1st–3rd levels (5–10 ppm) is localized along a right tributary of the Choque River. Sporadic anomalous Mo points were detected in the left-bank territory at headwaters of the Campanayos and nameless dry valleys.

Gold is characterized by a high background concentration and low differentiation with formation of extended anomalous zones of the 1st–3rd level (0.02–0.04 ppm) and local anomalous points of the 4th–5th levels (0.04–0.12 ppm), which are localized in the upper reaches of the dry Campnayos and Tararure valleys, where they are confined to the fields of metasomatic alteration. The anomalous field in the lower reaches of the dry Muertos Valley and its nameless left tributary is most likely related to small zones of veins and veinlets; the Au content in one sample was as high as 0.113 ppm.

No Ag concentrations above the detection limit were established in the overwhelming majority of samples. Only four anomalous samples were noted at the left headwaters of the Muertos Valley in the eastern foothills of the Cerro Negro Mountains. In addition, two anomalous Ag points were detected at the eastern flank of the Copernic ore field.

The Pb concentrations in stream sediments commonly correspond to background values in bedrocks and are 2–3 times lower than global mean. In 50–60% of samples, the Pb content is below the detection limit (< 5 ppm). Four low-contrasting anomalous Pb points of the 1st–3rd level (20–50 ppm) were noted, as well as one local anomaly at the eastern flank of the Copernic ore field.

The Zn concentrations commonly correspond to background values in bedrocks. Three low-contrasting dispersion flows of the 1st–3rd levels (50–80 ppm) were established in the upper reaches of the Campanayos Valley and in the upper reaches and at the left headwaters of the Muertos Valley in the eastern foothills of the Cerro Negro Mountains. A local anomalous dispersion flow is documented at the eastern flank of the Copernic ore field.

Table 5.2-1. Statistical indices of concentration levels of elements in stream sediment samples

		Au	Ag	Al	Ba	Ca	Ce	Co	Cu	Cr	Fe	Ga	K	La	Mg	Mn	Mo	Na	Ni	P	Pb	Sr	Ti	V	Y_	Zn
Parámetros	Parameter	ppm	ppm	%	ppm	%	ppm	ppm	ppm	ppm	%	ppm	%	ppm	%	ppm	ppm	%	ppm	ppm	ppm	ppm	%			
Statistics		-0,005	-0,2	-0,01	-5	-0,01	-10	-1	-2	-1	-0,01	-5	-0,01	-2	-0,01	-2	-2	-0,01	-1	-10	-5	-1	-0,01	-1	-0,5	-5
Cantidad de Muestras	Number of samples	210	210	210	195	210	210	210	199	210	210	210	210	210	210	210	210	210	210	204	210	210	210	210	210	209
Valor Mínimo	Minimum value	0,003	0,10	0,31	32	0,11	5	2	3	34	1,06	3	0,06	3	0,08	151	1	0,03	2	85	2,5	6	0,03	15	2	9
Valor Máximo	Maximum value	**0,113**	0,40	3,12	150	2,74	56	30	66	264	**15,01**	26	0,50	29	1,29	867	**17**	0,35	17	1568	201	134	0,36	1256	14	**99**
Media aritmética (0)	Average	0,013	0,10	0,88	92	0,53	19	8	22,3	107	5,04	5	0,24	10	0,39	333	3	0,10	8	535	8,01	30	0,16	172	7	36
	Median	0,012	0,10	0,83	87	0,46	16	7	21	105	3,68	5	0,24	9	0,35	317	3	0,09	8	485	6	25	0,16	101	6	34
	Average deviation	0,005	0,01	0,24	23	0,20	7	3	8,92	30	2,91	3	0,07	4	0,15	86	1	0,03	2	207	4,98	13	0,05	128	2	11
Desviación Estándar (S.D)	Standard deviation	0,009	0,03	0,34	28	0,30	9	4	11,3	39	3,85	4	0,08	5	0,19	115	2	0,04	3	276	14,6	21	0,06	197	2	14
Rangos	Coefficient of variatio	0,674	0,28	0,38	0	0,57	0	0,51	0,51	0,36	0,76	0,72	0,34	0,47	0,48	0,35	0,77	0,37	0,32	0,52	1,82	0,69	0,39	1,14	0,33	0,39
X	**C** background	**0,012**	**0,10**	**0,83**	**87**	**0,46**	**16**	**7**	**21**	**105**	**3,68**	**5**	**0,24**	**9**	**0,35**	**317**	**3**	**0,09**	**8**	**0**	**6**	**25**	**0,16**	**101**	**6**	**34**
x - {x + S.D.}	Ca1	0,021	0,13	1,17	115	0,76	25	11	32,3	143	7,52	9	0,32	14	0,54	432	5	0,13	11	276	20,6	46	0,22	298	8	48
{x + S.D.} – {x + 3(S.D)}	Ca3	0,038	0,19	1,84	170	1,35	44	19	54,9	221	15,21	17	0,49	23	0,92	662	10	0,20	16	828	49,8	87	0,35	692	13	76
> {x+ 5(S.D.)}	Ca5	0,056	0,25	2,51	225	1,95	63	26	77,5	299	22,90	25	0,65	33	1,30	892	15	0,28	21	1379	79,1	128	0,48	1086	17	104
		Au	**Ag**	Al	Ba	Ca	Ce	Co	**Cu**	Cr	**Fe**	Ga	K	**La**	Mg	Mn	**Mo**	Na	Ni	P	**Pb**	Sr	**Ti**	V	Y	**Zn**
CLARC	**Global mean**	g/t	ppm	%	ppm	%	ppm	ppm	ppm	ppm	%	ppm	%	ppm	%	ppm	ppm	%	ppm	ppm	ppm	ppm	%	ppm	ppm	ppm
roca acid	**Intermediate igneous rocks**	0,001	0,05	7,81	750	1,64	90	10	20	25	2,61	20	3,23	45	6,63	540	1	2,75	15	870	*16*	290	0,25	35	31	60
roca medio	**Acid igneous rocks**	0,0005	0,1	9,12	350	4,69	38	24	55	60	5,04	18	1,52	19	1,96	1160	1,1	2,68	30	1050	*16*	400	0,47	150	21	72

Table 5.2-2. Statistical indices of concentration levels of elements in bedrock samples beyond the Copernic ore field

		Au	Ag	Al	As_	Ba	Ca	Ce	Co	Cr	Cu	Fe	Ga	K	La	Li	Mg	Mn	Mo	Na	Ni	P	Pb	S	Sc	Sr	Ti	V	Y	Zn
Parámetros	Parameter	ppm	ppm	%	ppm	ppm	%	ppm	ppm	ppm	ppm	%	ppm	%	ppm	ppm	%	ppm	ppm	%	ppm	ppm	ppm	%	ppm	ppm	%	ppm	ppm	ppm
		-0,005	-0,2	-0,01	-5	-5	-0	-10	-1	-1	-2	-0,01	-5	-0	-2	-5	-0	-2	-2	-0,01	-1	-10	-5	-0	-1	-1	-0	-1	-0,5	-5
Cantidad de Muestras	Number of samples	339	578	578	578	578	578	561	578	578	577	578	561	578	578	561	578	578	578	578	578	578	578	578	561	578	578	578	561	578
Valor Mínimo	Minimum value	0,003	0,10	0,06	2,5	5,0	0,01	5,0	0,5	13,0	1,0	0,20	2,5	0,01	1,0	2,5	0,01	16,0	1,0	0,01	0,50	5,0	2,5	0,01	0,5	2,0	0,01	1,0	0,25	2,5
Valor Máximo	**Maximum value**	**0,076**	**20,90**	**8,89**	**129,0**	**2985,0**	**6,11**	**101,0**	**37,0**	**269,0**	**9239,0**	**15,01**	**23,0**	**0,90**	**63,0**	**32,0**	**6,48**	**6526,0**	**2086,0**	**0,88**	**29,00**	**1787,0**	**336,0**	**4,45**	**10,0**	**445,0**	**0,43**	**799,0**	**20,40**	**1214,0**
Media aritmética (0)	Average	0,011	0,38	1,25	3,4	128,6	0,65	12,1	6,6	79,8	207,1	2,63	4,7	0,31	7,0	7,4	0,56	340,2	16,3	0,13	7,11	509,1	6,4	0,08	2,3	43,4	0,15	61,5	4,46	49,3
	Median	**0,010**	**0,10**	**1,12**	**2,5**	**105,0**	**0,55**	**12,0**	**7,0**	**69,0**	**25,0**	**2,48**	**5,0**	**0,27**	**6,0**	**7,0**	**0,60**	**309,0**	**3,0**	**0,11**	**7,00**	**536,0**	**2,5**	**0,01**	**2,0**	**30,0**	**0,17**	**61,0**	**4,20**	**41,0**
	Average deviation	0,004	0,44	0,51	1,7	67,1	0,37	4,5	2,8	27,5	299,5	0,88	2,2	0,15	2,7	3,3	0,26	140,1	23,1	0,06	2,02	190,6	5,3	0,12	0,9	28,6	0,07	32,5	1,51	23,5
Desviación Estándar (S.D)	**Standard deviation**	**0,007**	**0,86**	**0,93**	**6,4**	**144,8**	**0,66**	**8,0**	**4,2**	**37,1**	**688,6**	**1,72**	**2,7**	**0,18**	**5,1**	**4,3**	**0,40**	**335,2**	**63,8**	**0,11**	**2,89**	**250,9**	**17,0**	**0,32**	**1,2**	**50,1**	**0,09**	**59,4**	**2,19**	**62,8**
Rangos	Coefficient of variation	0,640	2,24	0,75	1,9	1,1	1,02	0,7	0,6	0,5	3,3	0,65	0,6	0,58	0,7	0,6	0,71	1,0	3,9	0,85	0,41	0,5	2,7	4,13	0,5	1,2	0,57	1,0	0,49	1,3
X	**C** background	**0,01**	**0,10**	**1,12**	**2,5**	**105,0**	**0,55**	**12,0**	**7,0**	**69,0**	**25,0**	**2,48**	**5,0**	**0,27**	**6,0**	**7,0**	**0,60**	**309,0**	**3,0**	**0,11**	**7,00**	**536,0**	**2,5**	**0,01**	**2,0**	**30,0**	**0,17**	**61,0**	**4,20**	**41,0**
x - {x + S.D.}	Ca1	0,02	0,96	2,05	8,9	249,8	1,21	20,0	11,2	106,1	713,6	4,20	7,7	0,45	11,1	11,3	1,00	644,2	66,8	0,22	9,89	786,9	19,5	0,32	3,2	80,1	0,26	120,4	6,39	103,8
{x + S.D.} – {x + 3(S.D)}	Ca3	0,03	2,67	3,91	21,7	539,3	2,54	36,0	19,5	180,3	2090,7	7,64	13,0	0,80	21,2	19,8	1,79	1314,7	194,3	0,44	15,67	1288,6	53,4	0,96	5,6	180,4	0,43	239,3	10,78	229,3
> {x+ 5(S.D.)}	Ca5	0,05	4,38	5,78	34,5	828,8	3,87	51,9	27,9	254,5	3467,8	11,09	18,3	1,16	31,3	28,4	2,59	1985,2	321,9	0,67	21,45	1790,4	87,4	1,60	8,0	280,7	0,61	358,1	15,17	354,8

		Au	Ag	Al	As	Ba	Ca	Ce	Co	Cr	Cu	Fe	Ga	K	La	Li	Mg	Mn	Mo	Na	Ni	P	Pb	S	Sc	Sr	Ti	V	Y	Zn
CLARC	**Global mean**	g/t	ppm	%	ppm	ppm	%	ppm	ppm	ppm	ppm	%	ppm	%	ppm	ppm	%	ppm	ppm	%	ppm	ppm	ppm	%	ppm	ppm	%	ppm	ppm	ppm
roca acid	**Intermediate igneous rocks**	0,001	0,05	7,81	1,5	750	1,64	90	10	25	20	2,61	20	3,23	45	35	6,63	540	1	2,75	15	870	*16*	0,03	6	290	0,25	35	31	60

5.2.2. Sampling of bedrocks

Statistical parameters of samples taken from bedrocks beyond the Copernic ore field are given in Table 5.2-2. The elements characterized by less than 25–30% significant determinations have been omitted from statistical processing. Concentrations below the detection limit were substituted by half of this limit.

Comparison of background and global mean concentrations in intermediate and acid igneous rocks has shown the following relationships:

- The Au and Mo background concentrations are 10 and 3 times higher than the global mean concentrations, respectively (gained elements or local specialization).
- The Ag and Pb background concentrations are at least 10 times lower than the global mean concentrations (elements of loss); in most samples concentrations are below the detection limit;
- The Co, Cr, Cu, Fe, Li, Mn, P, V, and Zn background concentrations are approximately equal to global mean concentrations;
- The As, S, Ba, Ca, Ce, Ga, La, Ni, and Ti background concentrations are 3–4 times lower than global mean concentrations;
- To all appearances, ICP analysis underestimates Al. K, Na, Mg, Ca, Sr, Y, and La concentrations by more than 10 times.

As follows from spatial distribution of the major ore elements displayed in monoelemental geochemical maps (Appendix 3, sheets 1, 2), the anomalous Cu and Mo contents emphasize the ore field boundaries and anomalous sites at its flanks. In addition, local Cu anomalies (500–2000 ppm) related to small zones of veins and veinlets are contoured in the southwest of the studied territory (Cayan 5 and Cayan 8 concessions). At the same time, no promising, highly contrasting anomalies were revealed. Only exception is the eastern slope of the Cerro Negro, where prerequisites for discovery of copper mineralization exist in the contact zone of Atirmey and Copernic granitoids with sedimentary and volcanic rocks of the Pararin Formation.

Several scattered low-contrasting Mo anomalies (2–20 ppm) are noted. A local anomaly (8–10 samples; 8–100 ppm Mo) on the right bank of the Choque River merits further verification.

Statistical parameters of samples taken from particular intrusive complexes beyond the ore field (except for anomalous values) are shown in Table 5.2-3.

The maximal average and median Cu concentrations are characteristic of granite and granite porphyry of the Copernic Complex. The background Cu concentrations decreases then in the following order:

- Atirmey Complex, metagranodiorite;
- Trinchera Complex, andesite dikes;
- Choque Complex, gabbro, gabbrodolerite, and diorite;
- Atirmey Complex, leucogranite;
- Atirmey Complex, amphibole–biotite granodiorite.

The maximal average and median Mo concentrations are also characteristic of granite and granite porphyry pertaining to the Copernic Complex. The background Mo concentrations decreases in the following order:

- Atirmey Complex, metagranodiorite;
- Atirmey Complex, leucogranite;
- Trinchera Complex, andesite dikes;
- Atirmey Complex, amphibole–biotite granodiorite;
- Choque Complex, gabbro, gabbrodolerite, and diorite.

Thus, the above relationships support the suggestion that intrusive rocks of the Copernic Complex are ore-bearing, whereas metagranodiorite (biotitized granodiorite) of the Atirmey Complex are the host rocks for Cu–Mo mineralization.

Table 5.2-3. Results of statistical processing of chemical analyses of igneous rocks (amomalous analyses are omitted)

		Au	Ag	Al	Ba	Be	Bi	Ca	Cd	Ce	Co	Cr	Cu	Fe	Ga	K	La	Li	Mg	Mn	Mo	Na	Ni	P	Pb	S	Sc	Sr	Ti	V	Y	Zn
		ppm	ppm	%	ppm	ppm	ppm	%	ppm	ppm	ppm	ppm	ppm	%	ppm	%	ppm	ppm	%	ppm	ppm	%	ppm	ppm	ppm	%	ppm	ppm	%	ppm	ppm	ppm
Trinchera Complex: andesite dikes	average	0,009	0,1	2,39	101	0,2	4,65	1,4	0,6	12,7	8,4	44	67	2,9	7,65	0,4	6,9	8,3	0,8	376	2,7	0,3	5,4	795	7,7	0,0	2,1	117	0,2	70	5,1	53
	median	0,007	0,1	2,54	92	0,1	1,25	1,6	0,5	12,0	9,0	28	60	3,3	9,00	0,2	6,0	10,0	1,0	349	3,0	0,2	5,0	910	2,5	0,0	2,0	143	0,2	58	4,4	65
Copernic Complex: granite, granite porphyry	average	0,011	0,2	0,85	110	0,2	1,78	0,3	0,5	8,6	2,0	83	**125**	1,6	2,75	0,3	5,7	3,3	0,3	236	**35,0**	0,1	3,9	347	4,2	0,1	1,7	36	0,1	20	3,2	39
	median	0,012	0,1	0,85	110	0,1	1,25	0,2	0,3	5,0	2,0	80	**119**	1,5	1,25	0,3	6,0	1,3	0,3	244	**9,0**	0,1	4,0	296	2,5	0,0	1,0	32	0,1	14	2,8	33
Atirmey Complex: metagranodiorite	average	0,011	0,1	1,28	137	0,2	1,73	0,5	0,5	11,2	6,3	70	99	2,6	4,61	0,4	6,7	6,3	0,6	381	**10,2**	0,1	6,4	504	6,0	0,0	3,1	43	0,2	64	5,0	58
	median	0,011	0,1	1,19	129	0,1	1,25	0,5	0,3	12,0	6,0	70	70	2,6	5,00	0,4	6,0	6,0	0,6	367	5,0	0,1	6,0	543	2,5	0,0	3,0	33	0,2	62	4,9	53
Atirmey Complex: biotite–amphibole granodiorite	average	0,010	0,1	1,19	150	0,1	1,52	0,7	0,3	11,5	7,0	68	25	2,5	4,47	0,3	6,5	8,5	0,7	325	2,9	0,1	7,1	573	4,0	0,0	2,3	36	0,2	65	4,3	41
	median	0,010	0,1	1,16	137	0,1	1,25	0,6	0,3	12,0	7,0	66	11	2,5	5,00	0,3	6,0	8,0	0,7	326	2,0	0,1	7,0	586	2,5	0,0	2,0	30	0,2	67	4,2	40
Atirmey Complex: leucogranite	average	0,011	0,1	0,57	70	0,1	4,83	0,2	0,3	14,6	3,3	107	28	1,4	2,24	0,2	9,6	3,4	0,2	202	3,6	0,1	6,9	261	3,8	0,0	1,3	13	0,1	23	5,5	24
	median	0,011	0,1	0,45	61	0,1	5,00	0,2	0,3	16,0	2,0	100	17	1,2	1,25	0,2	9,0	1,3	0,1	155	3,0	0,1	7,0	202	2,5	0,0	1,0	10	0,1	9	5,7	14
Choque Complex: gabbro, gabbrodolerite, diorite	average	0,012	0,1	**3,32**	88	0,2	1,76	2,0	0,4	6,5	10,8	51	47	3,3	7,48	0,2	4,9	8,1	0,8	291	2,6	0,4	9,1	651	5,3	0,0	3,0	160	0,2	143	3,6	51
	median	0,012	0,1	**3,16**	78	0,1	1,25	1,9	0,3	5,0	10,0	46	37	3,4	7,00	0,1	4,0	7,0	0,8	282	2,0	0,4	7,0	660	2,5	0,0	3,0	155	0,2	138	3,2	44

Elements with insufficient number of significant determinations: **Ag Be Bi Cd Pb**

Elements practically devoid of significant determinations: As Ge Hg In Nb Re Sb Se Sn Te Tl U W Zr

Correlation coefficients and matrices were calculated for the selections characterizing particular intrusive complexes (Appendix 10). The youngest Trinchera Complex almost unaffected by metasomatic alteration stands out in degree of contrast (occurrence of significant positive and negative correlation coefficients). The degree of contrast decreases further in the following order:

- Atirmey Complex, leucogranite;
- Copernic Complex, granite and granite porphyry;
- Atirmey Complex, amphibole–biotite granodiorite;
- Atirmey Complex, metagranodiorite (the rocks metasomatically altered under effect of intrusions pertaining to the Copernic Complex);
- Choque Complex, gabbro, gabbrodolerite, and diorite (the oldest intrusive rocks in the studied area).

Except the dikes of the Trinchera Complex, copper does not reveal linear correlation with other chemical elements. This indicates that copper was redistributed in the course of superimposed processes and now occurs largely in form of supergene minerals, at least, at the surface.

5.3. Results of geochemical exploration in the Copernic ore field

The common selection of samples created for the Western site covers the entire mineralized zone. Statistical parameters of this selection are shown in Table 5.3-1. The average Cu content is 1715.63 ppm (median is 1083 ppm); the average Mo content is 75.14 ppm (median is 37 ppm). Correlation coefficients and correlation matrix are presented in Table 5.3-2. Cu reveals significant correlation with Ag and Li, whereas Mo is correlated (to a certain extent) with Au.

Statistical parameters of the selections of samples pertaining to the main ore zones in the Copernic ore field (Fig. 52) computed with Excel and Spss 10.0 programs were used for calculation of series of normalized productivities for all detected chemical elements (5.3-3). The selection principle of separation, localization of samples from anomalous zones, taking into account their hypsometric position

The normalized productivity is a ratio of the average concentration of elements to the local background value of unaltered rocks or global mean value.

The following conclusions can be drawn from the consideration of these series.

(1) The ore field is divided in a number of sites differing in geochemical specialization.

(2) In set of elements and concentration factor, series 1, 6, and probably 3 correspond to the geochemical series characteristic of porphyry Cu–Mo mineralization.

(3) Series 2 reflects the most intense redistribution of copper due to the superimposed hydrothermal process and subsequent supergene alteration.

(4) Series 4 and 5 characterize the sites with the most active postore hydrothermal and tectonic processes.

(5) Series 7 is based on the samples taken beyond the ore field and reflects, in our opinion, local geochemical specialization of rocks.

Correlation graphs and matrices for the above selections are shown in Appendix 7.

Table 5.3-1. Results of statistical processing of chemical analyses from the Western site of the Copernic ore field

	Au	Ag	Al	Ba	Be	Bi	Ca	Cd	Ce	Co	Cr	Cu	Fe	Ga	K	La	Li	Mg	Mn	Mo	Na	Ni	P	Pb	S	Sc	Sr	Tl	V	Y	Zn
min	0,00	0,05	0,02	7,00	0,13	1,25	0,01	0,25	0,25	0,25	15,00	11,00	0,21	1,25	0,00	0,50	1,25	0,01	28,00	0,50	0,00	1,00	0,25	1,25	0,00	0,25	3,00	1,25	1,00	0,13	1,25
max	0,03	10,10	4,45	566,00	1,20	23,00	2,02	2,00	42,00	219,00	327,00	10000,00	15,00	36,00	0,97	21,00	18,00	3,05	2956,00	1557,00	0,24	49,00	3182,00	901,00	3,91	6,00	649,00	11,00	563,00	32,90	623,00
average	0,01	0,67	1,27	110,26	0,25	1,91	0,40	0,35	12,94	10,47	80,67	1715,63	2,34	3,34	0,22	6,31	4,58	0,64	354,87	75,14	0,07	6,51	525,82	10,69	0,07	2,24	62,45	1,40	39,70	5,55	64,98
median	0,01	0,50	1,21	86,50	0,13	1,25	0,36	0,25	13,00	7,00	74,00	1083,00	2,25	1,25	0,18	6,00	1,25	0,59	284,00	37,00	0,06	6,00	521,50	2,50	0,01	2,00	44,00	1,25	36,00	5,05	58,00

Table 5.3-2. Correlation coefficient matrices: the Western site of the Copernic ore field

	AU	AG	AL	BA	BE	BI	CA	CD	CE	CO	CR	CU	FE	GA	K	LA	LI	MG	MN	MO	NA	NI	P	PB	S	SC	SR	TL	V	Y	ZN
AU	1	0.393	-0.27	-0.22	-0.06	-0.01	-0.09	-0.42	-0.16	-0.06	-0.05	0.304	0.103	-0.05	-0.26	-0.1	-0.06	-0.13	-0.1	0.476	-0.29	-0.15	0.072	0.199	0.131	-0.34	-0.04	.	0.109	-0.07	-0.05
AG	0.393	1	0.081	-0.03	0.197	0.015	0.019	-0.02	-0.28	0.153	-0.13	0.605	0.314	0.521	-0.18	-0.17	0.264	0.153	0.069	0.206	-0.2	0.043	0.087	0.535	-0.03	-0.09	-0.09	-0.04	0.39	-0.01	0.141
AL	-0.27	0.081	1	0.153	0.298	-0	0.77	0.112	0.071	0.413	-0.55	0.233	0.455	0.196	0.16	-0.09	0.627	0.896	0.627	-0.16	0.231	0.339	0.386	-0.03	-0.22	0.819	0.373	0.212	0.501	0.212	0.671
BA	-0.22	-0.03	0.153	1	-0.09	-0.08	-0.11	0.097	0.295	-0.08	-0.16	-0.08	0.186	0.27	0.608	0.213	0.08	-0.01	-0.06	0.018	0.414	-0.12	0.06	-0.07	0.098	0.515	0.436	-0.01	0.153	-0.02	-0.1
BE	-0.06	0.197	0.298	-0.09	1	0.005	0.206	-0.26	-0.18	0.3	-0.04	0.454	0.059	-0.21	-0.12	-0.12	0.418	0.29	0.123	-0.04	-0.24	0.315	0.081	-0	0.032	0.162	0.074	.	0.01	0.16	0.156
BI	-0.01	0.015	-0	-0.08	0.005	1	-0.04	-0.09	0.142	0.047	-0.04	0.077	0	-0.13	-0.04	0.09	-0.05	-0.01	-0.01	0.087	-0.12	0.017	-0.08	-0.02	-0.05	-0.19	0.002	-0.01	0.002	-0.03	-0.03
CA	-0.09	0.019	0.77	-0.11	0.206	-0.04	1	0.199	0.025	0.446	-0.36	0.147	0.277	0.076	-0.19	-0.16	0.489	0.717	0.653	-0.17	0.104	0.381	0.472	0.019	-0.2	0.501	0.249	0.198	0.333	0.395	0.643
CD	-0.42	-0.02	0.112	0.097	-0.26	-0.09	0.199	1	-0.03	0.183	0.049	-0.07	0.22	0.35	0.11	0.038	0.113	0.085	0.278	0.019	0.225	0.098	0.088	0.151	0.064	0.105	-0.03	0.009	0.198	-0.05	0.255
CE	-0.16	-0.28	0.071	0.295	-0.18	0.142	0.025	-0.03	1	-0.07	-0.11	-0.29	-0.15	-0.04	0.208	0.894	-0.17	-0.11	-0.03	-0.22	0.214	-0.23	0.388	-0.16	-0.17	0.026	0.168	.	-0.15	0.491	-0.1
CO	-0.06	0.153	0.413	-0.08	0.3	0.047	0.446	0.183	-0.07	1	-0.19	0.369	0.184	-0	-0.12	-0.06	0.559	0.372	0.792	-0.03	-0.12	0.535	0.231	0.071	-0.11	0.289	0.006	0.027	0.134	0.39	0.442
CR	-0.05	-0.13	-0.55	-0.16	-0.04	-0.04	-0.36	0.049	-0.11	-0.19	1	-0.18	-0.28	-0.25	-0.13	-0.04	-0.41	-0.48	-0.29	0.101	-0.15	0.19	-0.18	0.008	0.148	-0.53	-0.25	-0.08	-0.31	0.012	-0.32
CU	0.304	0.605	0.233	-0.08	0.454	0.077	0.147	-0.07	-0.29	0.369	-0.18	1	0.074	0.046	-0.2	-0.12	0.561	0.294	0.246	0.035	-0.26	0.16	0.088	0.151	-0.15	0.098	-0.05	0.016	0.084	0.167	0.317
FE	0.103	0.314	0.455	0.186	0.059	0	0.277	0.22	-0.15	0.184	-0.28	0.074	1	0.657	0.212	-0.14	0.088	0.437	0.313	0.197	0.23	0.141	0.373	0.49	0.377	0.168	0.246	0.141	0.79	-0.03	0.363
GA	-0.05	0.521	0.196	0.27	-0.21	-0.13	0.076	0.35	-0.04	-0	-0.25	0.046	0.657	1	0.265	-0.07	0.046	0.15	0.148	0.123	0.28	-0.17	0.165	0.736	-0.05	0.287	0.023	.	0.862	-0.04	0.141
K	-0.26	-0.18	0.16	0.608	-0.12	-0.04	-0.19	0.11	0.208	-0.12	-0.13	-0.2	0.212	0.265	1	0.193	0.033	-0	-0.11	-0	0.508	-0.06	0.023	-0.12	0.155	0.646	0.266	0.009	0.217	-0.05	-0.12
LA	-0.1	-0.17	-0.09	0.213	-0.12	0.09	-0.16	0.038	0.894	-0.06	-0.04	-0.12	-0.14	-0.07	0.193	1	-0.08	-0.2	-0.09	-0.11	0.223	-0.2	0.105	-0.15	-0.05	0.072	0.072	-0.06	-0.17	0.423	-0.12
LI	-0.06	0.264	0.627	0.08	0.418	-0.05	0.489	0.113	-0.17	0.559	-0.41	0.561	0.088	0.046	0.033	-0.08	1	0.843	0.642	-0.1	-0.17	0.305	0.185	-0.04	-0.2	0.432	-0.03	.	0.15	0.267	0.634
MG	-0.13	0.153	0.896	-0.01	0.29	-0.01	0.717	0.085	-0.11	0.372	-0.48	0.294	0.437	0.15	-0	-0.2	0.843	1	0.635	-0.15	0.042	0.366	0.395	0.013	-0.23	0.708	0.141	0.233	0.482	0.283	0.727
MN	-0.1	0.069	0.627	-0.06	0.123	-0.01	0.653	0.278	-0.03	0.792	-0.29	0.246	0.313	0.148	-0.11	-0.09	0.642	0.635	1	-0.1	0.011	0.454	0.373	0.104	-0.16	0.365	0.103	0.139	0.268	0.362	0.704
MO	0.476	0.206	-0.16	0.018	-0.04	0.087	-0.17	0.019	-0.22	-0.03	0.101	0.035	0.197	0.123	-0	-0.11	-0.1	-0.15	-0.1	1	-0.02	-0.06	-0.11	0.243	0.248	-0.23	0.013	-0.03	0.141	-0.15	-0.12
NA	-0.29	-0.2	0.231	0.414	-0.24	-0.12	0.104	0.225	0.214	-0.12	-0.15	-0.26	0.23	0.28	0.508	0.223	-0.17	0.042	0.011	-0.02	1	-0.13	0.065	-0.05	0.224	0.313	0.378	0.016	0.205	-0.19	0.031
NI	-0.15	0.043	0.339	-0.12	0.315	0.017	0.381	0.098	-0.23	0.535	0.19	0.16	0.141	-0.17	-0.06	-0.2	0.305	0.366	0.454	-0.06	-0.13	1	0.132	0.02	-0.08	0.01	-0.01	0.122	0.138	0.25	0.375
P	0.072	0.087	0.386	0.06	0.081	-0.08	0.472	0.088	0.388	0.231	-0.18	0.088	0.373	0.165	0.023	0.105	0.185	0.395	0.373	-0.11	0.065	0.132	1	0.081	-0.07	0.263	0.108	0.084	0.265	0.819	0.363
PB	0.199	0.535	-0.03	-0.07	-0	-0.02	0.019	0.151	-0.16	0.071	0.008	0.151	0.49	0.736	-0.12	-0.15	-0.04	0.013	0.104	0.243	-0.05	0.02	0.081	1	0.023	-0.12	-0.06	0.012	0.662	-0.05	0.169
S	0.131	-0.03	-0.22	0.098	0.032	-0.05	-0.2	0.064	-0.17	-0.11	0.148	-0.15	0.377	-0.05	0.155	-0.05	-0.2	-0.23	-0.16	0.248	0.224	-0.08	-0.07	0.023	1	-0.24	0.066	-0.01	-0.04	-0.24	-0.18
SC	-0.34	-0.09	0.819	0.515	0.162	-0.19	0.501	0.105	0.026	0.289	-0.53	0.098	0.168	0.287	0.646	0.072	0.432	0.708	0.365	-0.23	0.313	0.01	0.263	-0.12	-0.24	1	0.209	.	0.28	0.234	0.424
SR	-0.04	-0.09	0.373	0.436	0.074	0.002	0.249	-0.03	0.168	0.006	-0.25	-0.05	0.246	0.023	0.266	0.072	-0.03	0.141	0.103	0.013	0.378	-0.01	0.108	-0.06	0.066	0.209	1	0.051	0.205	-0.01	0.066
TL	.	-0.04	0.212	-0.01	.	-0.01	0.198	0.009	.	0.027	-0.08	0.016	0.141	.	0.009	-0.06	.	0.233	0.139	-0.03	0.016	0.122	0.084	0.012	-0.01	.	0.051	1	0.161	.	0.244
V	0.109	0.39	0.501	0.153	0.01	0.002	0.333	0.198	-0.15	0.134	-0.31	0.084	0.79	0.862	0.217	-0.17	0.15	0.482	0.268	0.141	0.205	0.138	0.265	0.662	-0.04	0.28	0.205	0.161	1	0.002	0.332
Y	-0.07	-0.01	0.212	-0.02	0.16	-0.03	0.395	-0.05	0.491	0.39	0.012	0.167	-0.03	-0.04	-0.05	0.423	0.267	0.283	0.362	-0.15	-0.19	0.25	0.819	-0.05	-0.24	0.234	-0.01	.	0.002	1	0.267
ZN	-0.05	0.141	0.671	-0.1	0.156	-0.03	0.643	0.255	-0.1	0.442	-0.32	0.317	0.363	0.141	-0.12	-0.12	0.634	0.727	0.704	-0.12	0.031	0.375	0.363	0.169	-0.18	0.424	0.066	0.244	0.332	0.267	1

Table 5.3-3. Series of normalized productivity in (1–6) ore halos and (7) beyond the ore field

Selection	Site - Lote	1	2	3	4	5	6	7	8	9	10	11	12	13	14	15	16	17	18	19	20	21	22	23	24	25	26	27	28
1	Western, NW subzone	**Mo**	**Cu**	S	**Ag**	Cr	Sr	La	Y	Ga	Ce	**Pb**	Ba	**Au**	P	**Zn**	K	Na	Sc	Ni	**Fe**	Al	Co	Mn	Ca	Li	Mg	Ti	V
	Oeste, subzona N-Oeste	**162,03**	**33,55**	22,62	**4,31**	1,71	1,55	1,54	1,52	1,48	1,45	**1,32**	1,23	**1,22**	1,17	**1,10**	1,06	1,03	0,85	0,84	**0,82**	0,75	0,69	0,67	0,66	0,59	0,58	0,51	0,49
2	Western	**Cu**	**Mo**	**Ag**	**Pb**	Co	S	Ga	**Zn**	Li	Y	Sc	Sr	Mn	**Au**	Mg	Ni	Al	La	Ca	P	Cr	Ba	**Fe**	V	Ti	K	Ce	Na
	Oeste	**172,30**	**77,00**	**9,98**	**6,26**	2,35	2,23	1,94	**1,91**	1,73	1,65	1,49	1,42	1,34	**1,29**	1,28	1,19	1,18	1,16	1,05	1,03	1,00	0,99	**0,95**	0,89	0,88	0,76	0,66	0,65
3	Central	**Mo**	**Cu**	**Ag**	S	**Pb**	Sr	Ca	Co	Sc	**Zn**	**Au**	Na	Al	Ni	Li	Cr	Mn	**Fe**	Y	P	Mg	V	Ti	La	Ba	Ce	K	Ga
	Centro	**35,35**	**28,60**	**7,16**	6,45	**3,65**	1,64	1,56	1,54	1,41	**1,40**	**1,36**	1,27	1,20	1,15	1,14	1,13	1,08	**1,08**	1,06	1,00	0,99	0,95	0,92	0,77	0,71	0,70	0,59	0,47
4	Eastern	**Cu**	**Ag**	**Mo**	S	**Pb**	**Zn**	Ca	**Au**	Sr	Ga	Na	Ni	Mn	Sc	Al	Cr	**Fe**	Co	Mg	Li	Y	Ba	P	V	K	La	Ti	Ce
	Este, cota 1809	**128,62**	**26,04**	**22,47**	3,73	**3,30**	**1,80**	1,71	**1,59**	1,54	1,49	1,45	1,41	1,41	1,38	1,38	1,12	**1,07**	1,05	1,04	1,00	0,98	0,95	0,95	0,94	0,93	0,90	0,83	0,80
5	Eastern, NW subzone	**Mo**	**Cu**	S	**Ag**	Ga	Sc	Ba	K	**Pb**	Sr	**Zn**	Na	Al	V	Ti	Ca	Mg	Mn	**Au**	**Fe**	Y	Co	Li	P	La	Ni	Cr	Ce
	Este, subzona N-Oeste	**44,88**	**30,08**	7,78	**4,11**	2,39	2,32	2,23	2,15	**2,04**	1,88	**1,79**	1,73	1,60	1,60	1,51	1,48	1,47	1,42	**1,41**	**1,28**	1,27	1,18	1,16	1,09	1,06	1,05	0,89	0,65
6	Northern	**Mo**	**Cu**	S	**Ag**	**Zn**	Mn	Ga	Sc	Mg	Ni	Li	Ti	Co	**Pb**	K	Ba	Ca	V	Al	**Fe**	Cr	Na	Y	P	La	Sr	**Au**	Ce
	Norte	**86,12**	**25,38**	13,06	**11,93**	**3,39**	2,30	1,88	1,84	1,64	1,55	1,52	1,46	1,41	**1,36**	1,35	1,35	1,33	1,32	1,27	**1,21**	1,19	1,16	1,16	1,14	1,05	0,96	**0,86**	0,74
7	Beyond the ore field, **Rocas no alteraciones**	**Mo**	**Cu**	**Ag**	S	**Pb**	Ga	Ca	Na	La	V	Li	Ba	K	Ni	Ti	Co	Ce	Sc	Y	**Zn**	**Au**	Cr	Mn	**Fe**	Al	Sr	P	Mg
		4,59	**4,54**	**3,51**	3,36	**2,46**	2,01	1,60	1,47	1,45	1,37	1,31	1,27	1,25	1,19	1,16	1,16	1,15	1,14	1,13	**1,10**	**1,09**	1,08	1,05	**1,05**	1,04	1,04	0,99	0,96

Elements with concentrations mainly below the detection limit (omitted from calculation)

Be	Bi	Cd	Ge	Hg	In	Nb	Re	Sb	Se	Sn	Te	U	W	Tl
ICP/AQR														
ppm	ppm	ppm	ppm	ppm	ppm	ppm	ppm	ppm	ppm	ppm	ppm	ppm	ppm	ppm
0,5	5	1	10	1	10	10	5	5	5	10	5	10	10	5

Elements of ore level (active gain)

Elements of weak gain

Elements of background level

Elements of removal

Fig. 52. Location of mineralized sites and zones in the Copernic ore field.

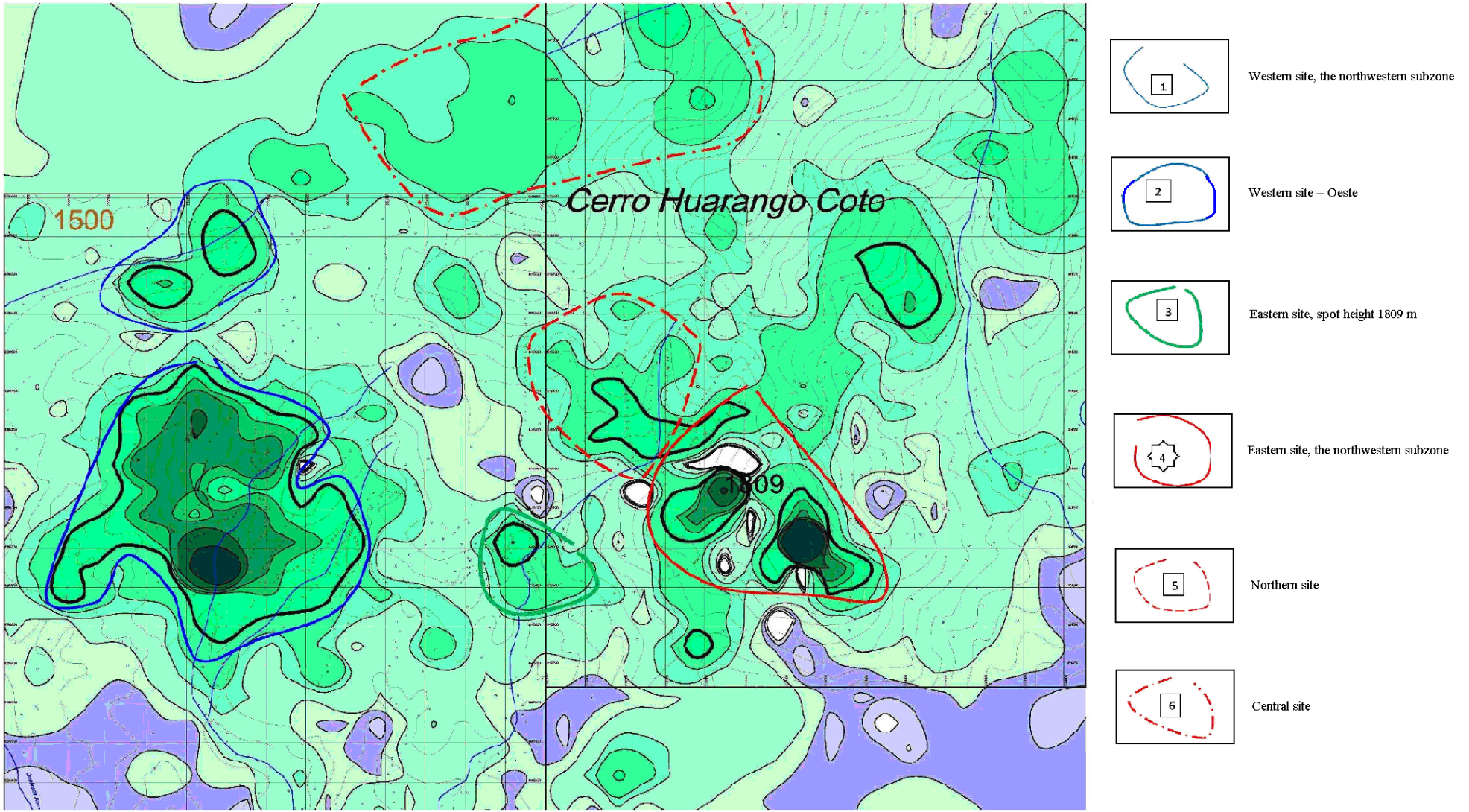
1500
Cerro Huarango Coto
1809
1
Western site, the northwestern subzone
2
Western site – Oeste
3
Eastern site, spot height 1809 m
4
Eastern site, the northwestern subzone
5
Northern site
6
Central site

5.4. Conclusions

(1) The results of statistical processing of the selections characterizing intrusive rock complexes (except the samples with anomalous concentrations) support the suggestion that intrusive rocks of the Copernic Complex are ore-bearing, whereas metagranodiorite (biotitized granodiorite) of the Atirmey Complex are the rocks that host Cu–Mo mineralization.

(2) The Copernic ore field and its concentrically zoned structure is clearly displayed in the maps of monoelemental geochemical anomalies in the studied area (primary halos in bedrocks) on a scale of 1 : 25 000 and 1 : 10 000. The centers of Mo anomalies are shifted somewhat outward relative to Cu anomalies.

(3) The Cu and Mo anomalies extend from west to east for more than 4 km as a belt about 2 km wide, which is dismembered into a number of blocks.

(4) Several local, highly contrasting Cu anomalies are localized within the ore field. One of such anomalies corresponds to the Western site, and the second, more elongated, partly contours the Eastern site (Appendix 8, sheet 1).

(5) Highly contrasting Mo anomalies are localized at the margins of the Western site (outer zone of the stockwork) and in the north of the ore field (Appendix 8, sheet 2).

(6) In general, the geochemical links between Cu, Mo, Pb, Ag, and Zn and the levels of their anomalous concentrations, as well as their configuration and mutual arrangement correspond or, at least, are very close to the anomalies characteristic of porphyry copper mineralization.

(7) The postmineral tectonics and related hydrothermal redistribution of metals exerted appreciable effect on the Western and Central sites. These sites are distinguished by higher Co, Mo, Mn and Mg concentrations, likely, as a result of deeper erosion level.

Fig. 53. Interpetation of geochemical anomalies in the Copernic project area.

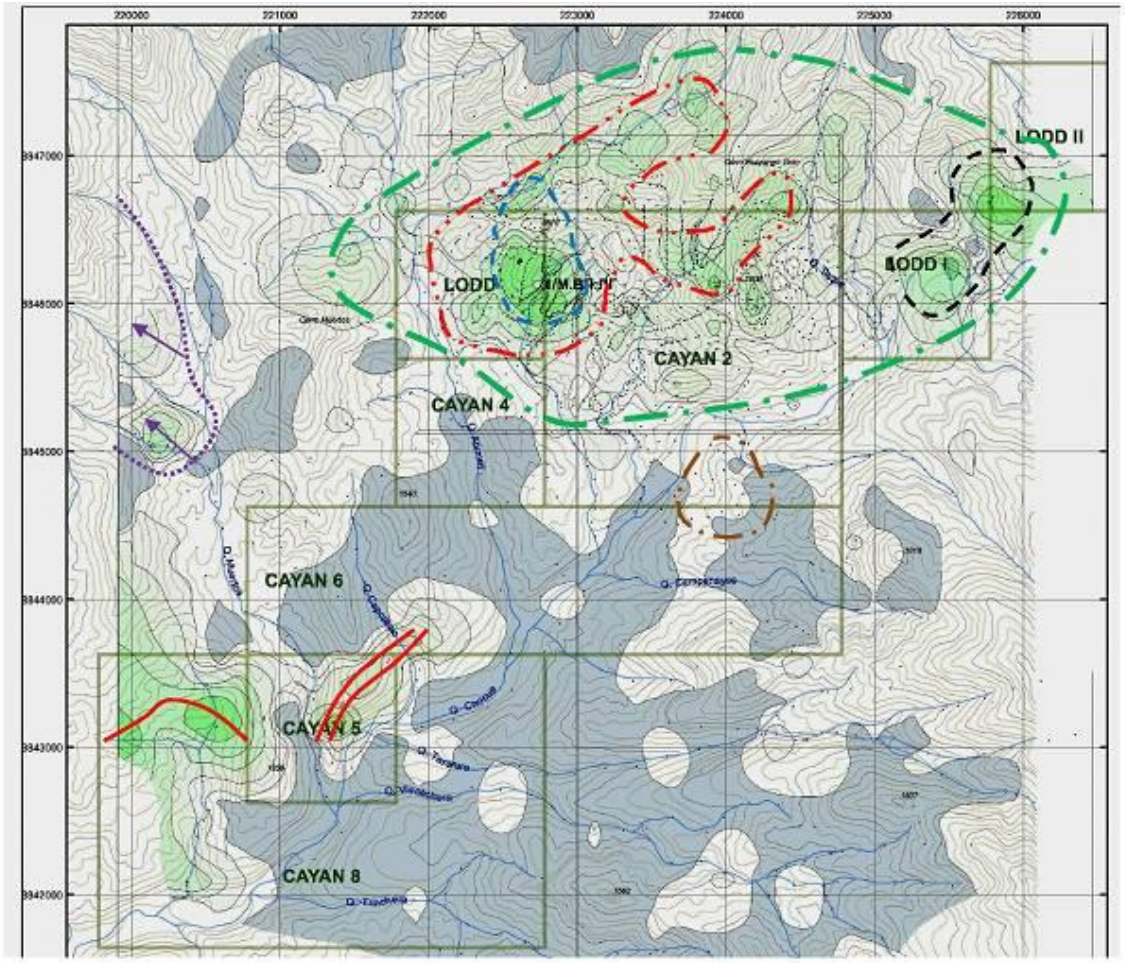

Boundary of the Copernic ore field

Quartz–sulfide zones in Cayan 5 concession

Promising zone on the eastern slope of the Cerro Negro Mountains

Mo anomaly in the left-bank area of the Choque River basin

Inferred Eastern zone of sulfide mineralization

Site of local sulfide occurrences

Inferred boundary of the Western zone

6. PRELIMINARY CHARACTERIZATION OF ORE

To date, only oxidized copper mineralization is known in the studied area. The results of prospecting performed in 2010 give grounds to suggest occurrence of sulfide Cu and Cu–Mo ores. The samples taken in some samples contain visible sulfide mineralization.

The oxidized copper mineralization is widespread and especially in stockworks. The so-called copper greens are mainly composed of secondary copper minerals such as: atacamite, malachite, azurite, chrysocolla etc. The local geological practice generalizes all the secondary copper oxide minerals and ore to "oxide copper ore»-« los minerales oxidos de cobre» or «oxiCu». Their composition varies considerably, depending on the source of ores and host rocks.

Copper greens are the most abundant in stockworks hosted in propylitized metagranodiorite and in ore-bearing granite porphyry. “OxiCu” veinlets are as thick as fractions of a millimeter and only rarely reach 5–8 mm in thickness. Copper greens are often dispersed in rocks, which in this case acquire greenish hue. Such a hue is clearly seen at washed surfaces in dry valleys and in rocky outcrops at drainage divides. The samples taken from the high-grade oxidized ore contain higher than 1 % Cu. Copper greens develop after quartz veinlets, quartz–feldspar veins, zones of propylitization, along fractures, and in rock as a whole. The areas with copper greens are shown in the geological map by a special pattern and out-of-scale symbols.

Pyrite, chalcopyrite, and molybdenite were identified in the studied area. In quartz veins and stockworks, copper sulfides are often associated with hematite (less 1%).

At OP 2644, a block of biotite–hornblende granodiorite incorporated into the tectonic zone contains chalcopyrite and molybdenite grains a few millimeters in size (up to 5–10%).

At OP 302, a quartz vein 15–30 cm thick contains molybdenite and Fe hydroxides replacing sulfides.

At OP 1527, pyrite and chalcopyrite were identified in granodiorite. Sulfide grains as large as a few millimeters occupy up to 5% of rock volume.

At OP 2972, a composite vein comprises veinlets (15–50 cm) of white quartz and sheets of silicified host rock replaced with chlorite and epidote, which are sandwiched between the veinlets; quartz breccia is noted. Ore minerals—hematite, pyrite, and chalcopyrite—occur as grains a few millimeters in size.

It is suggested that sulfide ore occurs beneath the oxidized mineralization at a depth of no less than 50 m, where it is hosted in metagranodiorite crossed by quartz veinlets. A transition zone probably exists between sulfide ore and products of their oxidation.

The sulfide mineralization related to gabbro and diorite is noteworthy. At OP 2871, a tectonic zone developing after diorite contains balls of melanocratic medium-grained diorite 10–20 cm in diameter with pyrite and sporadic chalcopyrite grains <1 mm in diameter.

The set of 30 representative samples of oxidized copper ore collected in 2009 was analyzed in order to estimate their leachability (Supplementary Appendix 5). The results obtained for the samples with different Cu content are summarized in Table 6-1. As can be seen from this table, the higher Cu grade in the oxidized ore the higher percentage of leached copper (recovery) is. At average Cu grade in ore ≥ 0.3%, about 85–90% Cu can be recovered. Under industrial conditions, recovery of 80–85% seems to be feasible.

Table 6-1. Leachability of various copper species in oxidized ore.

	Oxidized copper	Copper dissolved in H2SO4	Bulk copper	% CuOx of bulk Cu	**% CuSsulf of bulk Cu**	% CuSsulf – % CuOx	Bulk Cu – % CuSsulf
Analysis	ISP-112	ISP-137	ISP-140				
	CuOx	CuSsulfurico	**Cu**				
Intervals of Cu content	AA	H_2SO_4/AA	AA	AA	**H_2SO_4/AA**		
	ppm	ppm	ppm				
	1	2	3	4	5	6	7
Aver. <0.3% Cu	1 446	1 618	2 127	69,91	**77,64**	7,73	22,36
Aver. 0.3-1.0% Cu	4 717	5 127	5 970	81,77	**89,31**	7,54	15,96
Aver. > 1.o% Cu	25 054	25 760	28 620	83,70	**89,09**	5,39	10,91

Speciation of Mo remains poorly studied. In the occurrences with identified molybdenite, the Mo content does not exceed 0.05%, whereas in geochemical anomalies Mo concentrations reach 0.1–0.5%. On the basis of indirect data, it may be suggested that near the surface Mo is fixed in ferrimolybdite $Fe_2O_3 \cdot 2MoO_3 \cdot 7H_2O$ that contains 60 wt % Mo; a part of Mo occurs as molybdenite in quartz veins.

7. ESTIMATION OF RESOURCES

7.1. Copper

On the basis of the available data, the origin of the Copernic ore field, at least, as concerns the Western and Central sites is suggested as follows:

- a porphyry-type Cu–Mo deposit with stringer–disseminated mineralization hosted in the Late Cretaceous granitoids was formed first;
- then it was involved in faulting and affected by hydrothermal solutions; as a result, quartz veinlets and veins were formed;
- low-temperature hydrothermal solutions oxidized and redistributed the primary sulfide mineralization and formed oxidized ore containing 0.1–1.0% Cu.

The forecasted copper resources were estimated on the basis of two hypothetical models of the deposit considered in 2009. It was assumed that the deposit is composed of only oxidized copper and molybdenum ore in contours of anomalies bounded by conditionally cutoff of 0.1% Cu; the average Cu grade within this contour is above 0.3% Cu. On the basis of geophysical data it is suggested that the depth of ore is no less than 200–250 m, i.e., approximately 100 m below the lowermost samples involved in calculation.

The forecasted resources were estimated separately for the Western (Oeste), Central (Centro), and Eastern (Este) sites. In the degree of their substantiation, the resources fit category P_3 in the classification adopted in Russia (speculative resources).

The samples used in estimation were taken from dig holes, trenches, and outcrops. The average Cu grade in ore was accepted to be average of the sum of all samples within the cutoff contour of 0.1% Cu. The vertical range of copper mineralization corresponds to a distance between the lowermost and uppermost samples with significant Cu concentrations within every contour of anomaly. The lower edge of a hypothetical orebody is horizontal and the uppermost edge coincides with present-day topography.

Graphic modeling and estimation of resources were conducted using AutoCAD and Geol-DH programs. The location of contours bounding the areas involved in estimation of copper resources is shown in Appendix 8, sheet 1. The scheme is based on a digital topographic

map on a scale of 1 : 25 000 (map sheet 21h-II-SE) with solid contour lines drawn at intervals of 25 m acquired from the Organismo de formalizacion del a propiedad informal.

The Western site (Oeste). Contours with Cu content > 0.1% Cu (278 samples) have been drawn. The volume of ore was calculated in two variants: at the lowermost samples within these contours (above 1400 masl) and at a level 100 m deeper (above 1300 masl). The volume of ore was calculated as a sum of volumes between the adjoining contour lines limited in the horizontal direction by contours of conditionally cutoff contents 0.1% Cu. The lower edge of the orebody is accepted at 1400 masl. In addition, the isolated anomalies at the northern flank of the site within the inferred stockwork were involved in calculation.

The Central site(Centro). The area within a contour of 0.1% Cu (31 samples) has been selected. Because of insufficient number of samples, the average Cu grade within this contour was accepted by analogy with the Western site.

The Eastern Site (Este). The area within a contour of 0.1% Cu (93 samples) has been selected. The volume of ore was calculated as a sum of the volumes between adjoining contour lines limited by the chosen cutoff content.

The calculated mass of ore within the contours with cutoff 0.1% Cu is shown in Tables 7.1-1 and 7.1-2. The total forecasted copper resources of the Western and Eastern sites are given in Table 7.1-3.

Table 7.1-1. Calculated ore mass within anomalous contours (cutoff is 0.1% Cu) in the Western site of the Copernic ore field

Copernic ore field, site "OESTE"									
Level	Area 1	Area 2	Area 3	Area at a level, m2	Volume between the adjacent planes, m3	Total volume at different depths, m3	Mass of ore, t at density of 2.55 t/m3	Mass of metal, t at average grade of 0.3514.7% Cu	Mass of metal, lb at average grade of 0.3514.7% Cu
1550	6 386	247		6 634					
1525	36 825	4 464		41 289	599 037				
1500	67 195	18 209	527	85 931	1 590 249				
1450	219 662			219 662	7 639 813				
1400	297 400			297 400	12 926 543	22 755 641	**58 026 885**	**203 947**	449 625 839
1350	297 400			297 400	14 869 988				
1300	297 400			297 400	14 869 988	52 495 617	**133 863 824**	**470 491**	1 037 254 268
Northern part of stockwork "OESTE"									
1525	9 318			9 318					
1500	31 289			31 289	507 588				
1450	42126,55			42 127	1 835 399				
1400	42126,55			42 127	2 106 328	4 449 315	**11 345 752**	**39 877**	87 913 446
1350	42126,55			42 127	2 106 328				
1300	42126,55			42 127	2 106 328	8 661 970	**22 088 023**	**77 633**	171 150 764
							1400	**ИТОГО**	**537 539 285**
							1300		**1 208 405 032**

Table 7.1-2. Calculated ore mass within anomalous contours (cutoff is 0.1% Cu) in the Eastern site of the Copernic ore field

Copernic ore field, site "ESTE"									
Level	Area 1	Area 2	Area 3	Area at a level, m2	Volume between the adjacent planes, m3	Total volume at different depths, m3	Mass of ore, t at density of 2.55 t/m3	Mass of metal, t at average grade of 0.3514.7% Cu	Mass of metal, lb at average grade of 0.3514.7% Cu
1800	2 893			2 893					
1750	49 404			49 404	1 307 432				
1700	106 732	2 450		109 182	3 964 643				
1650	135 877	14 093		149 970	6 478 785				
1600	166 601			166 601	7 914 271				
1550	166 601			166 601	8 330 049				
1500	166 601			166 601	8 330 049	36 325 229	92 629 334	**299 378**	**660 014 742**

Table 7.1-3. Speculative copper resources of the Eastern and Western sites (cutoff is 0.1% Cu)

Copernic ore field, site "ESTE"				
Level	Area 1	Total volume at different depths, m3	Mass of ore, t at density of 2.55 t/m3	Mass of metal, t at average grade of 0.3232.0% Cu
1500	166 601	36 325 229	92 629 334	**299 378**
Copernic ore field, site "OESTE"				
Level	Area 1	Total volume at different depths, m3	Mass of ore, t at density of 2.55 t/m3	Mass of metal, t at average grade of 0.3514.7% Cu
1400	297 400	22 755 641	**58 026 885**	**203 947**
1300	297 400	52 495 617	**133 863 824**	**470 491**
Northern part of stockwork "OESTE"				
1400	42126,55	4 449 315	**11 345 752**	**39 877**
1300	42126,55	8 661 970	**22 088 023**	**77 633**
		Total	1400	**243 824**
			1300	**548 124**
Total in all sites			**minimum**	**543 202**
			maximum	**847 502**

7.2. Molybdenum

The estimation of Mo resources is complicated by fragmentation of Mo anomalies into a number of isolated zones partly coinciding with contours of Cu anomalies. Because of this, those parts of Mo anomalies, which are enclosed into the contour of Cu anomalies (cutoff 0.1% Cu), are involved in calculation (Appendix 8, sheet 2).

The calculated speculative Mo resources are shown in Table 7.2-1. It should be noted that the estimated Mo resources are at least three times lower than the geochemical resource potential and can be increased substantially in the future.

Table 7.2.1. Speculative molybdenum resources of the site "OESTE"within the cutoff contour of 0.1% Cu

Level	Area 1	Area 2	Area 3	Area at a level, m2	Volume between the adjacent planes, m3	Total volume at different depths, m3	Mass of ore, t at density of 2.55 t/m3	Mass of metal, t	Mass of metal, lb
								at average grade of 100 ppm Mo	
1550	2 688	247		2 936					
1525	31 281	11 508		42 789	571 566				
1500	60 572	26 923	1 022	88 517	1 641 327				
1475	155 909			155 909	3 055 317				
1450	223 005			223 005	4 736 423				
1425	276 488			276 488	6 243 663				
1400	283 503			283 503	6 999 881	23 248 177	59 282 852	**5 928**	**13 069 616**
1375	283 503			283 503	7 087 567				
1350	283 503			283 503	7 087 567	37 423 311	95 429 442	**9 543**	**21 038 566**

Appraisement

Mo	**RJ prognosis LongTerm (2009/04)**	lb/t	$US
$/lb	**11**	21 038 566	**231 424 222**
$/t	**24 250,820**	9 543	**231 424 222**
	LME Q1 2009		
$/lb	**9,8**	21 038 566	**206 177 943**
$/t	**21 605,276**	9 543	**206 177 943**

8. ECONOMIC EVALUATION OF THE OBJECT

The main parameters of this project are compared with those of medium and large porphyry and other copper deposits of Peru at different stages of geological exploration. The Haquira, Canariaco, the 1st order of priority, and Magistral are the closest in basic parameters.

Table 8-1. The main parameters of some porphyry and other copper deposits in Peru

Deposit	Company	Deposit type	Stripping ratio	Cutoff, % Cu	Average grade, % Cu	Resource category	Ore, Mt	Copper, kt	Average grade, % Mo	Ore type
Copernic	Upstream Mining SAC	Porfido+oxi	***0,5***	***0,1***	**0,353**	Speculative	203,6-239,8	732,1-857,5	***0,01***	**oxi**
				0,3	**0,483**		89,0-121,3	473,1-568,4	***0,025***	**oxi**
Haquira	Minera Antares Peru SAC. 100% Antares Minerals	Porfido	1,2	**0,2**	0,389	Inferred	293,31	557,96		oxi
				0,3	0,483	Inferred	179,10			oxi
Canariaco, the 1st order of priority	Candente Resource Corp.	Porfido+oxi	0,6-1,3	0,3	0,359	Inferred	106,90	287,83		oxi+sulf
Canariaco Norte	Candente Resource Corp.	Porfido+ oxi	>1,0	0,3	*0,446*	Inferred	*820,00*	*3 674,00*		oxi+sulf
Pinaya	Acero-Martin Exploration Inc	Porfido	>1,0	?	0,52	Speculative	**?**	52,10	Au0,4g/t, res. 15,4 t	oxi+sulf
Quechua	Pan Pacific Copper Co., Ltd.	Porfido и skarn		0,48	0,98	Inferred	100,00	980,00	**0,011**	sulf
			>1,0	0,4	0,61	Hypothetical	260,00		0,005	sulf
Constancia	Norsemont Peru S.A.C	Porfido	1,19-1,25	0,2	0,33-0,5	Inferred	412,60	1 813,90	0,01-0,012	sulf
Magistral	Inca Pacific Resources Inc	Porfido	1.78, prefeas. Study	0,4	0,51	Inferred	*250,90*	*1 308,16*	0,042	sulf
		skarn	**2.2, feas. Study**	**0,4**	**0,49**	**Proven+ Probable**	**113,50**	**556,11**	**0,05**	**sulf**
Mina Justa	Chariot Resources Ltd.	**IOCG**	approx.	0,3	0,6-0,71	Inferred	81,3-331,8			oxi+sulf
	2008 FinModel		**0.8, open pit**	0,3	**0,67**	Inferred	**228,10**	*1 520-1 733*	**174,1**	**oxi**
				0,3	**0,76**	Inferred			**54**	**sulf**

9. CONCLUSIONS

The prospecting performed in 2009–2010 gave the following results:

- outlook for the future of the Copernic project has been specified substantially and its reliability increased;
- the Western site became more promising, and the contours of forecasted economic mineralization therein became more specific;
- new geophysical data give grounds to expect shallow-seated sulfide mineralization in the Western site and its extension in the northern and northeastern directions;
- showings of visible oxidized and sulfide copper mineralization are traced northward and northeastward beyond the concession areas belonging to the JV Copernic Exploraciones S.A.C.;
- the distinct, highly contrasting Cu and Mo geochemical anomalies likely correspond to extensive zones of economic mineralization;
- new evidence for occurrence of primary sulfide porphyry copper–molybdenum ore at a depth substantially increases ore resource potential of the Copernic ore field;
- first of all, economic mineralization should be expected in the Western site, where economic Cu (0.1–1.0%) and Mo (0.01–0.1%) were detected;
- Mo resource potential of the Copernic ore field remains vaguely estimated, however, promise for economic Cu-Mo mineralization is rather high;
- speculative copper resources of the Copernic ore field have been estimated;
- it seems realistic that 80–85% recovery of copper from oxidized ore can be achieved;
- the main parameters of inferred orebodies in the Copernic ore field are comparable with those of medium and large porphyry copper deposits currently explored in Peru by other companies;
- the estimated copper resources of the Copernic ore field fits a small- or medium-sized deposit;
- the forecasted deposit will be suitable for open-pit mining with expected stripping ratio of 0.5 for oxidized copper ore and subsequent vat- or heap-leaching and SX/EW copper recovery;
- the infrastructure of the territory, where the deposit is situated, is favorable for geological exploration, development, and mining.
- IN SUMMARY, the Copernic project is a promising object for further geological exploration.

10. RECOMMENDATIONS

The results obtained in 2010 allow us to recommend further development of geological exploration.

The next stage of drilling should be aimed at tracing mineralization to a depth and its qualitative and quantitative characterization.

The Western site (zona Oeste) is a high-priority object for drilling, where ascertained the most contrasting geochemical anomalies of copper and molybdenum, which partly overlaps with the anomalies of the IP. Drilling profiles must cross the zone of stockwork «Oeste» in submeridional direction and sublatitudinally NW segment of the anomalous contour IP. At the first stage, the drilling must be focused on substantiation of the forecasted sulfide mineralization at a depth and estimation of inferred resources for the entire ore stockwork.

To resolve these problems, it is necessary to drill 3000–3500 m (8–10 holes of diamond core drilling). At least six holes are necessary to intersect ore intervals of stockwork and 3–4 holes for verifying geophysical anomalies presumably caused by sulfide mineralization. Drilling

will be accompanied by sampling of cores and logging. In the case of positive drilling results, its footage can be increased.

The Eastern site will be involved in drilling after positive results obtained in the Western site.

Chief geologist A.Yu. Mar'yan

November 5, 2010